Acoustic field influence in the kinetics of thermochemical degradation during biomass torrefaction

Influência de um campo acústico na cinética de degradação termoquímica durante a torrefação de biomassa

Influence d'un champ acoustique dans la cinétique de dégradation thermochimique pendant la torréfaction de la biomasse

Edgar Amaral Silveira

Brasília, May 2018

UNIVERSITY OF BRASÍLIA

FACULTY OF TECHNOLOGY

MECHANICAL ENGINEERING DEPARTMENT

TESE DE DOUTORADO EM CIÊNCIAS MECÂNICAS
PhD THESIS IN MECHANICAL SCIENCES

EDGAR AMARAL SILVEIRA

BRAZIL

DIRECTION: PROF. ARMANDO DE AZEVEDO CALDEIRA-PIRES
ORIENTADOR: PROF. ARMANDO DE AZEVEDO CALDEIRA-PIRES

CO-DIRECTION: PROF. MARCUS VINICIUS GIRÃO DE MORAIS
COORIENTADOR: PROF. MARCUS VINICIUS GIRÃO DE MORAIS

FRANCE

DIRECTION: PROF. ANÉLIE PÉTRISSANS
ORIENTADOR: PROF. ANÉLIE PÉTRISSANS

CO-DIRECTION: PROF. PATRICK ROUSSET
COORIENTADOR: PROF. PATRICK ROUSSET

PUBLICAÇÃO: ENM-DT 48/2018
BRASÍLIA/DF: MAIO - 2018

AGRADECIMENTO

Dedico este trabalho ao meu pai, minha mãe e meus avós que nunca mediram esforços para garantir minha educação e mostrar o caminho a ser seguido, e a todas as pessoas que contribuíram para realização deste projeto: professores, amigos, namorada, meus irmãos e familiares. Agradeço ao meu orientador e co-orientador Armando Caldeira-Pires e Marcus Vinícius Girão por todos os ensinamentos diários, atenção e disponibilidade em todas as etapas do projeto no Brasil, assim como, meus orientadores e co-orientadores da parte francesa: Mathieu e Anélie Pétrissans; Patrick Rousset. Muito obrigado pela experiência incrível de trabalho com uma equipe de ponta dentro do laboratório Lermab. Obrigado por todas as oportunidades profissionais, momentos de aprendizado e pela amizade. Gostaria de agradecer a Thierry Duvaut (Universidade de Reims) e Divino Eterno Teixeira (Laboratório de Produtos Florestais) pela atenção como revisores da tese. Agradeço aos pesquisadores e amigos Luiz Gustavo Galvão e Bruno Sant'Anna Chaves pelo excelente trabalho desenvolvido em parceria com o Laboratório de Produtos Florestais, no Brasil. Na França, agradeço aos amigos Baptiste Colin e Bo-Jhih Lin por toda a atenção e aprendizado ao longo desses dois últimos anos. Agradeço à toda equipe de trabalho da IUT Hubert-Curien por todo acolhimento e momentos inesquecíveis durante o meu período de trabalho em Épinal, França. Agradeço ao Conselho Nacional de Desenvolvimento Científico e Tecnológico (CNPQ) pela oportunidade e apoio financeiro para o meu aperfeiçoamento profissional no exterior e pela bolsa de estudos no Brasil e à Fap-Df e ao DPG pelo suporte em congressos. Agradeço ao PCMEC da Universidade de Brasília pela atenção e dedicação aos alunos, ao programa Labex-Arbre e Cost Action por todo o suporte em congressos e formações internacionais.

ACKNOWLEDGEMENT

I dedicate this work to my father, my mother and my grandparents who always tried to guarantee my education and show the way to be followed, and to all the people who contributed to the realization of this project: teachers, friends, girlfriend, my brothers and relatives. I would like to thank my director and co-director Armando Caldeira-Pires and Marcus Vinícius Girão for all the daily teaching, attention and availability in all stages of the project in Brazil, as well as my French director and co-director: Mathieu and Anélie Pétrissans and Patrick Rousset. Thank you so much for the incredible experience of working with a leading team within the Lermab laboratory. Thanks for all the professional opportunities, moments of learning and friendship. I would like to thank Thierry Duvaut (University of Reims) and Divino Eterno Teixeira (Forest Product Laboratory) for the attention as Thesis reporters. I would like to thank the researchers and friends Luiz Gustavo Galvão and Bruno Sant'Anna Chaves for the excellent work developed in partnership with the Laboratory of Forest Products in Brazil. In France. I would like to thank my friends Baptiste Colin and Bo-Jhih Lin (John) for all the attention and learning over the last two years. I would like to thank the entire IUT Hubert-Curien staff for all the welcome and unforgettable moments during my period of work in Épinal, France. I would like to thank the CNPQ for the opportunity and financial support for my professional development abroad and scholarship in Brazil, DPG and Fap-Df for the support in congresses. I would like to thank the PCMEC of the University of Brasilia for the attention and dedication to the students, the Labex-Arbre and Cost Action programs for all the support in international congresses and training.

ABSTRACT

Considered a mild form of pyrolysis, torrefaction appears as an alternative thermal treatment where the biomass is heated at temperatures between 200-300°C in partial or total absence of oxygen to produce a more hydrophobic, homogeneous and higher calorific solid fuel when compared to the raw material. Several torrefaction technologies have already been developed and implemented in the industry. The present work has as main objective to deepen the knowledge in the biomass thermo-degradation process during torrefaction. For this, an innovative experimental apparatus was developed aiming to improve the wood heat treatment by coupling an acoustic field to the temperature parameter. The assumption is that an acoustic field within a reactor modifies the pressure field and consequently the velocity of the particles around the sample by altering the interaction between the gaseous environment and the released volatile around the wood surface, accelerating its degradation process. With this objective, an acoustic system was implemented in a reactor. A characterization and mapping of the acoustic behavior contemplating the measurement of acoustic flux rate and its intensity was performed. The physical and chemical torrefaction experiments were performed for two treatment temperatures with and without influence of the acoustic, providing the mass yield evolution, the temperature curves and the chemical properties of the torrefied material. Concomitantly, a numerical model of kinetics and elemental composition was established for the mass yield and the composition prediction in terms of carbon hydrogen and oxygen during the degradation. The torrefaction experimental results, as well as the chemical analysis and pyrolysis of the final product, provided evidence such as: reduction of residence time, increase of the samples internal temperature during treatment and a greater calorific power for the samples treated under acoustic influence. A final comparison between experimental and simulation results allowed the evaluation of the torrefaction numerical model and the influence of the acoustics on the degradation kinetics.

Keywords: biomass, torrefaction, acoustic, kinetics, energy properties.

RESUMO

Considerada uma forma suave de pirólise, a torrefação aparece como alternativa de tratamento térmico da biomassa, onde essa é aquecida a temperaturas de 200 - 300 ° C em ausência parcial ou total de oxigênio visando produzir um combustível sólido mais hidrofóbico, homogêneo e com maior teor de carbono quando comparado à matéria-prima. Várias tecnologias de torrefação já foram desenvolvidas e implementadas na indústria. O presente trabalho tem como objetivo principal aprofundar o conhecimento no processo de termo-degradação da biomassa durante a torrefação. Para isso um inovador aparato experimental foi desenvolvido visando aprimorar o tratamento térmico da madeira acoplando um campo acústico ao fator temperatura. O pressuposto é que um campo acústico dentro de um reator modifica o campo de pressão e, consequentemente, a velocidade das partículas ao redor da amostra alterando a interação entre o ambiente gasoso e os voláteis na superfície da madeira, acelerando o seu processo de degradação. Com este objetivo, um sistema acústico foi implementado em um reator. Uma caracterização e mapeamento do comportamento acústico contemplando a aferição da taxa de fluxo acústica e da sua intensidade foi executada. Os experimentos físicos e químicos da torrefação foram realizados para duas temperaturas de tratamento com e sem influência da acústica, fornecendo o rendimento mássico, as curvas de temperaturas e as propriedades químicas do material torrificado. Concomitantemente, foi estabelecido um modelo numérico da cinética e da composição elementar para a predição do rendimento mássico e da composição em termos de carbono hidrogênio e oxigênio durante a degradação. Os resultados experimentais da torrefação, bem como a análise química e pirólise do produto final, forneceram evidências como: redução do tempo de residência, aumento da temperatura interna da amostra e um maior poder calorífico para as amostras tratadas sobre influência da acústica. Uma comparação final entre resultados experimentais e numéricos permitiram a avaliação da precisão do modelo para o tratamento de torrefação e a influência da acústica na cinética de degradação.

Palavras-chave: biomassa, torrefação, acústica, cinética, propriedades energéticas.

RÉSUMÉ

Considérée comme une forme douce de la pyrolyse, la torréfaction apparaît comme une alternative au traitement thermique de la biomasse où elle est chauffée à des températures de 200-300 ° C en absence partielle ou totale d'oxygène pour produire un combustible solide plus hydrophobe, homogène et de meilleure qualité par rapport à la matière première. Plusieurs technologies de torréfaction ont déjà été développées et mises en œuvre dans l'industrie. Le présent travail a pour objectif principal d'approfondir les connaissances dans le processus de thermo-dégradation de la biomasse pendant la torréfaction. Pour cela, un appareil expérimental innovant a été développé visant à améliorer le traitement thermique du bois en couplant un champ acoustique au facteur température. L'hypothèse est qu'un champ acoustique dans un réacteur modifie le champ de pression et par conséquent la vitesse des particules autour de l'échantillon en modifiant l'interaction entre l'environnement gazeux et les volatiles à la surface du bois, accélérant son processus de dégradation. Avec cet objectif, un système acoustique a été mis en place dans un réacteur. Une caractérisation et une cartographie du comportement acoustique envisageant la mesure du débit acoustique et de son intensité ont été réalisées. Les expériences physiques et chimiques de la torréfaction ont été effectuées pour deux températures de traitement avec et sans influence de l'acoustique, fournissant le rendement massique, les courbes de température et les propriétés chimiques du matériau torrifié. Concomitamment, un modèle numérique de la cinétique et de la composition élémentaire a été établi pour la prédiction du rendement en masse et de la composition en termes de carbone, d'hydrogène et d'oxygène au cours de la dégradation. Les résultats expérimentaux de la torréfaction, ainsi que l'analyse chimique et la pyrolyse du produit final ont fourni des preuves telles que: réduction du temps de séjour, augmentation de la température interne de l'échantillon et pouvoir calorifique supérieur pour les échantillons traités sous l'influence de l'acoustique. Une dernière comparaison entre les résultats expérimentaux et numériques a permis d'évaluer la précision du modèle pour le traitement de torréfaction et l'influence de l'acoustique sur la cinétique de dégradation.

Mots-clés: biomasse, torréfaction, acoustique, cinétique, propriétés énergétiques.

SUMMARY

LIST OF FIGURES

LIST OF TABLES

LIST OF SYMBOLS

c	Speed of sound	(m.s^{-1})
ρ	Air density	(kg.m^{-3})
$\vec{v}$	Acoustic velocity vector field	(m.s^{-1})
p	Acoustic pressure	(Pa)
$P(\vec{x})$	Pressure	(Pa)
$\vec{V}(\vec{x})$	Velocity magnitude	(m.s^{-1})
ω	Frequency	(Hz)
Φ	Phase angle	°
Δx	Distance between two microphones	(m)
$\hat{S}_{xy}$	Cross-spectral density function	
$R_{xy}(\tau)$	Cross-correlation function	
ϕ_{xy}	Phase shift	°
$x(t)$	Acoustic signal in x coordinate	(Pa)
$y(t)$	Acoustic signal in y coordinate	(Pa)
$\gamma_{xy}^2(f)$	Coherence spectrum	
B	Bandwidth	(Hz)
$z(t)$	Analytic signal	
$\tilde{x}(t)$	Time function	
$\mathcal{H}[x(t)]$	Hilbert transform	
C	Carbon	(wt%)
H	Hydrogen	(wt%)
N	Nitrogen	(wt%)
O	Oxygen	(wt%)
η_S	Solid yield	(wt%)
η_E	Energy yield	(wt%)
F	Acoustic frequency within the reactor	(Hz)
T	Temperature	(°C)
ε_{ij}	Error of the statistical model	
μ	Constant of statistical model	
A	Raw biomass pseudo-component	(kg)
B	Intermediate solid fraction pseudo-component	(kg)
C	Final solid fraction (biochar) pseudo-component	(kg)

V_1	First step reaction volatile group pseudo-component	(kg)
V_2	Second step reaction volatile group pseudo-component	(kg)
$E_{a,i}$	Activation energies of the reactions	(J.mol^{-1})
$k_{0,i}$	Pre-exponential factors of the reactions	(s^{-1})
R	Universal gas constant	(J.mol^{-1}.K^{-1})
T	Absolute temperature	(K)
$Y_{cal}^{T}(t)$	Instantaneous calculated solid yield	(wt%)
S	Sum of A, B and C pseudo-components	(kg)
t	Time	(s)
β	A relative rate of reaction	
v	V_1 relative rate of reaction	
γ	B relative rate of reaction	
ξ	V_2 relative rate of reaction	
m_0	Dried mass before torrefaction	(kg)
m_i	Solid mass during torrefaction	(kg)
HHV_0	Higher heating value of untreated samples	(MJ. kg^{-1})
HHV_i	Higher heating value of torrefied	(MJ. kg^{-1})
$diff^{(T)}$	Deviation between experimental and calculated yield	

UnB	University of Brasília
LPF	Forest Product Laboratory
SFB	Brazilian Forest Service
IBAMA	Brazilian Institute of Environment and Renewable Natural Resources
LEA	Laboratory of Energy and Environment
GDS	Dynamic System Group
LERMAB	Laboratory of Studies and Research in Wood
Toe	Tonne of oil equivalent
TGA	Thermogravimetric analysis
DTG	Derivative of thermogravimetric
FTIR	Fourier transform infrared spectroscopy
HPLC	High performance liquid chromatography
GC	Gas chromatography
IR	Infrared spectroscopy
ASTM	American Society for Testing and Materials

ODE	Ordinary Differential Equation
ANOVA	Analysis of variance
CV	Coefficient of variation
EMCI	Energy-mass co-benefit index

1. RESEARCH OBJECTIVES AND MOTIVATION

Present work is devoted to deep the knowledge in biomass thermo-degradation torrefaction process. The advanced experimental and numerical methodologies developed at this work allowed the conception of an innovative concept technology to improve the wood heat treatment by coupling acoustic field and temperature.

The hypothesis is that the introduction of an acoustics field within a torrefaction reactor could change the pressure distribution and flow field around the wood sample modifying the interaction between reactor gaseous environment and volatiles at wood sample surface, consequently, improving the degradation processes.

With this aim a sound system was implemented within an existing torrefaction reactor (ROUSSET et al., 2012) and acoustically characterized thereafter. Torrefaction experiments were performed to analyze the temperature profiles and wood sample weight dynamics during the heat treatment with and without acoustic. The torrefied product assessment via its pyrolysis and chemical analyses provided information about the effect of the temperature and acoustic frequencies coupling. A numerical model to simulate the influence of the acoustic field on biomass thermodegradation has been developed and validated with the performed experiments results.

The study involves the cooperation between the Forest Products Laboratory (LPF - SFB), Laboratory of Energy and Environment (LEA - University of Brasília) and GDS (Dynamic System Group), in Brazil, and Laboratory of Studies and Research in Wood (LERMAB - University of Lorraine), in France. The research work is split into five steps:

Experimental

a) Conception and implementation of an acoustic system within a torrefaction reactor;

b) Reactor acoustic characterization with different methodologies in time and frequency domain;

c) Torrefaction experiments in micro-particle scale to characterize the torrefaction process;

d) Torrefaction experiments in macro-particle scale with and without acoustic influence;

Numerical

d) Two different numerical models for torrefaction process simulation:

- Wood thermodegradation kinetics model;
- Wood elemental composition prediction model;

1.1 Research Outline

The document is broken into four main chapters. In Chapter 2 a detailed state of the art is provided. In a first step, a summarized worldwide and Brazil energy context was presented. The introduction to biomass characterization and properties are reviewed next. Biomass properties evolution during torrefaction is also described. The chapter continues with a biomass torrefaction process/technologies literature review. In addition to describing how torrefaction affects biomass physical properties and wood compounds degradation, it is detailed the existing kinetics and composition evolution models for torrefaction and its limitations. Finally, the emphasis is placed on the acoustic, describing the acoustic techniques applied in this work.

Chapter 3 describes the case of study. It starts with the experimental acoustic apparatus proposition, development and implementation within a torrefaction reactor. It details the physical modifications that have been made to adapt the acoustic system in to the existing reactor and the experimental characterization to determine the optimum operation acoustics parameters. The chapter continues with the biomass torrefaction experimental study. It is presented the biomass selection, the methodology and the applied parameters for the micro and macro-scale experimental analysis. Finally, a new numerical modelling methodology to determine the kinetic and elemental composition evolution is presented.

Chapter 4 presents the obtained results. In a first stage, the results for the acoustic characterization are presented. Next, the *Eucalyptus grandis* torrefaction in micro-scale results, providing a basis of comparison for the thermo-acoustic discussion via the physical assessment. Thereafter, the torrefaction results are presented with and without the influence for the macro-scale particle. Two new biomass models, kinetics and composition prediction, are presented, validated and applied to the case of study. The two new methodologies allowed the predicting of the solid yield evolution and its composition in time for coupled acoustic and temperature treatments.

Chapter 5 presents the conclusions and the perspectives of the research.

2. STATE OF ART

2.1 Energy context

The demand for alternative energy sources drives technological development in such a way that many fuels and energy conversion processes, once judged to be inadequate or even unviable, are now competitors of fuels and so-called traditional processes. The increase in energy consumption in recent years is justified by the socio-economic progress of developing countries. Also, factors such as population growth, economic structure, patterns of social development, among others, make the projection of world energy expenditure ever increasing. Figure 1 illustrate de global energy demand for 2015.

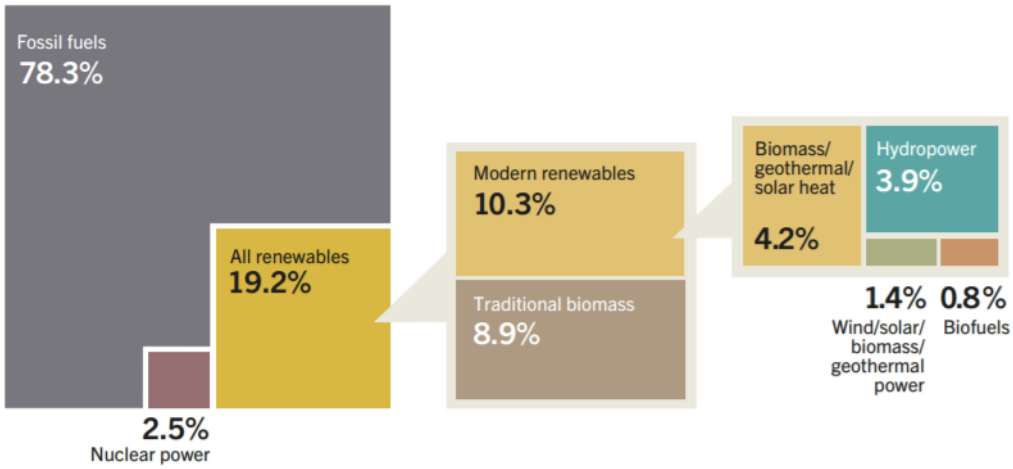

Figure 1. Global energy demand 2016 (REN21 - GSR, 2016).

About 80% of the energy supply comes from coal, oil and natural gas on a global average. This energy system based on the use of fossil fuels results in the economic dependence of non-producing countries on raw materials, implying even military and geopolitical conflicts. Another problem is the damage to the environment and to society, such as the destruction of ecosystems, damage to forests and aquifers, diseases, reduction of agricultural productivity, deterioration of the ozone layer or acid rain, greenhouse effect, as well as the collateral effects as accidents in oil drilling and coal mines or contamination by chemical or fuel spills. In addition, the depletion of reserves and the consequent rise in prices of fossil fuel derivatives are observed.

Biomass global production continued to increase in 2015, helping to meet rising energy demand in some countries and contributing to environmental objectives. However, the sector also faced several challenges, in particular from low oil prices and policy uncertainty in some markets. Bio-heat production for buildings and industrial uses grew slowly in 2015, with

modern uses of bio-heat rising by approximately 3% from 2014 levels. There has been marked growth in the use of biomass for district heating in the Baltic and Eastern European regions. The use of bio-power has increased more quickly - averaging some 8% annually - with rapid growth in generation notable in China, Japan, Germany and the United Kingdom. Ethanol production increased by 4% globally, with record production levels in the United States and Brazil. Global production of biodiesel fell slightly due to constrained production in some Asian markets, although growth continued in the major producing countries (the United States and Brazil). Blend mandates sheltered demand for biofuels from falling fossil fuels prices, but uncertainty about future markets constrained investment in new production capacity during the year (REN21 - GSR, 2016).

Bioenergy contributes more to primary global energy supply than any other renewable energy source. Total energy demand supplied from biomass in 2015 was approximately 60 exajoules (EJ). The use of biomass for energy has been growing at around 2% per year since 2010. The bioenergy share in total global primary energy consumption has remained relatively steady since 2005, at around 10%, despite a 24% increase in overall global energy demand between 2005 and 2015. Bioenergy plays a role in all three-main energy-use sectors: heat (and cooling), electricity and transport. The contribution of bioenergy to final energy demand for heat (traditional and modern) far outweighs its use in either electricity or transport (Figure 2).

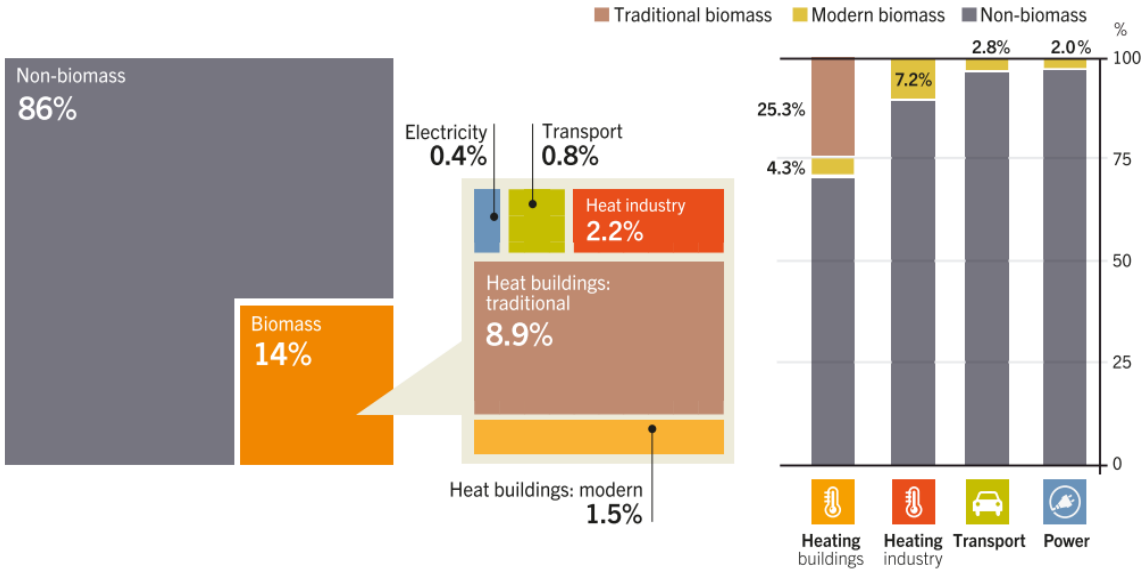

Figure 2. Shares of Biomass in Total Final Energy Consumption and in Final Energy Consumption by End-use Sector, 2014 (REN21-GSR2016).

Solid biomass represents the largest share of biomass used for heat and electricity generation, whereas liquid biofuel represents the largest source in the transport sector (Figure 3) (REN21-GSR2016).

In the case of Brazil, energy matrices distribution has a huge difference when compared to the world average due to the large share of renewable sources, mainly biomass and hydropower. Brazilian energy scenario (year 2015 as a base) is shown in Figure 4.

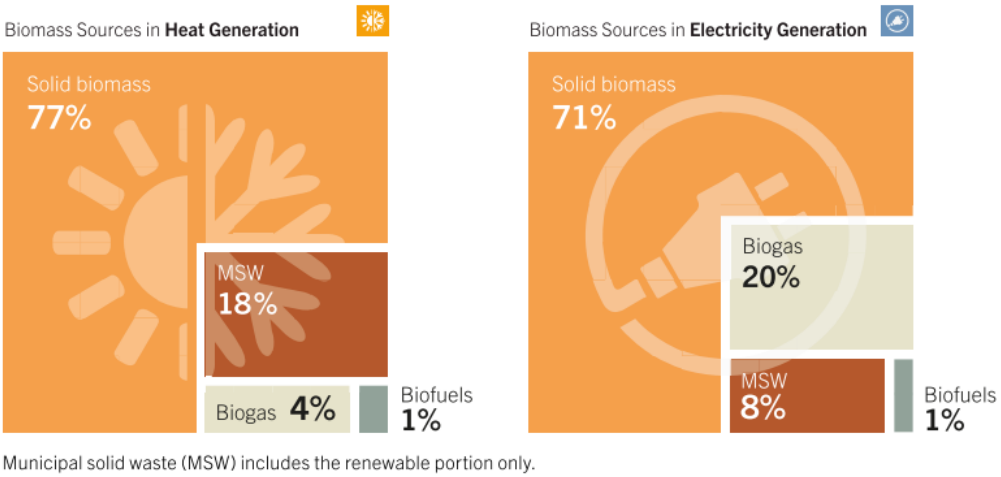

Figure 3. Shares of biomass sources in global heat and electricity generation, 2015 (REN21-GSR2016).

From the 2016 Synthesis Report of the Ministry of Mines and Energy, the Internal Energy Supply in 2015 in Brazil was 299.2 million toe, which meant a decrease of 2.1% in relation to the year previous. In 2015, the share of renewable sources in the Brazilian Energy Matrix remained among the highest in the world with the percentage of 41%. This year there was an increase of 2.3% due to the higher supply of sugarcane derivates and wind compared to 2014. The bioenergy parcel, which corresponds to 25.1% of the total, is composed mainly of sugarcane biomass, firewood and charcoal.

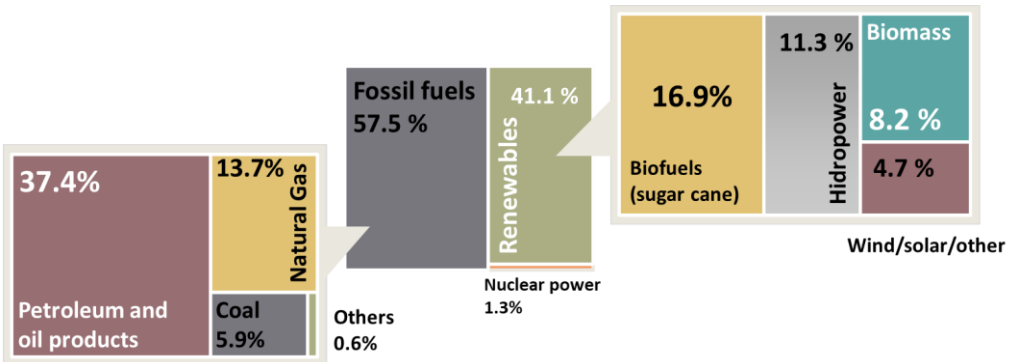

Figure 4. Brazil domestic energy supply (EPE, 2016 - Modified).

At the beginning of the studies the Brazilian energy matrix was dominated by renewable sources, with 58.4% of the total offered versus 41.6% of non-renewable sources. However, this relationship was reversed over the years, and three decades later non-renewable energy accounted for the largest share of the energy supply with 60%. This inversion demonstrates the

adoption of a development pathway based mainly on oil, and this scenario continues to this day, with 58.8% of non-renewable and 41.2% of renewables.

The crisis of prices of this fossil fuel in the 1970's stimulated in part the search for alternative sources. Many countries have invested in new technologies for energy use of renewable natural resources, including public policies were created, as in the case of PROALCOOL in 1975 (RODRIGUES et al., 2009). To minimize the use of natural resources and at the same time supply energy in a sustainable way, the importance of research aiming to improvement and developing of renewable energy technologies must be considered. Brazil is prominent in the world due mainly to biomass energy use in two areas: the production of sugarcane ethanol for motor vehicles and the production of charcoal from planted forests.

The Brazilian forestry sector is one of the most developed and competitive in the world. According to the Brazilian Association of Planted Plantain Producers (ABRAF), in 2012 the Brazilian planting area of Eucalyptus and Pinus reached 6.66 million hectares. Eucalyptus plantations represent 76.6% of the total area and Pinus 23.4% (ABRAF, 2013).

Biomass torrefaction has been subject of numerous studies in recent years. A detailed state of the art seems therefore indispensable to understand biomass global position, constitution, thermochemical degradation pathways and identify the main advances into thermal modifications treatments. The objective of this bibliographic study is therefore to establish a knowledge base necessary to understand the phenomena involved in torrefaction pre-treatment and to highlight the technological aspects that require further study. With this aim, a review of wood biomass constitution and composition will be presented. Torrefaction treatment mechanisms will then be described and related to thermal modified biomass properties. Emphasis will also be placed on wood numerical model to simulate kinetic and elemental composition during thermal modification. Finally, the acoustic phenomena whose characterization is indispensable for the conception of the lab-scale reactor will be detailed.

2.2 Torrefaction

2.2.1 Biomass

Biomass can be considered as one of the solar energy resources. Plants grow by absorbing carbon dioxide from the atmosphere as well as water and nutrients from soils followed by converting them into hydrocarbons through photosynthesis. All carbon contained in biomass is gained from carbon dioxide; in other words, carbon is cycled in the atmosphere when biomass is consumed as a fuel (CHEN et al., 2015).

All plant derived biomass contains an inedible lignocellulose portion which provides structure in the form of trunks, stems, leaves, and branches. Certain plants may additionally produce edible fruits and seeds which contain carbohydrates (starch and sugar), fat, and protein. Woody plants like trees, shrubs, and vines are characterized by stems covered in thickened bark and are non-herbaceous. This means that they maintain a perennial stem above the ground. Trees can be further divided into hardwoods (angiosperms), which are deciduous and lose their leaves annually, and softwoods (gymnosperms), which are coniferous, and do not lose their needles. Herbaceous plants, which include most types of grasses, have stems and leaves which die annually at the end of the growing season (BATES, 2012).

2.2.1.1 Composition and structure

The constituents in biomass include cellulose (a polymer glucosan), hemicelluloses (which are also called polyose), lignin (a complex phenolic polymer), organic extractives and inorganic minerals (also called ash) (CHEN et al., 2015).

The first three constituents are the main components in biomass and their weight percent depend on biomass species. For example, the softwood typically consists of 42% cellulose, 27% hemicelluloses, 28% lignin and 3% organic extractives; the hardwood comprises 45% cellulose, 30% hemicelluloses, 20% lignin and 5% organic extractives (PENG et al., 2013).

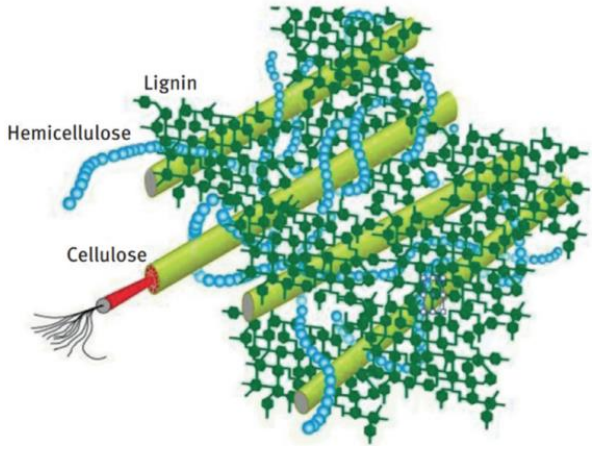

Figure 5. Cellulose, hemicellulose and lignin in plant cells (WANG et al., 2017).

Inorganic minerals are usually less than 1% of the content in wood. A clear understanding of the nature and behavior of these constituents is conducive to elucidating biomass torrefaction and densification characteristics (CHEN et al., 2015). The properties of cellulose, hemicellulose and lignin are summarized in table 1.

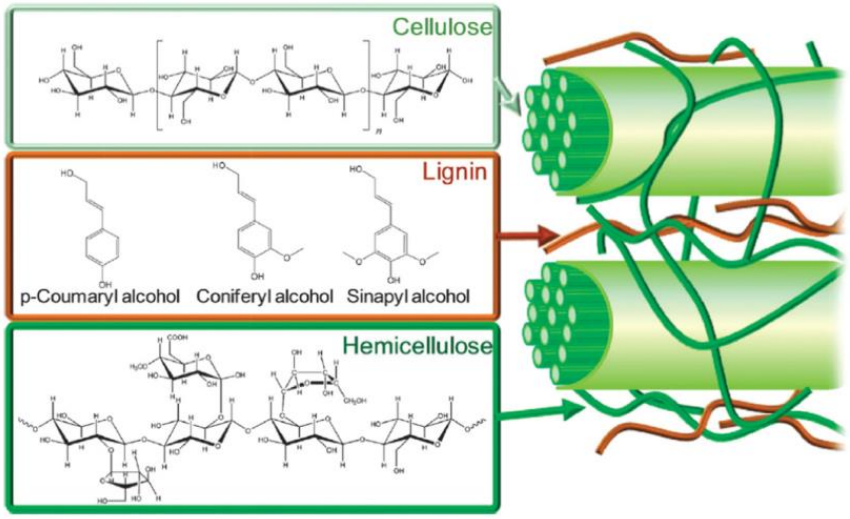

Figure 6. Molecular structures for cellulose, hemicelluloses (xylan), and lignin (NAG, 2010).

2.2.1.1.1 Cellulose

Cellulose is a linear homopolysaccharide composed of β-D-glucopyranose units linked together by (1-4)-glycosidic bonds (BALAT et al., 2008). Crystalline and amorphous structures are contained in cellulose and can be expressed by $(C_6H_{10}O_5)_m$ where subscript m is the degree of polymerization (CHEN et al., 2015). Cellulose is the primary component of most kinds of biomass and is earth's most common organic compound. It is a long linear chain polymer formed by 10,000-15,000 glucose units linked by glycosidic bonds (NAG, 2010). The hydroxyl groups which project from the sides of the cellulose chain contribute to intrachain hydrogen bonds (RAVEN & EICHHORN, 2005).This orderly arrangement and tight winding together of fibrils contributes to the mechanical strength of the plant cells.

Table 1. Summary of the properties of cellulose, hemicellulose, and lignin in biomass (CHEN et al., 2015)

	Cellulose	**Hemicelluloses**	**Lignin**
Structure	Linear	Branched	Three-dimensional
Formula	$(C6H10O5)_m$[a]	$(C5H8O4)_m$	$[C_9H_{10}O_3(OCH_3)_{0.9\text{-}1.7}]_m$
Atomic O/C	0.83	0.80	0.47–0.36
Atomic H/C	1.67	1.60	1.19–1.53
TDT[b] (°C)	315–400	220–315	160–900
Component	Glucose	Xylose, glucose, mannose, galactose, arabinose and glucuronic acid	Phenylpropane
Thermal behavior	Endothermic (exothermic if char formation is significant)	Exothermic	Exothermic

[a] m: degree of polymerization.
[b] TDT: thermal decomposition temperature.

2.2.1.1.2 Hemicelluloses

Hemicelluloses is a branched mixture of various polymerized monosaccharides, such as xylose, glucose, mannose, galactose, arabinose and glucuronic acid (MOHAN et al., 2006). Its basic structure can be represented by $(C_5H_8O_4)_m$. While herbaceous biomass contains primarily arabinoxylan, deciduous woods contain primarily xylan (80-90% weight), and coniferous woods contain 60-70% glucomannan and 15-30% arabinogalactan (GAUR & REED, 1998)

2.2.1.1.3 Lignin

Lignin is a three-dimensional, highly branched and polyphenolic substance that consists of an irregular array of variously bonded “hydroxy-” and “methoxy-” substituted phenylpropane units (CHEN et al,. 2011). Its chemical formula is represented by $[C_9H_{10}O_3 .(OCH_3)_{0.9\text{-}1.7}]m$ (CHEN et al., 2011). The strength of the carbon-carbon linkages is what provides lignin with high resistance to thermal and chemical degradation. Deciduous woods tend to contain guaiacylpropane units while coniferous woods contain the guaiacylpropane and syringylpropane units (GAUR & REED, 1998). Lignin is found primarily in the middle lamella and binds together adjacent cells. By encasing the hemicellulose and cellulose components, it protects the plant from enzymatic and microbial attack.

2.2.1.1.4 Extractives

Extractives are nonstructural compounds including proteins, oils, starches, and sugars. They provide plants with odor, color, and durability and can be extracted by hot water or other solvents (NAG, 2010).

2.2.1.1.5 Ash

Ash is inorganic solid residue remaining after a fuel undergoes complete combustion. It often contains carbonates, phosphates, and sulfates of silica, calcium, magnesium, sodium, and potassium. Ash components vary between biomass types and sources. Some mineral components may not be inherently contained in the biomass, and they may actually be from dirt and other impurities picked up during the collection process (BATES, 2012).

2.2.1.1.6 Moisture

Due to water's role in transpiration, photosynthesis and fluid transport, raw biomass contains characteristically high amounts of moisture. Moisture can be divided into free (also called external or imbibition) and inherent (also called bound or saturation) moisture. The former is defined as moisture above the fiber saturation point (FSP) and generally resides

outside the cell walls in the cavities of conductive vessels (FRANCESCATO et al., 2015). The inherent moisture content resides within the cell walls and is a function of relative humidity and air temperature (BASU, 2010).

Moisture content can be measured on a wet or dry basis. The difference is whether the moisture mass is divided by the original wet mass or the final dry mass, respectively. For very wet biomass like manure, moisture content on a dry basis exceeds 1 (BATES, 2012).

2.2.2 Thermochemical conversion pathway

The use of forest residues is carried out by thermo-chemical conversion processes such as liquefaction, torrefaction, pyrolysis, combustion and gasification. In addition to these, biological processes are also used to produce ethanol. The thermochemical pathway uses heat input for direct energy generation or to produce secondary fuels with higher energy density. When it is desired to obtain an intermediate product between dry wood and charcoal the process is called torrefaction and its main product is a solid material which retains 75-95% of the original energy content (PRINS et al., 2006). The thermo-chemical valorization channels illustrate in Figure 7 presents the main thermo-chemical valorization pathways for biomass.

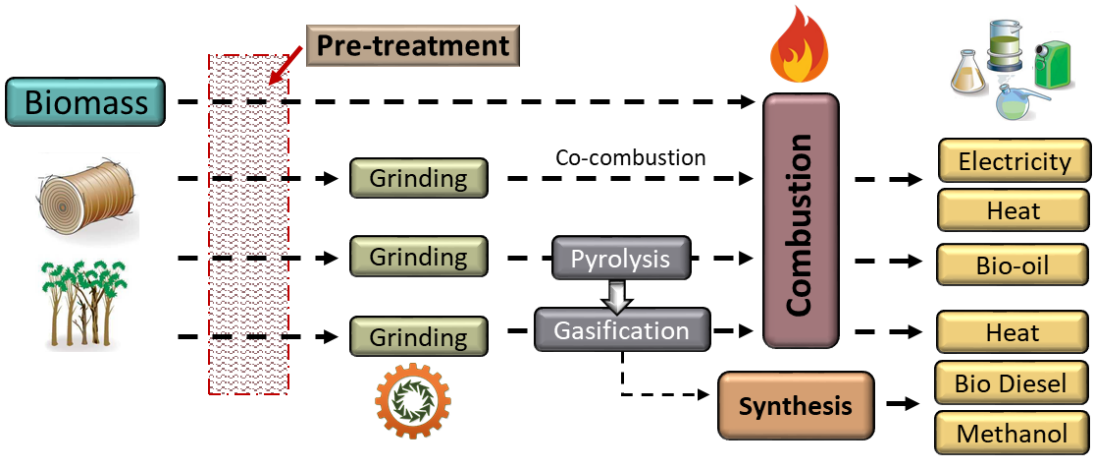

Figure 7. Main thermochemical biomass valorization pathway.

At present, the most industrially represented sectors are those of combustion and co-combustion (simultaneous combustion of biomass and coal) because these processes have been controlled and exploited for several years already allowing heat and electricity production (CAILLAT et al., 2010; ROGAUME, 2005).

The other value chains are mainly pyrolysis and gasification (DEGLISE and DONNOT, 2004). Pyrolysis is a thermal process carried out conventionally at temperatures between 500 and 1000°C under an inert atmosphere. During the rise in temperature, the biomass undergoes

first a drying phase and then a phase of thermochemical reaction which leads to the release of volatile materials. These volatiles are composed of condensable (oils) and non-condensable gases and the solid residue is the coal. These three fractions are then recoverable energetically or chemically. The proportions of these different phases are mainly controlled by the heating rate and the treatment temperature (DEGLISE and DONNOT, 2004). A so-called "rapid" pyrolysis at 500°C mainly leads to the production of oil, whereas at 1000°C, non-condensable gases are favored and a so-called "slow" pyrolysis favors the production of coal whatever the temperature.

Finally, gasification is also a heat treatment process at temperatures above 900°C under a slightly oxidizing atmosphere (CO_2, H_2O, O_2 or sub stoichiometric air). In a gasifier, the biomass is therefore successively subjected to a drying step and then to a pyrolysis step. The charcoal obtained (as well as the pyrolysis gases) are then reacted by gasification reactions to produce combustible gases (mainly CO, H_2, CH_4) and incombustible (CO_2) gases. The combustible gases produced can then be recovered by combustion, in a boiler or in a motor, to produce heat and/or electricity. Another way of valorization for these gases is the production of bio-fuels (bio-diesel, DME, methanol) via a chemical synthesis step (BROUST et al., 2008).

In the case of direct combustion, a pretreatment step is necessary when the biomass is to be transported over long distances. Indeed, because of the low apparent energy density of wood chips (2.2 to 4 GJ/m^3) (BATIDZIRAI et al., 2013), the densification of this biomass can considerably reduce transport and handling costs (ZWART and BOERRIGTER, 2006).The conventional pretreatment is pelletization, which makes it possible to obtain an energy density of 7.8 to 10.5 GJ/m^3 (BATIDZIRAI et al., 2013). However, pelletization requires grinding the biomass to a particle size of a few millimeters maximum (STELTE et al., 2011; MEDIAVILLA et al., 2012) which represents a high energy cost (20 to 80 kW_e/MW_{th} depending on the biomass and granulometry of the ground material, according to (BERGMAN et al., 2005).

Other sectors (co-combustion and gasification in particular) generally require the injection of biomass in pulverulent form. A fine grinding step is therefore also indispensable (SVOBODA et al., 2009). The costs incurred by these grinding stages therefore justify the search for a pretreatment capable of weakening the material. This is the case of torrefaction, which is one of the most promising ways to integrate efficiently into energy production chains from biomass (USLU etal., 2008; PÉREZ-FORTES et al., 2014).

2.2.3 Torrefaction process

Torrefaction pertains to a thermal pretreatment of biomass where raw biomass is heated in an inert atmosphere at temperatures of 200-300°C for upgrading solid biomass fuel (TRAN et

al., 2013). Nitrogen is the commonly used as carrier gas to provide a non-oxidizing atmosphere in most laboratory tests. Since torrefaction is conducted at conditions like those of pyrolysis which usually takes place between 350 and 650°C (DEMIRBAS, 2009), torrefaction has also been called mild pyrolysis. As described earlier, raw biomass is characterized by its high moisture content, low calorific value, hygroscopic nature, and larger volume or low bulk density. The evidences from recent research suggest that after undergoing torrefaction the properties of biomass are improved to a great extent (VAN DER STELT et al., 2011; CHEW et al., 2011). Figure 8 shows a summary of changes in biomass properties before and after torrefaction. The benefits accomplished by torrefaction include:

- Higher heating value or energy density;
- Lower atomic O/C and H/C ratios and moisture content;
- Higher hydrophobicity or water-resistivity;
- Improved grindability and reactivity;
- More uniform properties of biomass.

When biomass is torrefied, the pretreatment can be further classified into light, mild and severe torrefaction processes, corresponding to the temperatures of approximately 200–235, 235-275 and 275-300°C, respectively (CHEN et al., 2011). With light torrefaction, the moisture and low molecular weight volatiles contained in biomass will be released. Hemicellulose in biomass is the most active constituent among hemicellulose, cellulose and lignin; it is thermally degraded to a certain extent from light torrefaction, whereas cellulose and lignin are only slightly or hardly affected (ROUSSET et al., 2011).

Therefore, the weight loss of biomass is slight and its energy density or calorific value increases only slightly. When biomass undergoes mild torrefaction, hemicellulose decomposition and volatile liberation are intensified. Hemicellulose is substantially depleted, and cellulose is also consumed to a certain extent. Regarding severe torrefaction, hemicellulose is almost depleted completely, and cellulose is oxidized to a great extent. Lignin is the most difficult constitute to be thermally degraded; its consumption within the temperature range of torrefaction is thus very low. Hemicellulose and cellulose are the main constituents of biomass. By substantial removal of hemicellulose and cellulose from biomass by severe torrefaction, the weight and energy yield of biomass are usually lowered significantly although the energy density of the fuel is intensified to a great extent. A comparison among light, mild and severe torrefaction is given in Table 2.

In addition to temperature, torrefaction time or duration is another important factor in determining the performance of torrefaction. Torrefaction can be carried out between several minutes (PRINS et al., 2006; PENG et al., 2012) to several hours (WANNAPEERA et al.,

2011). Biomass particle size is another parameter that can affect the mass loss of torrefied product. This effect may not be important for very small particles but may be relevant for large sizes. The energy density of produced solid fuel is enhanced from torrefaction, and an increase in duration raises the carbon content and energy intensity.

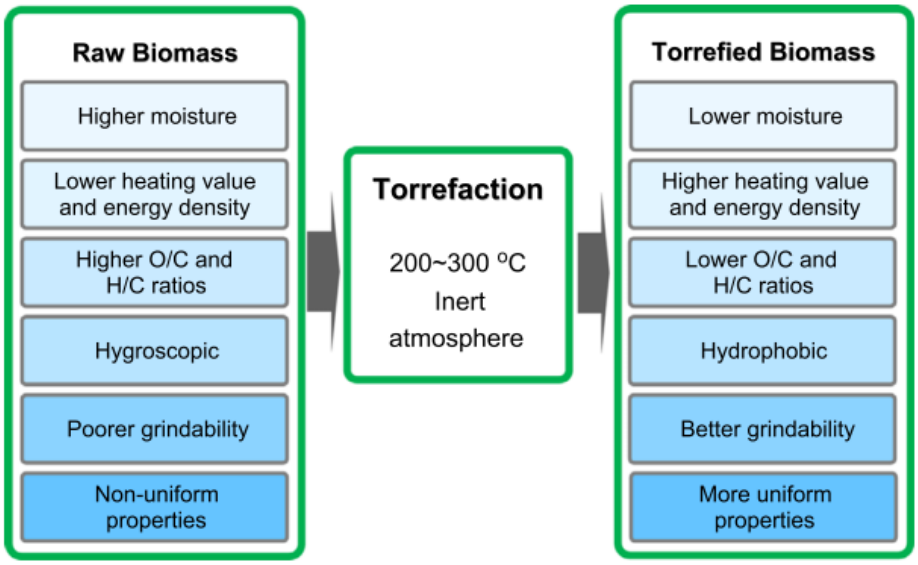

Figure 8. A schematic of property variation of biomass undergoing torrefaction (CHEN et al., 2015).

For example, in the study of Felfri et al., (FELFRI et al., 2005) when wood briquettes were torrefied at 250°C for 0.5, 1 and 1.5 h, the higher heating values of the biomass increased from 20.0 to 21.2, 22.1 and 22.7 $kJ.kg^{-1}$, respectively.

However, more energy for the thermal pretreatment is required if torrefaction duration is extended. From the TGA of biomass (CHEN et al., 2010) the thermal degradation of biomass is rapid at torrefaction time less than 1 h, and becomes very slow beyond 1 h. Therefore, torrefaction is normally controlled within 1 h (PENG et al., 2012; CHEW et al., 2011; CHEN et al., 2010). Overall, within the typical operating ranges of temperature and residence time, the influence of reaction temperature on the properties of biomass prevails over the residence time. Different combinations of temperature and residence time can be used to achieve a given degree of torrefaction, as represented by the weight loss (PENG et al., 2012). On the other hand, the key properties of the torrefied product, such as higher heating value and saturated moisture uptake, are primarily determined by the weight loss (PENG et al., 2013; LI et al., 2012).

Due to the dehydration process, moisture and volatiles are released. Torrefaction products presents a decrease of the volatile matter and increase of the amount of fixed carbon (CHEN, et al., 2015). Biomass loses more oxygen and hydrogen compared to carbon. In addition,

organic products reactions (acetic acid, furans, methanol) and gases (mainly CO_2 and CO) containing a considerable amount of oxygen can be mentioned.

Table 2. Torrefaction classification and torrefaction products (CHEN et al., 2015)

Classification	**Light**	**Mild**	**Severe**
Temperature (°C)	200–235	235–275	275–300
Consumption			
Hemicellulose	Mild	Mild to severe	Severe
Cellulose	Slight	Slight to mild	Mild to severe
Lignin	Slight	Slight	Slight
Liquid color	Brown	Brown dark	Black
Product			
Gas	H_2, CO, CO_2, CH_4, toluene, benzene and C_xH_y		
Liquid	H_2O, acetic acids, alcohols, aldehydes and ketones		
Solid	Char and ash		

Hydroxyl groups and lignin decomposition are considered the main reasons of torrefied biomass hydrophobicity increasing. Higher torrefaction temperatures has a favorable influence on hydrophobicity. Therefore, torrefaction process is a promising method for biomass pre-treatment, conferring a higher storage time without great losses of fuel quality.

Product density and volume are reduced due to the devolatilization. The shrinkage of the solid is due to water loss, chemical bonds rearrangement and graphite cores coalescence within the solid structure. Biomass passes through physical changes, increasing its fragile nature and reducing the polymeric fibers tenacity present in herbaceous and woody species biomasses, significantly reducing the energy required for wood grinding. (BRIDGEMAN et al., 2010).

Biomass product porosity increases, therefore, the torrefied product becomes more reactive during the combustion and gasification (PRINS et al., 2006a). According to Bergman (2005), a typical mass balance and energy balance of the thermal process is shown in Figure 9. Generally, 70% of the mass is maintained as a solid product containing 90% of the initial energy content and 30% of the biomass is converted into volatiles containing only 10% of the energy content of the biomass.

According to Prins et al., (2006a), the torrefied wood retains between 70% and 90% of the initial mass and decreases from 80% to 60-75% its volatile matter content and from 10% to 3% its moisture content. Ciolkosz and Wallace, (2011) reports that torrefaction process has an energy efficiency up to 80%. The efficiency of the thermal process can be increased by increasing the use of volatile and liquids as energy source, or by selecting processing conditions that maximize the biochar energy yield. Mass and energy balances shows the role

of the process final temperature: higher temperatures generate greater volatiles formation, therefore, larger mass losses (CIOLKOSZ and WALLACE, 2011).

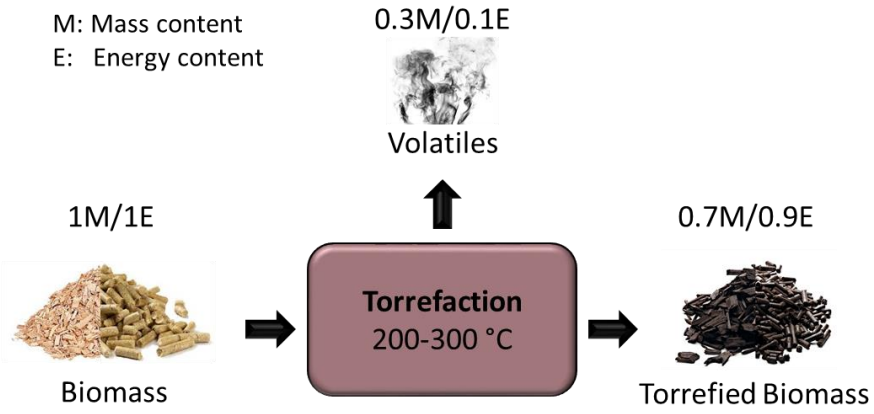

Figure 9. Mass/Energy balance of the roasting process (BERGMAN et al., 2005 - Modified).

2.2.4 Torrefaction technologies

As a promising bioenergy pre-treatment technology, torrefaction has the potential to make a major contribution to the thermal modification of biomass. (BATIDZIRAI et al., 2013) showed detailed insights into state of the art prospects of the commercial utilization of torrefaction technology over time identifying process performance characteristics such as thermal efficiency and mass yield and discussing their determining factors through analysis of mass and energy balances. The majority of the torrefaction technologies being developed are based on already existing reactor concepts designed for other purposes such as drying or pyrolysis (KIEL, 2011) and thus only require technical upgrading for torrefaction applications. The reactors being developed are in most cases established technologies that companies are familiar with and have been optimizing for torrefaction applications. Currently, no single technique is fundamentally superior to the others as all of them have their advantages and disadvantages (BATIDZIRAI et al., 2013). Proper selection of reactor is important as each reactor has unique characteristics and is well suited to handle specific types of biomass. Therefore, for given biomass properties and application, the proper technology can be selected. In recent years, many companies have invested in the development of roasting processes. The main technologies known to date and advantages and disadvantages of each technologies are presented in **Table 3.**

From the point of view of the product, the most important parameters are the efficiency of heat transfer and the quality of the mixture as they are essential for obtaining a homogeneous torrefied product. The energy source (electrical or thermal) and the ability to switch to industrial scale are also essential criteria for the selection of a technology. Among these

technologies, the most represented are mobile beds, multi-purpose furnaces and rotating kilns. Multiple solvent reactors have many advantages, including good control of temperature and residence time, as well as effective mixing, whereas moving beds and rotary kilns are already used on an industrial scale (COLIN, 2014).

Table 3. Torrefaction concepts reactor performance comparison under development (BATIDZIRAI et al., 2013).

Technology	Advantages	Disadvantages	Companies
Moving bed reactor	Simple and low cost High heat transfer High capacity No moving parts Wide range of biomass	High pressure drops Limited biomass size and type Temp. distribution is not uniform Unequal torrefaction Difficult temperature control Unproven scale-up	Buhler ECN Thermya
Torbed	Low residence time Fast heat transfer Scalable technology No moving parts Precisely control product	High utility fuel demand Vol. capacity limited Greater loss of volatiles Risk of tar formation	Topell Energy
Belt dryer	Better temperature control Wide range of biomass sizes Low investment costs Residence time good control Proven technology	Unequal torrefaction Limited upscaling potential Limited temperature control High maintenance costs	AgriTech producers 4EnergyInvesteAm New Earth EcoTech StramproyGreenInvelBiocoal
Rotary drum	Good process control Direct and indirect heating Uniform heat transfer Wide range of biomass Proven technology	Lower heat transfer Poor temperature control Increase of dust Limited upscaling ability High cost Large footprint	Torr-Coal, BIO3D Andritz, Stramproy Atmosclear, Earth,Care Prod., ETPC-Umea Torkapparater
Screw conveyer	Low cost Wide range of biomass Proven technology Better biomass flow	Unequal torrefaction Poor heat exchange Limited scaling potential	BioLake BTG Foxcoal
Multiple hearth furnace	Good heat transfer Good temp. control Wide range of biomass Scalable technology	Large footprint Process less sustainable	CMI-NESSA Integro

Fluidized bed	Good heat transfer Scalable technology	Selective particle size Slow temperature response Loss of fines Bed solids and biomass separation	River Basin Energy Alterna Ecotech/Sea2Sky Torrproc,Energex
Microwave	Radiation heat transfer High heat transfer Large size biomass Good temp. control Modular	Unproven technology Electric energy needed Heating is not uniform Requires integration with other conventional heaters	CanBiocoal Rotawave

2.2.5 Chemistry and kinetics

Biomass pyrolysis chemistry is complex due to the wide variety of chemical species generated, variabilities in feedstock characteristics, and the wide range of temperature, pressure, and heating rate conditions which must be considered. Moreover, it is technically difficult to separate the effects of secondary reactions and the catalyzing effects of mineral components. Chemistry research received a strong push after the oil embargo of the late 1970's and many seminal papers were published in the early 1980's. Similar economic motivations combined with recent technical advancements in instrumentation have caused a resurgence of this field.

Experimental methods for pyrolysis and torrefaction chemistry and kinetics are studied with a variety of experimental devices and some commonly used techniques include are TGA, DTG, Fourier transform infrared spectroscopy (FTIR), high performance liquid chromatography (HPLC), gas chromatography (GC), and bomb calorimetry. For a more comprehensive review on experimental analysis see (BAHNG et al., 2009). TGA analysis allows precise measurement of mass loss under controlled temperature profiles and is therefore used to validate and measure kinetic models and parameters. DTG shows the rate at which products are formed, and can be used to compare the pyrolysis and combustion profiles of raw and torrefied feedstocks (BRIDGEMAN et al., 2010). FTIR allows the real-time analysis of volatiles released during pyrolysis and torrefaction (CHEN et al, 2012a) (LV et al,, 2015). HPLC and GC can be used in tandem with TGA during batch experiments to perform mass balance and volatile composition analysis.

Based on the chemical formulas of the three constituents, the atomic O/C ratios in cellulose, hemicellulose and lignin are found to be 0.83, 0.80 and 0.47-0.36, respectively, and their atomic H/C ratios are 1.67, 1.6 and 1.19-1.53, respectively. In view of their distinct compositions and structures, cellulose, hemicellulose and lignin possess different thermal

decomposition characteristics. Generally speaking, the thermal decomposition temperature (TDT) of hemicellulose is the lowest among the three constituents at the range of 220 and 315°C. Cellulose decomposes at temperatures between 315 and 400°C. Lignin is featured by gradual decomposition for the temperature ranging from 160 to 900°C (LU et al., 2012) Figure 10a and b show the typical thermogravimetric (TGA) and derivative thermo-gravimetric (DTG) curves of the standard samples of cellulose (Alfa Aesar, A17730), hemicellulose (SIGMA, X-4252), lignin (Tokyo Chemical Industrial Co., L0045), xylose (SIGMA, X-1500) and glucose (Panreac Quimica SA, 131341). In some biomass samples, the decomposition peaks of cellulose and hemicellulose from DTG can be identified clearly (CHEN et al., 2010). Whereas the two peaks overlap in some biomass samples so that it is hard to be distinguished. (CHEN et al., 2015).

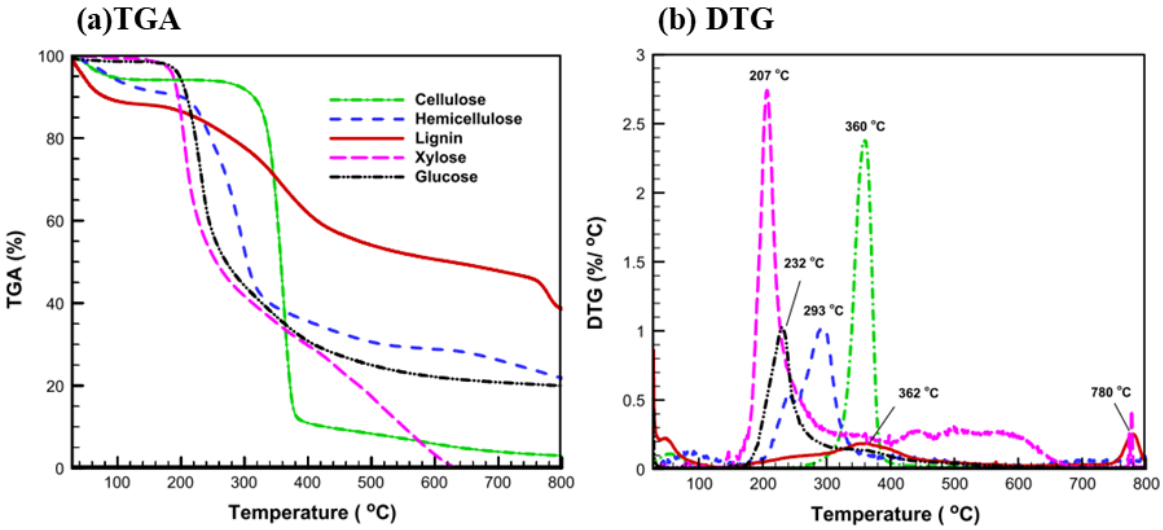

Figure 10. (a) Thermogravimetric analyses (TGA) and (b) derivative thermogravimetric (DTG) analyses of the standards of cellulose, hemicellulose, and lignin. (CHEN et al., 2015).

2.2.5.1 Hemicelluloses degradation

Hemicelluloses are branched polysaccharides composed of 5-carbon sugars such as xylan (the majority in hardwoods), and 6-carbohydrates, such as glucose and mannose (the majority in conifers) (TRIBOULOT et al., 2001) that plays a primordial role in the cell wall cohesion. Indeed, it allows the bonding between the cellulose fibers and lignin. Hemicellulose chains are amorphous and contain many hydroxyl groups which make it the most hydrophilic biomass compound. It is therefore considered to be the main responsible for the affinity of wood with water (COLIN, 2014).

Hemicelluloses are the most highly degraded polymers at torrefaction temperatures (NOCQUET et al., 2014; CHEN et al., 2011b). The main reactions involved in hemicelluloses

torrefaction are dihydroxylation, deacetylation and depolymerization (WEILAND and GUYONNET, 2003) . Under the most severe treatment conditions, almost all hemicellulose is degraded (CHEN et al., 2012). Finally, xylan is more sensitive to temperature than glucomannans, so deciduous trees have a greater loss of mass than conifers under identical treatment conditions (PRINS et al., 2006).

2.2.5.2 Cellulose degradation

Cellulose is the major biomass component. Cellulose chain is formed from 5,000 to 10,000 units of glucose (ROUSSET, 2004). These chains are assembled in the form of microfibrils which themselves form fibrils. It should be noted that some portions of the microfibrils are disordered (amorphous cellulose) while others are ordered (crystalline cellulose). It is possible to define a crystallinity index (crystalline cellulose / total cellulose ratio) which is generally between 0.6 and 0.7 for raw wood (TRIBOULOT et al., 2001).

Cellulose thermal degradation has been the subject of several studies TRIBOULOT et al., 2001; NOCQUET et al., 2014; CHEN et al., 2011b). It appears that cellulose has significant mass losses for temperatures above 250°C (NOCQUET et al., 2014; CHEN et al., 2011b). After product solid and the volatiles released analysis, it has been shown that at these temperatures the main degradation mechanism is dehydroxylation (SARVARAMINI et al., 2013). The loss of -OH groups would thus lead to the formation of a less hydrophilic cellulose containing unsaturated pyranoses. The molecules produced by these reactions are mainly water molecules, but also levoglucosan, CO and CO_2 at the highest temperatures (280-300°C).

Another trend often observed is the increase in the cellulose crystallinity index at low temperatures (120-180°C) (AKGÜL et al., 2006). This increase is mainly due to the preferential degradation of amorphous cellulose, which increases the proportion of crystalline cellulose (WIKBERG, 2004). However, other authors explain this evolution by a change in molecular organization that would transform amorphous cellulose into crystalline cellulose (MELKIOR et al., 2012; SINGH et al., 2013). It is therefore not impossible that these two phenomena occur simultaneously to lead to an increase in the crystallinity index. This increase has a direct impact on the properties of torrefied wood because the cellulose crystalline configuration limits the water penetration into the fibers, which makes the material less hygroscopic (TRIBOULOT et al., 2001; SINGH et al., 2013). However, it has been observed that for the treatments at the highest temperatures, the crystalline cellulose is degraded in turn, which can promote the return of water (HILL et al., 2013).

2.2.5.3 Lignin degradation

Lignin are amorphous compounds that rigidify the cell wall and allow cohesion between the different cells. These alcohols form polymers (mainly hydroxyphenyl, gaiacyl and syringyl units) which themselves form lignin whose composition differs according to the biomass considered. Lignin torrefaction studies have shown that degradation starts at lower temperatures than cellulose (about 150°C) (SARVARAMINI et al., 2013). However, mass loss is limited (less than 15wt%) for temperatures below 250°C (NOCQUET et al., 2014).

Indeed, if certain volatile materials are released (mainly water, CO, CO_2 and formaldehyde), in particular as a result of demethoxylation reactions, the main reactions occurring in the treatments temperature ranges are reactions of condensation (WINDEISEN et al., 2007; ROUSSET et al., 2009). These lead to the formation of crosslinked compounds derived from lignin. Depolymerization reactions are then carried out at temperatures above 250°C, whereas degradation of the monomers produced would only occur from 300°C (MELKIOR et al., 2012).

2.2.5.4 Volatile Materials

Produced volatile matter consists of condensable gases and permanent gases (non-condensable). The relative proportions of these two types of compounds depend on the biomass, the duration and treatment temperature (PRINS et al., 2006b). However, the condensable gases mass yield (ratio of the produced condensable mass to dry biomass initial mass) is always higher than non-condensable gases.

Condensable gases are mainly composed of water, acetic acid, formic acid, methanol, lactic acid and furfural. Water and acetic acid (markers of hemicelluloses degradation) are largely in the majority regardless of the treatment conditions (PRINS et al., 2006b; BATES and GHONIEM, 2012). The production of carbon monoxide seems to be favored by the high temperatures. Heavy condensable species (mainly aromatic compounds which can be subjected to material recovery), present in small quantities, have also been identified (CHEN et al., 2011b). Finally, recently, Nocquet et al., (2014) highlighted the importance of formaldehyde production as the second condensed species produced after water, as shown in Figure 11.

The incondensable gases commonly observed are CO_2 and CO, being CO_2 the majority Perhaps, CO/CO_2 ratio increases with the roasting temperature (PRINS et al., 2006b). Small amounts of CH_4 are also observed at higher processing temperatures, particularly when roasting agricultural residues (DENG et al., 2009).

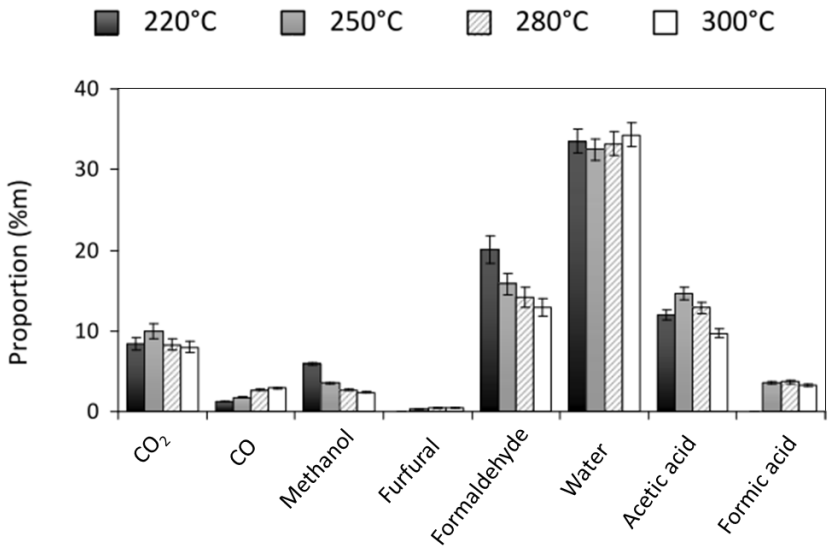

Figure 11. Volatile species yield after torrefaction of beech for 3 hours at different temperatures (NOCQUET, 2012).

2.2.5.5 Interaction between different biomass constituents

As previously discussed, the individual behavior of biomass main components subjected to torrefaction has been widely studied. However, their common evolution within the material remains little known. Indeed, there is still considerable uncertainty about the synergetic effect of cellulose, hemicelluloses and lignin degradation, but also on the role of ash in raw biomass.

Despite the lack of data on these phenomena, certain hypotheses have been put forward:

- Acetic acid released during the degradation of hemicelluloses acts as a catalyst for depolymerization of cellulose (WIKBERG et al., 2004; WINDEISEN et al., 2007) or even lignin (MELKIOR et al., 2012);
- Radical compounds formed by hemicelluloses degradation could react with the phenolic compounds of lignin (ROUSSET et al., 2009).
- Alkali metals (mainly potassium) in the ash would act as catalysts for roasting (SALEH et al., 2013; SALEH et al., 2013b; SADDAWI et al., 2012).

These hypotheses lead us to believe that the behavior of biomass can not be assimilated to the sum of the behaviors of its constituents (NOCQUET et al., 2014). They have compared the change in the mass yield of beech during torrefaction with the predicted evolution by additivity of the behavior of its various constituents: for temperatures above 250°C, the additivity law does not work. Moreover, the observation of the loss of mass of mixtures of the various pure components made it possible to demonstrate that the main interactions concern the cellulose-lignin and cellulose-hemicellulose mixtures (COLIN, 2014).

It therefore seems difficult to predict the thermal behavior of a biomass based solely on its cellulose-hemicellulose-lignin composition. Therefore, many studies have endeavored to describe biomass decomposition by kinetic models (COLIN, 2014).

2.3 Biomass thermal decomposition numerical models

2.3.1 Kinetic Model

Pyrolysis kinetics has been well studied and documented. Several review papers have been published on biomass pyrolysis reaction mechanisms and kinetic models subjects (ROUSSET, 2006; CHEW et al., 2011; VAN DER STELT et al., 2011). Since torrefaction is often considered as pyrolysis at low temperature, the pyrolysis models have recently been adapted to torrefaction case with the purpose to represent the mass loss curves.

Often, researchers tackle the complexity of biomass by first understanding the pyrolysis of pure lignocellulose components. They then use this knowledge to inform and provide a theoretical and/or empirical basis for the proposal of a kinetic model. The complexity, flexibility, and input/output model's requirements are dependent on variety of factors.

Several authors have attempted to develop biomass pyrolysis models based on a linear superposition of pure components decomposition (BIAGINI et al., 2006; COUHERT et al., 2009). Such a model has the advantages of flexibility and ease of application. Unfortunately, reasonable agreement between model and experiments results is possible only when mineral content is ignored. Moreover, these models are designed to reflect the experimental results of pyrolysis over a wide range of temperatures 100-1000°C and therefore their applicability to torrefaction treatment between 200-300°C for an extended period (15-60 minutes) would be inaccurate.

The difficulties encountered in numerical model's establishment are due to the need to find a scheme and kinetic parameters to accurately represent the mass loss evolution (or yield) over time whatever the treatment temperature.

In the literature, lots of studies proposed kinetic models to represent wood degradation during heat treatment. These models, usually applied to TGA (thermogravimetric analysis) measurements to simulate the intrinsic decomposition of biomass, can be sorted in three major sections: the detailed models, pseudo-components models and original models.

The most used detailed model was initially proposed by (RANZI et al., 2008) and further developed by (BLONDEAU et al., 2012; GAUTHIER et al., 2013; ANCA-COUCE et al., 2014). This model considers separately the decomposition of the three wood components and predicts the produced volatile matters. Its use requires determining the biomass in terms of

cellulose, hemicellulose and lignin. It is the only model based on the chemical reactions description occurring during treatment and is one of the only models that allow simultaneously solid mass loss and produced volatile composition prediction during pyrolysis. In the original model (RANZI et al., 2008) as well as in the model adapted by Gauthier et al. (2013), several hundreds of gas phase side reactions are taken into account.

In the model adapted by Blondeau and Jeanmart (2012), only intra-particular secondary reactions are considered. Anca-Couce et al. (2014) have applied this model to torrefaction by neglecting the gas phase reactions which are very limited at low temperature. They also showed that some modifications of this model were necessary to correctly predict the volatiles produced. Their final schema consists of 13 reactions whose velocity constants follow the Arrhenius law. The numerical results are compared with beech wood torrefaction experimental results at 250 and 285°C. The mass yield is overestimated by 3 and 6% for these two temperatures. Compared to the original model, a real improvement is observed on the prediction of main volatile materials production. However, this model is complex and hard to extend to various wood species or heat treatment conditions.

(WANG et al., 2016) developed a model-fitting method combining isoconversional method and Distributed Activation Energy Model (DAEM) method to determine the comprehensive kinetic models for pyrolysis of biomass components. The correlation between activation energy and conversion rate indicated that pyrolysis of hemicellulose and lignin are very complex and contained parallel reactions and successive reactions. The model proposed that the whole pyrolysis process of cellulose followed the *Avrami-Erofeev* nucleation reaction model, while the reaction-order model was more suitable for pyrolysis of hemicellulose and lignin. The model demands a series of experimental parameters and is complex to extend to another study.

Pseudo-components models are the most used in literature due to their simplicity and the quality of obtained results. The described models are shown in **Table 4**. For all models, A represents the raw biomass, B, C and D represent roasted solids and V represents the volatiles. The kinetic constants K is governed the Arrhenius law. Global mass loss can be represent based on a one-step reaction model (1), on several reactions in parallel schemes (2) and (3) or on two-step in series scheme (4) and (5).

REPELLIN et al., (2010) applied model (1) to adequately represent beech and spruce mass loss during torrefaction. However, because of its construction, this model always predicts the same distribution between biochar and volatile matter. It is therefore not possible to predict the solid yield evolution when the torrefaction temperature varies, which makes its use limited.

On several reactions in parallel schemes (CAVAGNOL et al., 2013) compared Model (2) with models (4) and (5) in a separated wood compounds degradation study for softwood and hardwood species. The one-stage model (2) does not correctly predict the solid mass loss. This is probably because considering only one step, the reactions slowing down over time (observed experimentally) can't be represented.

Table 4. The most used pseudo components kinetic models for torrefaction numerical analysis.

Model	Reactions	Studies
One Step Model	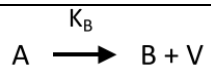	REPELLIN et al., 2010
Two parallel reaction one step	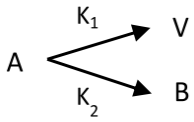	CAVAGNOL et al., 2013
Three parallel reaction one step	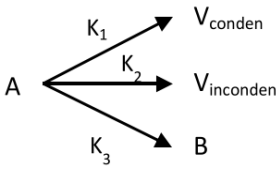	RATTE et al., 2009 RATTE et al., 2011
Two parallel reaction two steps	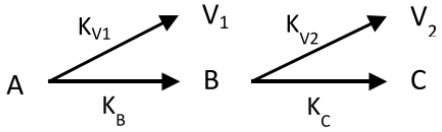	DI BLASI et al., 1997 BATES et al., 2012; JOSHI et al., 2014 PEDUZZI et al., 2014; COLIN, 2014 BACH et al., 2016;
Two parallel reaction three steps	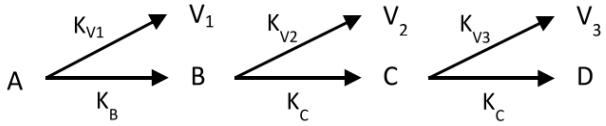	CAVAGNOL et al., 2013

Model (3), also called the Shafizadeh and Chin model, has the advantage of predicting product evolution in the three phases (solid, liquid and gas). This model was used in wood particles torrefaction numerical analysis (RATTE et al., 2009) and was subsequently integrated into a continuous torrefaction pilot device (RATTE et al., 2011). On a two-step in series scheme (DI BLASI and LANZETTA, 1997; PRINS et al., 2006a; BATES et al., 2012; JOSHI et al., 2014; PEDUZZI et al., 2014; COLIN, 2014; PARK et al., 2015; BACH et al., 2016) the two-stage model (4) correctly describes the mass loss curves during torrefaction. Whereas, on several steps in series schemes, model (5) provides only a small improvement compared to the complexity involved in taking into account one more reaction step (CAVAGNOL et al., 2013)

These observations are consistent with other published kinetics torrefaction studies. Indeed, model (4), also called the model of Di Blasi and Lanzetta, is the most commonly used model (PRINS et al., 2006a; BATES et al., 2012; BACH et al., 2016; COLIN, 2014). It was initially developed to describe the degradation of xylan during isothermal pyrolysis, what may explain its good adaptation to torrefaction case. It also has the advantage of being simple to implement. However, it should be noted that this model remains difficult to interpret physically being a numerical approach. In particular, it was noted that the representation of torrefied wood and the volatile matter production by separate reactions is erroneous (REPELLIN et al., 2010).

Finally, some original pyrolysis model are proposed in literature by (ROUSSET, 2006; REPELLIN et al., 2010; BASU et al., 2014). Rousset, 2006 developed a pyrolysis model taking in to account the degradation for each wood component as illustrated in Figure 12.

The model was developed based in *TransPore* drying model (PERRÉ et al., 1990). The studied coupled a "Reactions module" which allows to integrate the chemical reactions and their enthalpies during wood thermal treatment and a "Boundary conditions module " which allows the actual reactor conditions to be injected directly into the calculation engine.

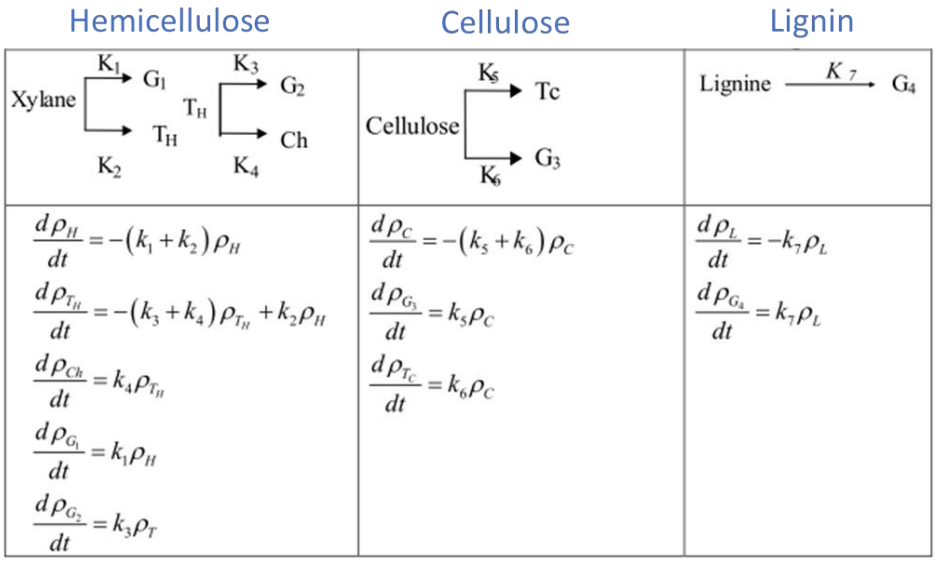

Figure 12. Pyrolysis model reaction mechanisms. (Rousset, 2006).

Repellin et al., (2010) based on Rousset (2006) study, developed a separately model wood components torrefaction according to the scheme presented in Figure 13. It is clear that this model is based on a superimposition of the simple models presented in Table 4. Although it is based on strong assumptions such as the absence of interactions between the various wood compounds, the study concludes that it is a good fit between numerical results and experimental values.

Based on Di Blasi and Lanzetta, 1997 model, (NOCQUET, 2012) propose to model the evolution of volatile matter composition over time considering that these two types of volatile matter have the same composition and degradation of the different wood compounds in biomass is modeled separately. The originality of the model lies in the consideration of a fourth compound, representing biomass acetyl groups, which makes it possible to model acetic acid production. The model is therefore difficult to extrapolate to other biomasses and other operating conditions.

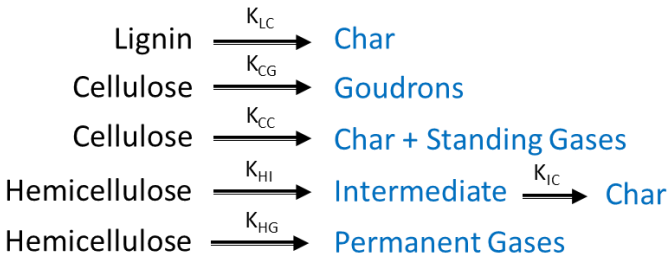

Figure 13. Kinetic model proposed by (REPELLIN et al., 2010).

In (BASU et al., 2014) model, biomass is first degraded by two parallel reactions, one leading to primary char production and the other to volatile materials production. A part of these volatile materials, rich in heavy hydrocarbons, are then redeposited on primary char surface. This re-deposition is considered by means of a coefficient δ which depends mainly on the size of the particles: the larger the particle size, the more limiting the transfer of matter and the more the volatiles recover. These re-deposited materials then react by cracking (to form new light volatiles) and by re-polymerization (to form a secondary coal). This model therefore considers other phenomena such as re-condensation and mass transfer, which is not the case in previous models which are models of intrinsic kinetics.

2.3.2 Composition Model

Very few models proposed in the literature for the process modelling of torrefaction consider the solid and gaseous yields, and their composition. Models used in techno-economic evaluations are generally relative to a single operating point (in terms of biomass composition, AWL (anhydric weight loss), and temperature) and therefore are represented by a single equation. The models based on empirical correlations, obtained under specific experimental conditions, do not describe the composition of the torrefied solid and evolution of the torrefaction gases during torrefaction. To address this need, several regression analysis and review studies (ALMEIDA et al., 2010; MEDIC et al., 2012; TUMULURU et al., 2010) have

been performed to predict the yield, heating value, energy yield, and composition of biochar. However, these empirical regressions models were based on only a few experimental points, thus their reliability and accuracy in further industrial applications might be limited. In addition, the studies provided no information about the torrefaction kinetics (e.g. activation energy) and the distribution of the products during the torrefaction process (e.g. how intermediate product is formed and degraded).

Based on (DI BLASI and LANZETTA, 1997) mechanism, Bates and Ghoniem (BATES et al., 2012) developed a method to estimate biochar elemental composition (e.g. C, H, N, and O contents) indirectly through released volatiles, which consist of 9 different species, detected by a gas chromatograph (GC) and a high-performance liquid chromatograph (HPLC). The model was calibrated with the volatiles produced by torrefaction of willow and experimentally measured employing thermogravimetric analysis technique by (PRINS et al., 2006a; PRINS et al., 2006b). This indirect method is interesting, but it requires well capturing and precisely analyzing all the volatiles, from which any leakage can lead to an inappropriate prediction of biochar composition. These models are generally independent from the torrefaction process design, as they do not consider the reactor technology, and heat and mass transfer mechanisms at the reactor scale.

(PEDUZZI et al., 2014) used experimental data from the literature and from previous studies carried out at CEA Grenoble to understand change in composition of the torrefied solid as a function of the anhydric weight loss. The developed numerical model is based on the torrefaction experiments carried out by (NOCQUET, 2012; NOCQUET et al., 2014a; NOCQUET et al., 2014b). The model simplifying assumption is that torrefied biomass composition depends only on the AWL, and therefore only indirectly on temperature and reaction time.

Norway spruce and birch branches at different torrefaction conditions have been studied using a thermogravimetric analyzer by (BACH et al., 2016). The study showed a direct method to predict the biochar elemental composition presenting good agreements with the literature with regards to increased carbon content and reduced hydrogen and oxygen contents during torrefaction. The model formulation is therefore incomplete, and the numerical solution is not presented in detail, being difficulty to understand some factors during calculation. To address the issues, it is necessary to develop a direct model to provide a simple and accurate numerical prediction, which is one of the objectives of this research.

2.4 Acoustics

Thermo-acoustic is responsible for some phenomena as combustion instabilities within experimental Rijke tube device (SANTOS et al., 2016; CINTRA, et al., 2016; MATVEEV et al., 2003) and thermo-acoustic heat engines (GUÉDRA et al., 2015). Some authors have shown relationships between thermal transfers and acoustic waves. (KOMAROV et al., 2003) discussed the possibility for enhancement of heat transfer between solids and ambient gas by application of powerful acoustic field. Results showed that the heat transfer rate between a preheated wire and ambient gas can be enhanced under the application of sound waves. The heat transfer coefficient increases with the sound strength in both standing and travelling sound waves. In (BENNETT et al., 2009) the interaction between a standing wave acoustic field in a duct and a heated section was experimentally examined to enhance the convective heat transfer.

New technologies coupled to thermal modification torrefaction reactors as vacuum atmosphere (CARRIER et al., 2012; GARCÌA-PÉREZ et al., 2007), microwaves (HUANG et al., 2016, 2017) and wet-torrefaction (BACH; SKREIBERG, 2016; BACH; TRAN; SKREIBERG, 2017) has been explored to improve the thermal pre-treatment. Some studies with ultrasound for biomass pre-treatment explore sonochemical and mechanoacoustic effects. The mechanoacoustic effect alters the surface structure of the biomass while sonochemical production of oxidizing radicals leads to chemical attack of the components of lignocellulose (BHUTTO et al., 2017).However, no work was found where torrefaction was combined with an acoustic field under pyrolysis or oxidative conditions. The assumption is that an acoustic field in a torrefaction reactor modifies the pressure and flux velocity field around the wood sample. The combined effect of heat and acoustics could modify the interaction between reactor gaseous environment and wood sample, modifying degradation processes development.

In this study, two experimental techniques to identify which acoustic frequency produces the ideal condition to a maximum acoustic flux around the sample were applied. Knowing the density of the fluid, optimum condition can be determined with identification and analysis of the shift phase between the two microphones. Due to the relationship between fluid particle velocity and acoustic pressure the pressure gradient is higher when the acoustic pressure signals are in opposition of phase. (FAHY, 1995).

2.4.1 Frequency domain

Determination of phase shift between two microphones was subject of some studies. (SAS, 2000) applied an approach called transfer function method which consists basically on

exposing two microphones to the same acoustic field to measure directly the phase shift between them. However, this method relies on a perfectly behavior of the microphones and do not compensate for different environmental conditions and non-linearities. In (CHUNG, 1978) it is shown a technique which in principle eliminates the phase mismatch when calculating the active intensity based on the finite difference method by taking the geometric average of the Cross Spectral Density between the microphones. (ROSSETO, 2001) applied (CHUNG, 1978) technique to correct (SAS, 2000) approach allowing an experimental identification of the phase shift between microphones 1 and 2.

2.4.2 Time domain

2.4.2.1 Lissajous Figures

Lissajous figures were discovered by the French physicist Jules Antoine Lissajous. Lissajous figures also called Bowditch curve pattern produced by the intersection of two sinusoidal curves the axes of which are at right angles to each other. First studied by the American mathematician Nathaniel Bowditch in 1815, the curves were investigated independently by the French mathematician Jules Antoine Lissajous in 1857–58. Lissajous used a narrow stream of sand pouring from the base of a compound pendulum to produce the curves (CUNDY and ROLLETT, 1989; GRAY, 1997).

When using an oscilloscope, it is possible to plot one sinusoidal signal along the x-axis against another sinusoidal signal along the y-axis, the result is a Lissajous figure. The oscilloscope displays a two-dimensional representation of one or more potential differences. The plot is normally of voltage on the y-axis against time on the x- axis, making the oscilloscope useful for displaying periodic signals (LAWRENCE, 1972).

For sine waves, this produces a Lissajous Figure from which it is possible to tell the phase difference between the two signals (AL-KHAZALI et al., 2012). In this study, the two analyzed signals are two microphone acoustic signals $p(\vec{x}_1, t)$ and $p(\vec{x}_2, t)$ assumed as harmonic functions (with excitation frequency $f = \omega/2\pi$ in Hz).

2.4.2.2 Hilbert transform

A quantitative measure of shift phase between microphones can be obtained applying a Hilbert Transform to the two analyzed signals are two microphone acoustic signals $p(\vec{x}_1, t)$ and $p(\vec{x}_2, t)$ (FELDMAN, 1994a; FELDMAN, 1994b). These methodologies were applied to a *Labview virtual instruments* development to obtain quantitative results for acoustic analyses.

3. CASE OF STUDY

Section 3.1 presents the thermo-acoustic torrefaction lab-scale reactor conception for the present study. In section 3.2 the mathematical formulation and acoustic characterization techniques utilized for the acoustics experimental procedure are exposed. Section 3.3 starts presenting the properties of the utilized biomass. The applied methodology for the torrefaction under temperature and coupled frequency/temperature effect are presented next. The section is closed presenting how the finals product was assessed. The mathematic formulation for the numerical model contemplating the kinetics and composition are presented in section 3.4.

3.1 Thermo-acoustic torrefaction lab-scale reactor conception

The motivation for this section arises from the potential coupling of an acoustic system to a torrefaction reactor to improve the wood heat treatment.

In torrefaction analysis references no work was found coupling torrefaction with an acoustic field over pyrolysis or oxidative conditions. The assumption is that an acoustic field within a torrefaction reactor modifies the pressure and particles velocities around the wood sample. The combined effect of heat and acoustics could modify the interaction between reactor gaseous environment and wood sample, modifying degradation processes development (SILVEIRA et al., 2017).

To that end, an acoustic system was applied inside an existing torrefaction reactor (ROUSSET et al., 2012) and subsequently characterized. Three different methodologies were used in terms of time and frequency domains. This characterization allowed the measurement of the flow rate and acoustic intensity at the exact spot where the sample was in the reactor. These acoustic results were analyzed and used to predict which acoustic frequency and intensity produced the ideal conditions for obtaining higher particles velocities around the wood sample. The acoustic system coupled to the existing torrefaction reactor (ROUSSET et al., 2012) is illustrated Figure 14.

The acoustic experiment was performed with a humidity of 50%, an average temperature of 24°C, speed of sound c =345 m.s^{-1} and an air density of ρ=1.23 kg.m^{-3}. Within the experimental acoustic system, the desired frequencies were produced by an *HP 33120A* wave generator with a broadband frequency of 20Hz - 20 kHz. The acoustic wave was delivered by a Selenium *D220TI 8* speaker connected by a flexible duct (ROSSETO, 2001) to the reactor cavity measuring 41×32×40 cm. Different acoustic frequencies produce different excitations of the reactor's cavity, hence a different pressure field. Frequencies were explored within a range of 0-3000Hz.

The acoustic signals were measured and processed by two *Brüel & Kjær 194537* microphones connected to a *Brüel & Kjær NEXUS* amplifier. Data acquisition was performed by a National Instruments CompactDAQ NI9174-NI9234 interfaced by a Labview device.

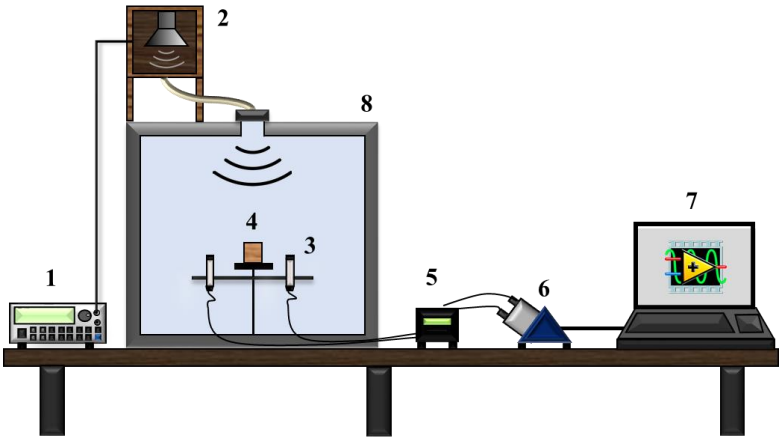

Figure 14. General scheme of experimental torrefaction acoustic system. 1) HP 33120A Signal Generator, 2) Selenium D220TI 8 Speaker, 3) Brüel & Kjaer Microphones, 4) Wood sample, 5) Nexus Brüel & Kjaer conditioner, 6) CompactDAQ NI9174 e NI9234, 7) Computer (Labview Software), 8) Reactor.

3.2 Acoustic characterization techniques

For the acoustics experimental procedure, two different microphones set ups were necessary. For the first analyze, in frequency domain, one microphone to measure the source signal was fixed in the end of the tube that connects the speaker and the reactor. The other microphone was placed inside the cavity, at the exact place of the biomass sample. The source signal was a logarithmic sweep sine with a broadband of 100-3000Hz and 2.5 Vpp of magnification. Two signal filters were used: (a) low-pass filter set to 100Hz, and (b) high-pass filter set to 2000Hz to assure that the acoustic experimental broadband covers the source band. With that set-up was possible to explore the calibrated source technique and performed a modal analysis of the reactor cavity (MELO, 2013; ROSSETO, 2001). It was observed that this technique has a limitation when higher frequencies are explored because of the modal density exponential comportment (GERGES, 2005; KINSLER et al., 1982) as illustrated in Figure 15.

Due to this limitation, two other techniques, in time domain (Lissajous curves/Hilbert transform) and the frequency domain (Cross spectrum density) were applied to improve the characterization and measurement of the phase shift in a higher frequencies range.

For the second analyze, two microphones were placed side-by-side and face-to-face on both side of the wood sample. This configuration is illustrated in Figure 16 and allowed to identify which frequency produce the desired shift phase between the two measured signals. The

microphones were disposed on that configuration set up for the three spatial axes (x, y and z) due to the vectoral characteristics of acoustic flow.

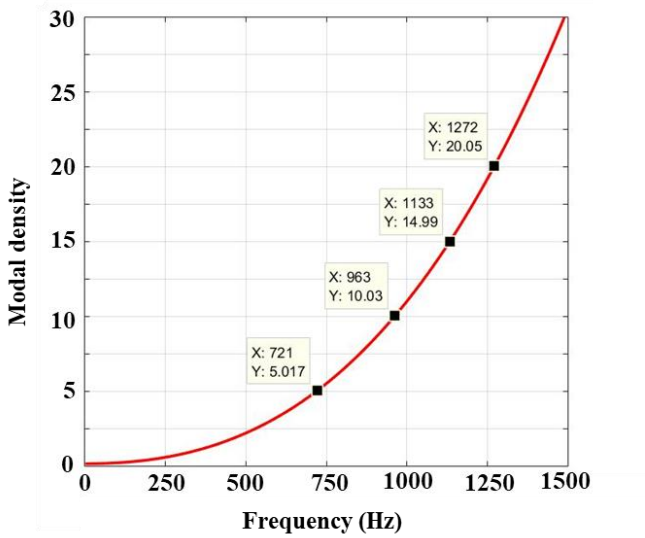

Figure 15. Modal density for explored frequencies.

Distance between microphones depends of the applied acoustic frequency (wave length) and air velocity. That configuration allowed to perform the Lissajous/Hilbert technique analyze in time domain and a cross spectrum analyses in frequency domain.

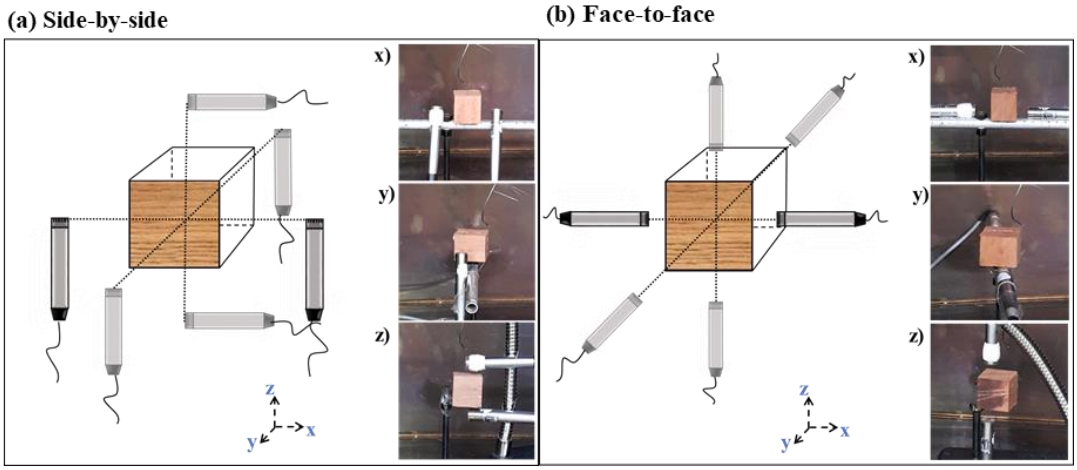

Figure 16. Experimental configuration for time (Lissajous/Hilbert) and frequency (Cross Spectrum) domain acoustic characterization.

3.2.1 Acoustic velocity/pressure formulation

The acoustic velocity vector $\vec{v}(\vec{x})$ was experimentally determined processing the acoustic pressure signal measured by the microphones. Using Euler equation adapted to acoustic processes of small amplitude, the linear inviscid force equation is described as:

$$\frac{\partial \vec{v}}{\partial t} = -\frac{1}{\rho}\nabla p \qquad (1)$$

where, $\vec{v}$ is the acoustic velocity vector field, p the acoustic pressure, and ρ the air density. Supposing the acoustic pressure p and acoustic velocity $\vec{v}$ described as a time harmonic wave:

$$p(\vec{x},t) = P(\vec{x}) \cdot exp(j\omega t) \tag{2}$$

$$\vec{v}(\vec{x},t) = \vec{V}(\vec{x}) \cdot exp(j\omega t + \Phi) \tag{3}$$

where $P(\vec{x})$ and $\vec{V}(\vec{x})$ are the pressure and velocity magnitude of a frequency ω, and phase angle Φ. Then, as function of frequency ω, the unidimensional linear inviscid force (Eq. 1) took the following form:

$$\vec{V}(\vec{x}) = \frac{j}{\rho\omega}\frac{\partial}{\partial x}P(x) \simeq \frac{j}{\rho\omega}\frac{P(x+\Delta x)-P(x-\Delta x)}{2\Delta x} = \frac{j}{\rho\omega}\frac{P(x_1)-P(x_2)}{2\Delta x} \tag{4}$$

where, $\Delta x = (\vec{x}_2 - \vec{x}_1)/2$ is the distance between the two microphones in space. The approximative determination of acoustic velocity field $\vec{V}(\vec{x})$ was made possible by this finite differential approach. The particle velocities for each frequency was obtained from the deviation of the acoustic pressure field $p(\vec{x})$ (FAHY, 1995). A similar technique is used to determine the acoustic intensity for each analyzed frequency (GERGES, 2005; FAHY, 1995).

In the following section, the techniques used to determine the particle velocity around the wood sample are presented. Firstly, the frequency-domain technique (Cross-Spectral Power Density Function), followed by the time-domain techniques (Lissajous curves/Hilbert Transform).

3.2.2 Frequency-domain

The cross-spectral density function $\hat{S}_{xy}$ was applied to determine the phase shift between the two measured acoustic signals in the frequency domain by the argument Eq. 5:

$$\hat{S}_{xy}(f) = \int_T^T R_{xy}(\tau)\mathrm{e}^{-j\,2\pi f}\,\mathrm{d}f = \left|\hat{S}_{xy}\right| \exp\left(-j\,\phi_{xy}\right) \tag{5}$$

where the cross-correlation function $R_{xy}(\tau)$ and phase shift ϕ_{xy} between signals $x(t)$ and $y(t)$ is given by Eq. 6 and Eq. 7 respectively.

$$R_{xy}(\tau) = \lim_{T\to\infty}\frac{1}{T}\int_{T/2}^{T/2} p(x,t)\; p(y,t+\tau)dt \tag{6}$$

$$\phi_{xy} = \arg \hat{S}_{xy} \tag{7}$$

Phase shift estimation by cross-spectral density function $\left(\arg \hat{S}_{xy}\right)$ is dominated by 'uncontrollable' influence of coherence spectrum $\gamma_{xy}^2(f)$ (SHIN and HAMMOND, 2008; JENKINS and WATTS, 1968). The variance of the phase shift is:

$$Var\left(\arg \hat{S}_{xy}(f)\right) \approx \frac{1-\gamma_{xy}^2(f)}{\gamma_{xy}^2} \cdot \frac{1}{2BT} \tag{8}$$

where, B and T are respectively bandwidth resolution and data length. The coherence function $\gamma_{xy}^2(f)$ is given by Eq. 9 and measures the degree of linear association with the two signals respective the interval $0 \leq \gamma_{xy}^2(f) \leq 1$.

$$\gamma_{xy}^2(f) = \left|\hat{S}_{xy}(f)\right|^2 / \left(\hat{S}_{xx}(f)\hat{S}_{yy}(f)\right) \tag{9}$$

A *virtual instrument* was developed in Labview to the cross-spectrum technique and is illustrated in Figure 17.

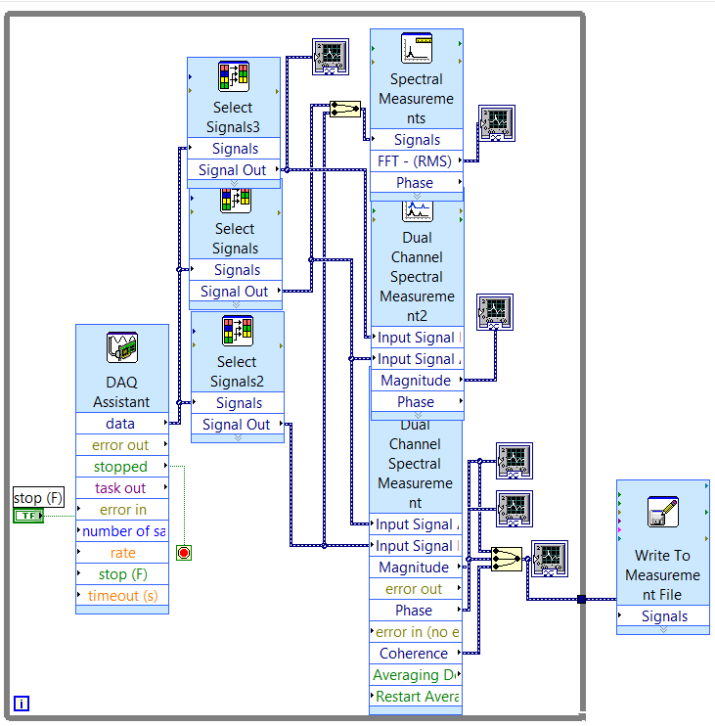

Figure 17. Cross-spectrum *virtual instrument* at Labview software.

3.2.3 *Time-domain*

The Lissajous curve, a qualitative technique in time domain, was applied to determine the phase shift between two microphones (AL-KHAZALI et al., 2012). A *virtual instrument* was developed in Labview for the identification of the Lissajous figures (Figure 18). The two microphone acoustic signals $p(\vec{x}_1, t)$ and $p(\vec{x}_2, t)$ were assumed as harmonic functions (with excitation frequency $f = \omega/2\pi$ in Hz):

$$p(\vec{x}_1, t) = P(\vec{x}_1)\sin(2\pi f t) \tag{10}$$

$$p(\vec{x}_2, t) = P(\vec{x}_2)\sin(2\pi f t + \phi) \tag{11}$$

where, $P(\vec{x}_i)$ $(i = 1{,}2)$ is the acoustic module in a determine position $\vec{x}_i$ in space, and ϕ the phase shift between both acoustic signals. The resulting phased harmonic signals acoustic normalization $p(\vec{x}_i, t)/P(\vec{x}_i)$ $(i = 1{,}2)$ has the similar amplitude. For a ratio of 1, the Lissajous curve is an ellipse, with special cases including circles ($P(\vec{x}_1) = P(\vec{x}_2)$, and $\omega = \pi/2$) and lines ($\omega = 0$). The identification of a circle represents a $\omega = \pi/2$ between the two microphones and a maximum pressure gradient, characterizing a maximum acceleration (flux) in the point of interest.

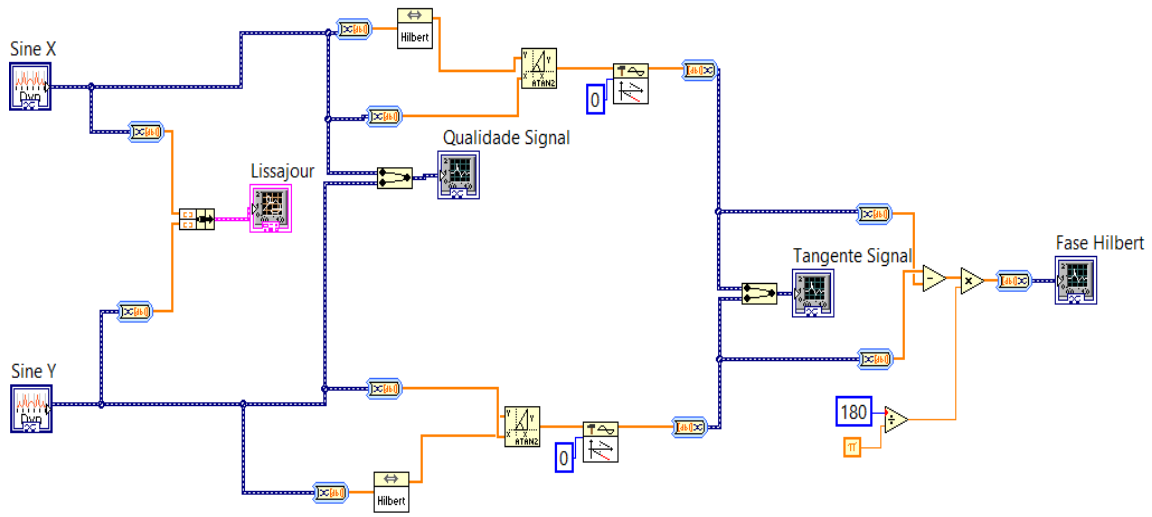

Figure 18. Lissajous virtual instrument at Labview software.

The Hilbert transform of the time signal $x(t)$ is also a time function $\tilde{x}(t)$:

$$z(t) = x(t) + j\,\tilde{x}(t) \tag{12}$$

where $z(t)$ is a analytic signal. The Hilbert transform has interesting properties, which enable a few useful applications (BENDAT; PIERSOL, 1986; OPPENHEIM, A.V. SCHAFER, 1989; FELDMAN, 1994a and 1994b). The definition of Hilbert transform in time domain is done by:

$$\tilde{x}(t) = \mathcal{H}[x(t)] = \frac{1}{\pi} \int_{-\infty}^{+\infty} \frac{x(\tau)}{t-\tau} d\tau \tag{13}$$

When the damped cosine signal $x(t)$ is analyzed, the Hilbert transform $\mathcal{H}[x(t)]$ act as a quadrature filter, according to Eq. 13. From the complex analytic function $z(t)$ it can be defined the instantaneous amplitude, instantaneous frequency and instantaneous phase of the signal $z(t)$:

$$z(t) = x(t) + j\,\tilde{x}(t) \quad \rightarrow \quad z(t) = A(t)e^{j\phi(t)} \tag{14}$$

The instantaneous amplitude $A(t)$ represents the signal envelop $z(t)$:

$$A(t) = \sqrt{x^2(t) + \tilde{x}^2(t)} \tag{15}$$

And, instantaneous frequency $f(t)$ and signal phase $\phi(t)$ was calculated by:

$$f(t) = \frac{1}{2\pi}\frac{d}{dt}[\phi(t)] \tag{16}$$

$$\phi(t) = \tan^{-1}\left(\frac{\tilde{x}(t)}{x(t)}\right) \tag{17}$$

Eq. 16 an Eq. 17 were applied to the present experimental setup to obtain the phase shift ϕ_{12} between two microphones signals:

$$p_1 = p(\vec{x}_1, t) = P(\vec{x}_1)\sin(\omega\, t + \phi_1) \tag{18}$$

$$p_2 = p(\vec{x}_2, t) = P(\vec{x}_2)\sin(\omega t + \phi_2) \tag{19}$$

$$\phi_{12} = \phi_1 - \phi_2 \tag{20}$$

This result gives the knowledge of which frequencies produces the highest acoustic flux around the wood sample. The virtual instruments developed for the measurement of the qualitative signal is illustrated in Figure 19. With the frequencies defined, a decibel meter was utilized to measure de intensity of the acoustic source inside de reverberant cavity for each identified frequency.

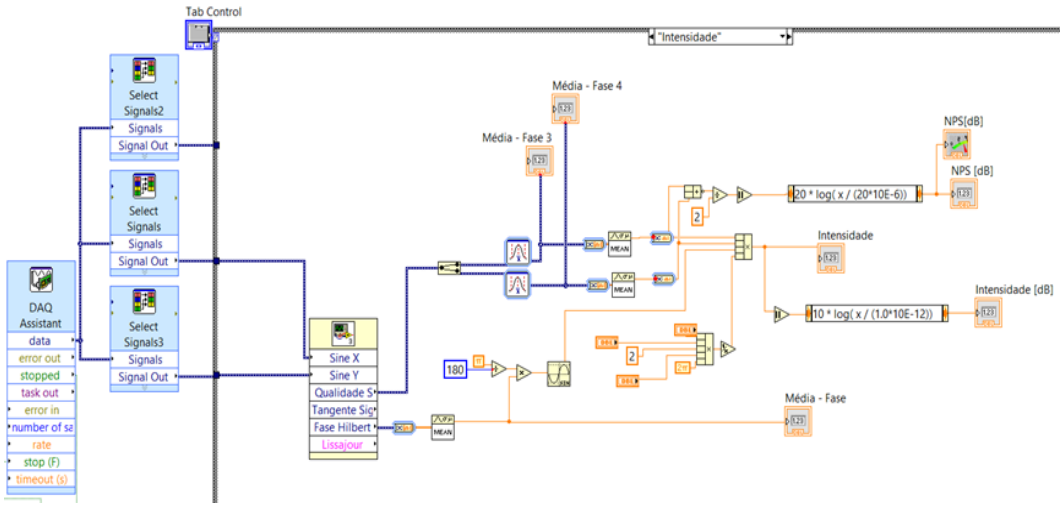

Figure 19. Hilbert Transform *virtual instrument* at Labview software.

3.3 Biomass thermodegradation

3.3.1 Feedstock

The biomass sample used in this study was *Eucalyptus grandis*, due to its large planting in Brazil, focused mainly for paper and celluloses industry and energy use. A 15-year-old *Eucalyptus Grandis* tree was extracted from *Fazenda água limpa*, UnB property for wood species controlled growing. Extraction process is illustrated in Figure 20.

The tree was divided into 6 large blocks. From the blocks, several rafters were made and stored in the LPF engineering room. Wood sample preparation was carried out in LPF laboratory. The proximate and ultimate analyses as well as energy content values for the raw material are shown in Table 5.

Figure 20. Wood sample confection of a 15-year-old species of *Eucalyptus Grandis*. Preparation of rafters in the LPF's carpentry.

Table 5. Proximate, elemental and calorific analyses of *Eucalyptus grandis*.

Raw material	*Eucalyptus Grandis*
Proximate analysis [a]	
Fixed carbon (F.C)	18.51
Volatile matter (V.M)	81.4
Ash	0.09
Elemental analysis [a]	
C	46.03
H	6.19
N	0.13
O [b]	47.65
HHV (MJ kg^{-1})	20.09

[a] Dry basis, [b] O (wt%) = 100–C–H–N-ASH

3.3.2 Biomass torrefaction

Aiming to clarify the thermal comportment and degradation mechanism for the raw material of this study (*Eucalyptus grandis*) some physic-chemical techniques were applied, specifically, thermal (TGA, TGA-FTIR) and chemical analysis (elemental, proximate and energetic analysis). Among all the techniques here selected, TGA-FTIR confirms to be a very useful tool since it was already successfully employed to unveil the amount and the nature of chemical evolved from different complex composite materials (CHEN; LU; TSAI, 2012a; CORAZZARI et al., 2015).

3.3.2.1 Thermogravimetric analysis TGA

Thermogravimetric analysis of a micro-particle sample of *Eucalyptus grandis* was performed to get information on solid mass evolution versus time and temperature. This analysis allowed the characterization of thermodegradation in micro-scale, providing information on the mass loss and volatile release dynamics (identification of functional groups throughout the treatment by a FTIR equipment connected in line with the TGA). These data were used for the discussions of thermoacoustic torrefaction and degradation kinetic model.

The thermal behaviors of the samples (about 15 mg of milled wood per run in ceramic crucibles with a 60 mesh) were investigated using a *SDT Q600 TA* which provides instantaneous measurement of mass variation (TGA). The samples were heated at a linear heating rate of 20°C.min^{-1} until 105°C and kept for 30 minutes to assure dry condition. After drying, a heating rate of 5°C.min^{-1} was imposed until the desired temperature of 210, 230, 250, 270 and 290 °C. Thereafter, they were torrefied for 60 minutes. Nitrogen was used as purging gas at a flow rate of 50 mL.min^{-1}. The torrefaction treatment parameters are listed in Table 6.

Table 6. Micro-particle torrefaction parameters.

Raw material	**Torrefaction conditions**		
	Duration	Heating rate	Final temperature
E. grandis	60 min	5°C.min^{-1}	210°C 230°C 250°C 270°C 290°C

3.3.2.2 FTIR spectroscopy

FTIR analysis of the gases released during thermogravimetry was performed using a THERMO SCIENTIFIC TGA / FTIR interface device. Evolved gases were then passed through a transfer line. The transfer line and gas cell were heated to an internal temperature of 190°C, and the gas cell temperature was limited to 200°C to avoid the condensation or adsorption of semi-volatile products. FT-IR spectra was recorded with a *Thermo Nicolet IS 10 FT-IR*. IR spectra were recorded between 400-4000 cm^{-1} a, with 68 scans collected at an interval of 4 cm^{-1}.

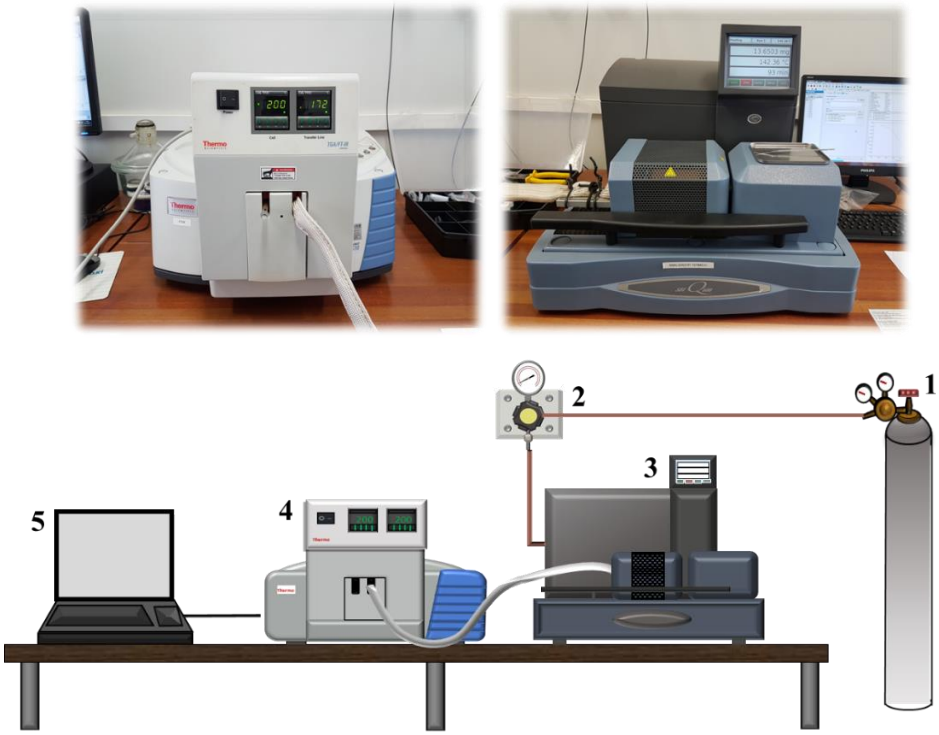

Figure 21. General scheme of the experimental system. 1) N_2 cylinder, 2) Gas control rotameter, 3) SDT Q600 TA, 4) THERMO SCIENTIFIC TGA / FTIR, 5) Computer (OMNIC and Qseries Software).

The results of the IR analysis provided the characterization of the functional groups released during thermodegradation for five different treatment temperatures. This allowed to validate the choice of the two temperatures used during the thermo-acoustic torrefaction treatment as well as the identification of the two stages of volatile releasing (BATES, 2012). The mass loss occurring during the faster first stage of torrefaction is primarily attributable to the hemicellulose decomposition with an increasing contribution from cellulose decomposition at higher temperatures. The mass loss during the slower second stage is primarily due to cellulose decomposition, with minor lignin decomposition and charring of the remaining hemicellulose (BATES; GHONIEM, 2012; PRINS; PTASINSKI; JANSSEN, 2006a, 2006b).

3.3.3 Biomass thermo-acoustic torrefaction

The reactor system located in the Forest Product Laboratory (Brasília, Brazil) and its schematic diagram are showed in Figure 22 and Figure 23 respectively.

The reactor included a square chamber with two internal electrical heaters. Oxygen concentration was maintained by N_2 injection. The reaction temperature was controlled by a proportional integral derivative (PID) temperature controller based on a PT100 placed in the centre of the reactor to record atmosphere temperature. Data acquisition was performed by two type K special thermocouples (*IEC 584-3*) with a bead size of 1 mm and a tolerance value of

1.1°C to measure wood surface and wood core temperatures and a mass balance (*Sartorius LP2200S*) with an accuracy of 10^{-3} grams. The system provide continues acquisition data with a 100Hz sampling rate (*e.bloxx A4-1TC Multichannel*) recording thermocouples temperature profiles and mass weight during the wood heat treatment.

The desired and identified frequencies (SILVEIRA et al., 2017) were produced by an *HP 33120A* wave generator and one *Selenium D220TI 8* speaker connected by a flexible duct (ROSSETO, 2001) to the reactor cavity to deliver the acoustic wave inside the reactor. Data were sent to a computer to control the reaction temperature and the nitrogen percentage, and record wood surface and core temperature profiles and mass loss during heat treatment with and without acoustic influence.

Figure 22. Physical thermo-acoustic reactor at the Forest Product Laboratory (LPF).

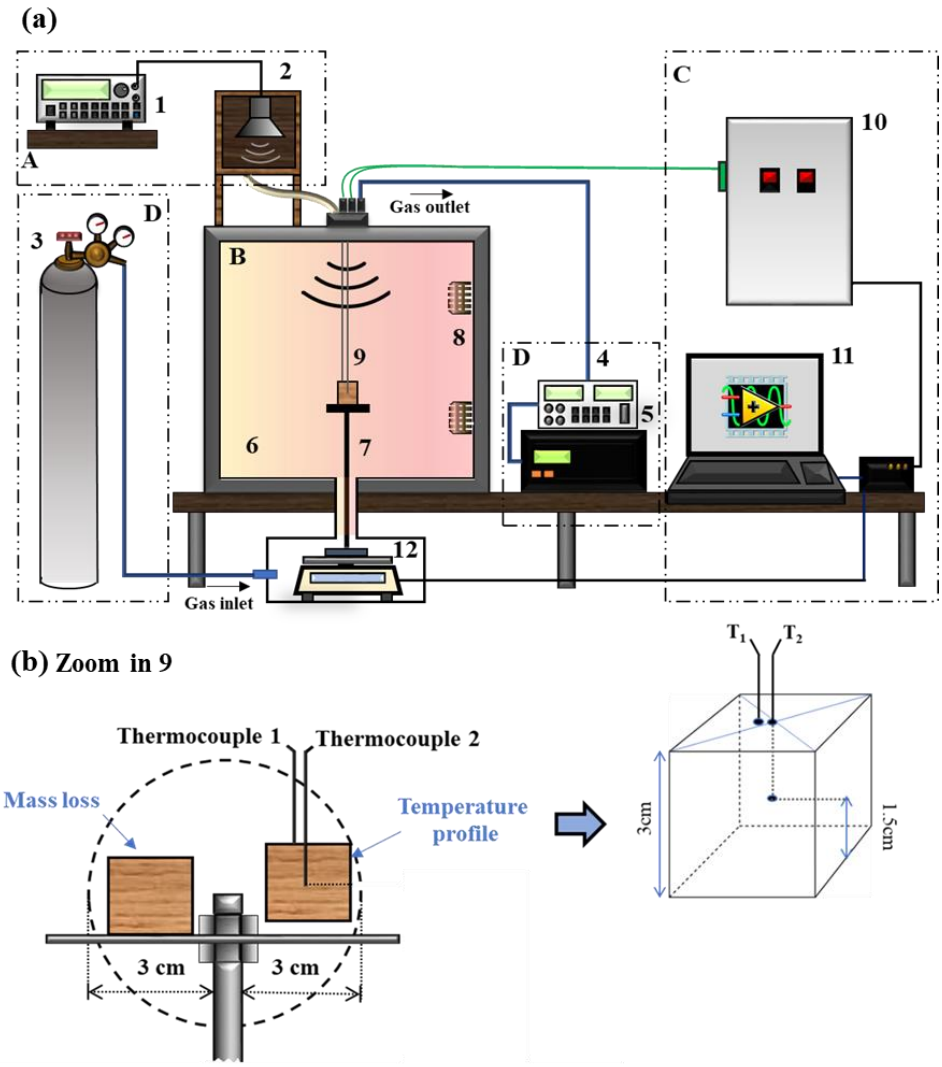

Figure 23. (a) Schematic of the laboratory-scale reactor with four subsystems: acoustic (A), heat treatment (B), power and recording (C) and gas feeding (D). Equipment list: 1) Wave generator; 2) Sound speaker 3) N_2 cylinder; 4) Gas pump; 5) O_2 control; 6) Reactor chamber; 7) Wood sample support; 8) Electric resistances for convection heating; 9) Thermocouples; 10) System control; 11) Computer; 12) Electric weight balance. (b) Detailed zoom in 9 for thermocouple positions.

3.3.3.1 Experimental procedure

For each experiment, two samples were analyzed in each trial run. One sample was placed to a precision balance to monitor mass loss and another with two thermocouples to monitor the internal and surface temperature (Figure 23b). The samples were heated at a linear heating rate of 5°C.min^{-1} until the desired temperature of 250 or 270°C. Thereafter, they were torrefied for 60 minutes. The carrier gas was continuously delivered into the reaction chamber to keep the system in an inert environment (10% O_2) (ROUSSET et al., 2012) and remove volatiles produced in the reactor. The torrefaction treatment parameters are listed in Table 7.

The controls experiments were performed without acoustic for both selected temperatures. The other sets of experiments were performed for both temperatures coupled to the 1411, 1810,

2478 and 2696Hz acoustic frequencies. Those frequencies were identified (SILVEIRA et al., 2017) and within the system have the capacity to produce the ideal conditions for maximum particle velocity around the wood sample affecting the interaction between gaseous environment and wood sample. Each frequency was maintained during all the experiment. For a statistical purpose, three experiments were performed for each condition. The effect of temperature and coupled acoustic and temperature were assessed by the analysis of the torrefied solid product.

Table 7. Thermo-acoustic torrefaction parameters.

Raw material	Torrefaction conditions			
	Duration	Heating rate	Atmosphere	Final temperature / frequency
E. grandis	60 min	5°C.min^{-1}	10% 0_2	250°C [a] / -
				250°C / 1411Hz
				250°C / 1810Hz
				250°C / 2478Hz
				250°C / 2696Hz
				270°C [a] / -
				270°C / 1411Hz
				270°C / 1810Hz
				270°C / 2478Hz
				270°C / 2696Hz

[a] Control experiments without acoustic.

3.3.4 Torrefied solid product analysis

3.3.4.1 Thermal decomposition dynamics

The thermal decomposition was evaluated by the calculated solid yield (η_S) and its derivative (DTG) in time, energy yield (η_E), and conversion rate α for the continuously weighed wood sample over time according to Eq. (21), Eq. (22) and Eq. (23) respectively.

$$\eta_S(t) = \frac{m_i(t)}{m_0} \times 100 \quad (21)$$

$$\eta_E(t) = \eta_S(t) \times \frac{HHV_i}{HHV_0} \quad (22)$$

$$\alpha = \frac{m_0 - m_i(t)}{m_0} \quad (23)$$

where m_0 (g) is the dried mass before torrefaction; m_i (g) is the solid mass during torrefaction; HHV_0 (MJ. kg^{-1}) is the higher heating value of untreated samples dry and ash-free basis; HHV_i (MJ. kg^{-1}) is the higher heating value of torrefied samples dry and ash-free basis.

This analysis allowed the characterization of thermodegradation in macro scale, providing information on the mass loss dynamics profiles and the influence of the heat transfer (due to the macro particle size). These data were used for the discussions of thermo-acoustic torrefaction results and degradation kinetic model.

3.3.4.2 Chemical analysis

The elemental analysis was conducted according to the American Society for Testing and Materials (ASTM E777 e E778) with a Perkin Elmer EA 2400 series II elemental analyzer, to detect the weight percentages of C, H, N for raw and torrefied biomass. The oxygen content was calculated by difference. Proximate analyses (fixed carbon, volatile matter and ash contents) were performed with the standard procedure of the ASTM D3172 - 13. The calorific values of raw and torrefied biomass samples were measured according to the standard ASTM D5865with a bomb calorimeter (PARR 6400).

The chemical analysis allowed to validate the standard torrefaction experiments with literature, establishing a basis of comparison (control) for the experiment and provided information concerning the effect of the coupled thermo-acoustic treatment on the torrefied product. These data were used for the discussion about the effect of the acoustic field during the thermal treatment.

3.3.4.3 Statistical analyses

Statistical analyses were conducted for thirty experimental tests using the *Assistat 7.7* software (FRANCISCO et al, 2016). Results for untreated and torrefied material were subjected to variance analysis (ANOVA) and the Tukey Test at a 5% significance level. Six variables in response to the experiments were analyzed and discussed: the solid yield (wt%), fixed carbon content (F.C%), volatile matter content (V.M%), ash content (Ash%), and the higher heating value (HHV). The general model for variance analysis is described by the Eq. 24:

$$Y_{ij} = \mu + [F_i + T_j + (F \times T)_{ij}] + \varepsilon_{ij} \quad (24)$$

where Y_{ij} is the value observed for the dependent variable for observation ij, F is the acoustic frequency within the reactor, T the temperature, ε_{ij} is the error of the model and μ is a constant.

3.3.4.4 Final product pyrolysis

Pyrolysis experiment of the torrefied product were performed to characterize how the torrefaction treatment affect the total degradation of the treated wood using a *SDT Q600 TA*, which provides instantaneous measurement of mass variation. The experiment was performed from 25 to 800°C with a heating rate of 20°C min^{-1} and a N_2 flow rate of 50 $mL.min^{-1}$. When the temperature reached 105°C, it was held for 10 min to ensure moisture removal. The pyrolysis experiment can provide information about the severity of the torrefaction treatments allowing to characterize the degradation of different wood constituents (hemicelluloses, cellulose and lignin) for each temperature in time via the analysis of the solid yield derivative.

3.4 Biomass torrefaction model

The biomass torrefaction model was developed in a particle scale (0D). Firstly, the kinetic, model was developed providing the solid and volatile yield evolution in time (section 3.4.1). In the sequence, the elemental composition model was established allowing to determine the *C*, *H* and *O* composition dynamics for the solid and volatile in time in section 3.4.2.

3.4.1 Wood kinetics model formulation

In the literature, lots of studies proposed kinetic models to represent wood degradation during the heat treatment. These models, usually applied to simulate the intrinsic biomass decomposition obtained from thermogravimetric analysis (TGA), can be classified in two major sections: detailed models and global pseudo-components models. The most used detailed model, initially proposed by (REPELLIN; GUYONNET, 2005) and further developed by (ANCA-COUCE et al., 2014; BLONDEAU; JEANMART, 2012; GAUTHIER et al., 2013b) considers separately the decomposition of the three main wood polymers and predicts the produced volatile components. This model, based on the description of all chemical reactions occurring during the treatment is however quite complex and hard to extend to various wood species or heat treatment conditions.

The pseudo-components models are commonly encountered in the literature because of their simplicity and the quality of obtained results. They aim to represent the global mass loss and can be based on a one-step reaction scheme (REPELLIN et al., 2010), on scheme of several

parallel reactions (CAVAGNOL et al., 2013; RATTE et al., 2009, 2011), on a two-step series reaction scheme (DI BLASI; LANZETTA, 1997; PRINS; PTASINSKI; JANSSEN, 2006a) or on scheme of several steps in series (CAVAGNOL et al., 2013; JOSHI et al., 2014). These models present the advantage of being simple and easily adaptable. A solid mass loss kinetic scheme originally proposed by (DI BLASI; LANZETTA, 1997) to describe pure hemicellulose decomposition in isothermal conditions has been adopted in this study. The macro-scale samples are considered as homogeneous particles in terms of composition and temperature distribution. The two steps pseudo-components degradation mechanism is summarized on Figure 24.

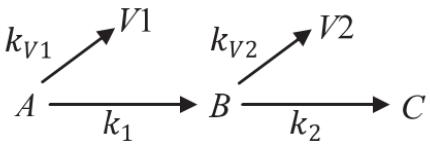

Figure 24. Di Blasi model schema.

The wood is initially assumed as solid chemical reactant A. Its decomposition leads to the formation of an intermediate solid fraction B and liberates a group of volatiles V_1. Under the effect of the temperature, intermediate B is transformed into a solid fraction C and volatiles V_2. Each reaction follows a specific decomposition law and requires the identification of model's parameters. The approach to determine the associated kinetic constants is proposed hereafter. Pseudo-components mass evolution is governed by a system of first-order differential equations (Eq. 25):

$$\begin{cases} \frac{dm_A(t)}{dt} = -(k_1 + k_{V1}) \times m_A(t) \\ \frac{dm_B(t)}{dt} = k_1 \times m_A(t) - (k_2 + k_{V2}) \times m_B(t) \\ \frac{dm_C(t)}{dt} = k_2 \times m_B(t) \\ \frac{dm_{V1}(t)}{dt} = k_{V1} \times m_A(t) \\ \frac{dm_{V2}(t)}{dt} = k_{V2} \times m_B(t) \end{cases} \quad (25)$$

where $m_j(t)$ are the instantaneous masses of the pseudo-components ($j = A, B, C, V_1, V_2$). The rate constant k_i (s^{-1}, $i = 1, 2, V_1, V_2$) obeying the Arrhenius law is calculated according to Eq. (26):

$$k_i = k_{0,i} exp\left(\frac{-E_{a,i}}{RT}\right) \quad (26)$$

where $E_{a,i}$ (J.mol^{-1}) and $k_{0,i}$ (s^{-1}) are respectively the activation energies and the pre-exponential factors of the reactions, R is the universal gas constant (J.mol^{-1}.K^{-1}) and T is the absolute temperature (K).

The system of equations (Eq. 25) was solved using the Matlab® software. The resolution needs a number of input data: the dynamic temperature profiles, the initial conditions concerning the masses of each pseudo-component, and eight kinetic parameters ($E_{a,i}$, $k_{0,i}$, $i = 1, 2, V_1, V_2$). Computation path is described hereafter. The temperature profiles come from the experimental data. Concerning mass initialization, the initial anhydrous mass m_0 is entirely allocated to the pseudo-component A (Eq.27).

$$\begin{cases} m_A\,(t=0) = 1 = m_0 \\ m_B\,(t=0) = 0 \\ m_C\,(t=0) = 0 \\ m_{V1}(t=0) = 0 \\ m_{V2}(t=0) = 0 \end{cases} \quad (27)$$

The kinetic parameters are firstly estimated from the literature then adjusted. This aspect will be more detailed in the next sections. The ODE (Ordinary Differential Equation) resolution provides the mass evolution of each pseudo component as a function of time. Instantaneous calculated solid yield $Y_{cal}^{T}(t)$ for a considered temperature T is obtained according to Eq. (28):

$$Y_{cal}^{(T)}(t) = \frac{m_A(t)+m_B(t)+m_c(t)}{m_0} \times 100 \quad (28)$$

The deviation $diff^{(T)}$ between experimental $Y_{exp}^{(T)}(t)$ and calculated $Y_{cal}^{T}(t)$ yield profiles can be evaluated using Eq. (29):

$$diff^{(T)} = \sqrt{\sum_t \left(\frac{Y_{exp}^{(T)}(t) - Y_{cal}^{(T)}(t)}{Y_{exp}^{(T)}(t)}\right)^2} \quad (29)$$

3.4.2 Biomass solid and volatile composition model

3.4.2.1 Solid composition

The composition model development was based in (BACH et al., 2016; BATES; GHONIEM, 2012). Bates and Ghoniem (2012) calculated the elemental composition of each pseudo-component indirectly through the known composition data of initial biomass and experimental data of the released volatiles obtained by (PRINS; PTASINSKI; JANSSEN, 2006b). During modelling, Bates et Ghoening (2012) assumed that the chemical compositions of the pseudo components V_1 and V_2 were constant and not dependent of the temperature. Bach et al (2016) simplified the methodo utilized by Bates, eliminating the need of a complex volatile analysys and basing the model on the final solid product elemental composition data. However, there was not a volatile compostion analysis during the modelling.

In this study, a method to provide a simple and accurate numerical prediction of carbon (C), hydrogen (H) and oxygen (O) evolution based on the kinetic evolution and the initial (raw biomass) and final (torrefied product) elemental analysis is proposed.

The solver was developed using a multidimensional unconstrained nonlinear minimization solver *Nelder-Mead* (Matlab® software). The resolution needs a number of input data: the solid pseudo-components ($Y_A, Y_B(t), Y_C(t)$) evolution in time (kinetic solver), the raw biomass elemental analysis ($\%C_A, \%H_A, \%O_A$) obtained experimentally and biochar elemental analysis ($\%C_S, \%H_S, \%O_S$). The formulation and computation path are described hereafter.

For the simulation some considerations were made: the simulation time runs from $t = 0$ until $t = t_f$ and, in $t = 0$, the solid yield is considered as 100% and composed only by A (raw biomass). The solid yield depends on treatment temperature being a mix of A, B and C and it is considered that $\frac{C(t)}{C(t=0)}$ increases with time and $\frac{H(t)}{H(t=0)}$, $\frac{O(t)}{O(t=0)}$ decreases with time. From the kinetic solver, the solid yield $Y_{cal}(t)$ at any time is calculated in function of pseudo components mass yield evolution with Eq. 30.

$$Y_{cal}(t) = Y_A(t) + Y_B(t) + Y_C(t) \tag{30}$$

A linear system for the pseudo-component evolutions can be established based on final solid product (S) experimental data and mass conservation equations for A, B and C:

$$Y_A(t).\%C_A + Y_B(t).\%C_B + Y_C(t).\%C_C = Y_{cal}(t).\%C_S$$

$$\begin{array}{l} Y_A(t).\%H_A + Y_B(t).\%H_B + Y_C(t).\%H_C = Y_{cal}(t).\%H_S \\ Y_A(t).\%O_A + Y_B(t).\%O_B + Y_C(t).\%O_C = Y_{cal}(t).\%O_S \\ \hline Y_A(t) \quad + \quad Y_B(t) \quad + \quad Y_C(t) \quad = \quad Y_{cal}(t) \end{array} \tag{31}$$

Knowing that the elemental composition for each pseudo component must correspond to 100% and solid yield ratios C/O and C/H increase with treatment time, a system of constraints is determined:

$$\begin{array}{l} \%C_B + \%H_B + \%O_B = 100 \\ \\ \%C_C + \%H_C + \%O_C = 100 \end{array} \tag{32}$$

$$\begin{array}{l} \%C_B > \%C_A \quad \%H_B < \%H_A \quad \%O_B < \%O_A \\ \\ \%C_C > \%C_B \quad \%H_C < \%H_B \quad \%O_C < \%O_B \end{array} \tag{33}$$

The resolution of the obtained linear system, in Eq. 31 and constraints in Eq. 32 and 33 by a minimization error function for $t = t_f$ gives the elemental composition ($\%C_i$, $\%H_{i\,\%}$ and $\%O_i$) of the pseudo-components ($i = B$ and C) evolution in time.

3.4.2.2 Volatile

Based on the kinetics mechanisms obtained from the solid mass loss kinetics a simplified volatile composition model was developed. The volatile composition calculation depends on the solid composition results from section 3.4.2.1. As inputs, the volatile solver needs a number of input data: the treatment temperature profiles, the pseudo-components ($Y_A, Y_B(t), Y_C(t)$) evolution in time (kinetic solver), the raw biomass elemental analysis ($\%C_A, \%H_A, \%O_A$) obtained experimentally and the resulting composition from the solid composition model ($\%C_B, \%H_B, \%O_B, \%C_C, \%H_C, \%O_C$).

The solid mass evolution characterized by the degradation/formation of pseudo-components based on (DI BLASI; LANZETTA, 1997) illustrated in Figure 24 is governed by the system of first-order differential equations presented in Eq. (25). The rate constant k_i (s^{-1}) is calculated with Eq. (26) and it is defined by the Arrhenius law for ($i = 1, 2, V_1, V_2$).

The step one reaction consists of 1 kg of A reacting competitively to form β kg of B and v kg of V_1. The step two reaction consists 1 kg of B kg reacting competitively to form γ kg of C and ξ kg of V_2. The two-step kinetic mechanism can be expressed by the two-step reaction mechanism shown:

$$A \rightarrow \beta B + vV1 \tag{34}$$

$$B \rightarrow \gamma C + \xi V2 \tag{35}$$

Where β, v, γ, ξ are dimensionless and represent the relative rates of reaction. In order to determine the relative rates, the rate laws must be written for each reaction. The first reaction step consists of three rate laws which define the specific reaction rates:

$$\begin{aligned} r_{A,1} &= \frac{dm_A(t)}{dt} = -(k_1 + k_{V1}) \times m_A(t) \\ r_{B,1} &= \frac{dm_B(t)}{dt} = k_1 \times m_A(t) \\ r_{V,1} &= \frac{dm_{V1}(t)}{dt} = k_{V1} \times m_A(t) \end{aligned} \tag{36}$$

Similarly, the second step consists of another three rate laws:

$$\begin{aligned} r_{B,2} &= \frac{dm_B(t)}{dt} = -(k_2 + k_{V2}) \times m_B(t) \\ r_{C,2} &= \frac{dm_C(t)}{dt} = k_2 \times m_B(t) \\ r_{V2,2} &= \frac{dm_{V2}(t)}{dt} = k_{V2} \times m_B(t) \end{aligned} \tag{37}$$

The relative rates are positive, dimensionless and defined by the formation rate of product divided by the decomposition rate of the reactant:

$$\begin{aligned} \beta &= \frac{r_{B,1}}{-r_{B,1}} = \frac{k_1 \times A}{(k_1 + k_{V1}) \times A} = \frac{k_1}{k_1 + k_{V1}} \\ v &= \frac{r_{V1,1}}{-r_{A,1}} = \frac{k_{V1} \times A}{(k_1 + k_{V1}) \times A} = \frac{k_{V1}}{k_1 + k_{V1}} \\ \gamma &= \frac{r_{C,2}}{-r_{B,2}} = \frac{k_2 \times B}{(k_2 + k_{V2}) \times B} = \frac{k_2}{k_2 + k_{V2}} \\ \xi &= \frac{r_{V2,2}}{-r_{B,2}} = \frac{k_{V2} \times B}{(k_2 + k_{V2}) \times B} = \frac{k_{V2}}{k_2 + k_{V2}} \end{aligned} \tag{38}$$

From the reaction mass balance defined previously, it is now possible to define the composition (i.e ultimate analysis) of V_1 and V_2. The six unknowns include the carbon, hydrogen, and oxygen content of V_1 and V_2.

$$\begin{aligned} V1_{\%C} &= \frac{A_{\%C} - \beta \times B_{\%C}}{\nu} \\ V1_{\%H} &= \frac{A_{\%H} - \beta \times B_{\%H}}{\nu} \\ V1_{\%O} &= \frac{A_{\%O} - \beta \times B_{\%O}}{\nu} \end{aligned} \tag{39}$$

$$\begin{aligned} V2_{\%C} &= \frac{B_{\%C} - \gamma \times C_{\%C}}{\xi} \\ V2_{\%H} &= \frac{B_{\%H} - \gamma \times C_{\%H}}{\xi} \\ V2_{\%O} &= \frac{B_{\%O} - \gamma \times C_{\%O}}{\xi} \end{aligned} \tag{40}$$

Knowing from literature (BATES; GHONIEM, 2012; PRINS; PTASINSKI; JANSSEN, 2006b) that for the volatile composition the pseudo-components V_1 and V_2 has a proportion, a system of constraints is determined:

$$\begin{gathered} \%C_{V2} > \%C_{V1} \qquad\qquad \%O_{V1} < \%O_{V2} \\ \%O_{V1} > \%C_{V1} > \%H_{V1} \qquad \%O_{V2} > \%C_{V2} > \%H_{V2} \end{gathered} \tag{41}$$

The solver provides as results the C, H and O evolution for V_1 and V_2 and total volatiles evolution in time

4. RESULTS

Section 4.1 presents the reactor conception and acoustic characterization for the innovative reactor technology. Obtained phase spectrum for the two methodologies in time and frequency domain are compared and validated. The acoustics analyses allowed to determine four frequencies and its intensities that produces conditions to enhance torrefaction process. In section 4.2 the torrefaction physical and chemical analysis results are exposed for the micro-scale experiments, characterizing the raw material that was used for all experiments and understanding the thermodegradation mechanism (solid degradations and volatile releasing).

Section 4.3 starts presenting the results of the standard torrefaction (without acoustic) for the macro-scale sample, allowing to observe the importance of the conductive heat transfer within the sample and providing data to be used as reference for the thermo-acoustic treatment comparison. The physical and chemical results and its statistical analysis for the thermo-acoustic treatments are reported for the 4 different acoustic frequencies. The identification of two optimum frequencies and a more detailed analysis was performed to understand the temperature and frequency interaction. The numerical model contemplating the kinetics and composition are presented in section 4.4. Experimental data allowed the validation of the two models and were used to explain the acoustic influence within all the degradation mechanism.

4.1 Reactor acoustics characterization

The phase spectrum obtained with the different methodologies in the time and frequency domains during the reactor acoustic characterization are compared and validated. A comparison was made between the obtained signal with the cross-spectrum technique in the frequency domain and Lissajous/Hilbert transform methods in the time domain. Identification of the desired frequencies that reproduced a phase shift of ± 90 degrees between the two measurement microphones combined with the intensity analysis revealed the acoustic configuration for higher particle velocities around the sample. Figure 25 illustrates the phase spectrum for the two methodologies versus the frequency. Three different experimental analyses were performed for each axis due to the vectorial characteristics. The results showed, as expected, different phase spectrum for each direction (SILVEIRA et al., 2017) and an accurate agreement between the two techniques used. The side-by-side microphone arrangement gave better results and agreement than the face-to-face configuration.

Frequencies of 1411, 1810, 2478 and 2696Hz were identified in both applied techniques and showed an approximate phase shift of ± 90 degrees between the microphones in all three spatial axes. An intensity measurement was carried out as displayed in Figure 26 for the

frequencies that showed an approximated phase spectrum behaviour for all cases in the side-by-side configuration.

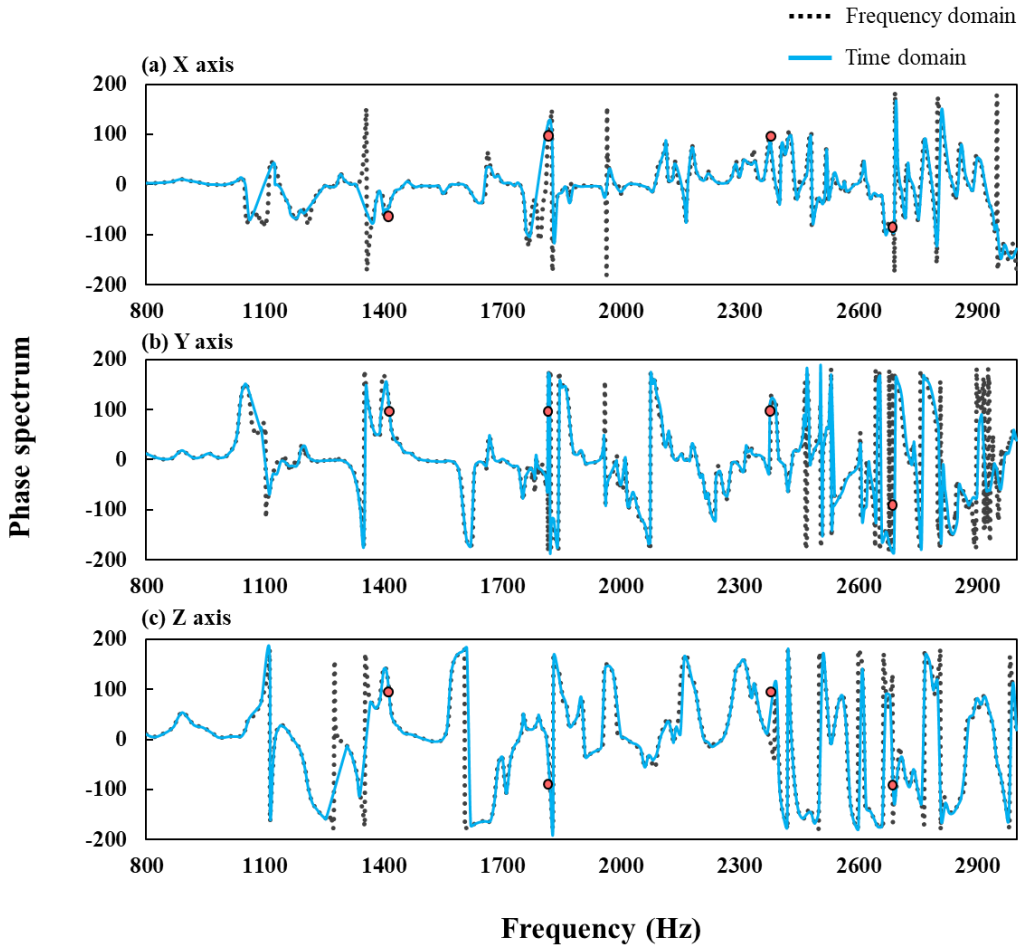

Figure 25. Time and frequency domain data comparison. Microphones side by side.

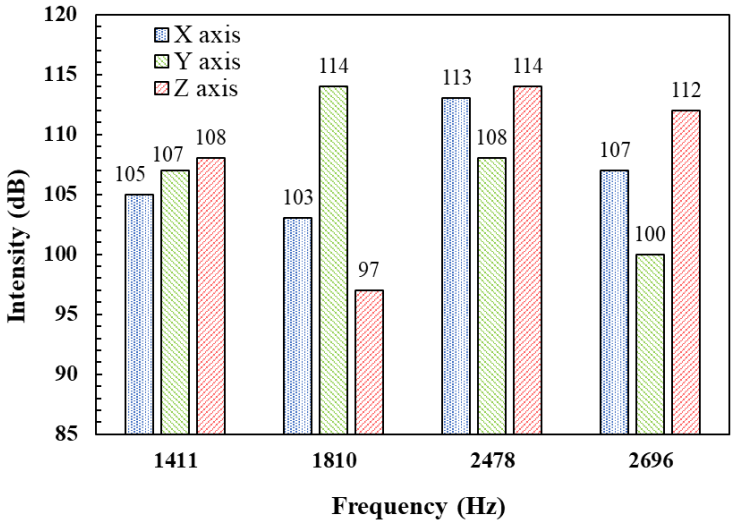

Figure 26. Selected frequencies for torrefaction experiment regarding the microphones configurations side-by-side.

The identified frequencies were applied to torrefaction experiments with the same parameter conditions with a view to obtaining different results for temperature profiles, solid yield and conversion rate during heat treatment.

4.2 Biomass torrefaction results

4.2.1 Thermogravimetric (TGA): Micro-samples results

The solid yield profiles are presented in Figure 27 to evaluate the thermal degradation dynamics of the micro-samples during torrefaction treatment.

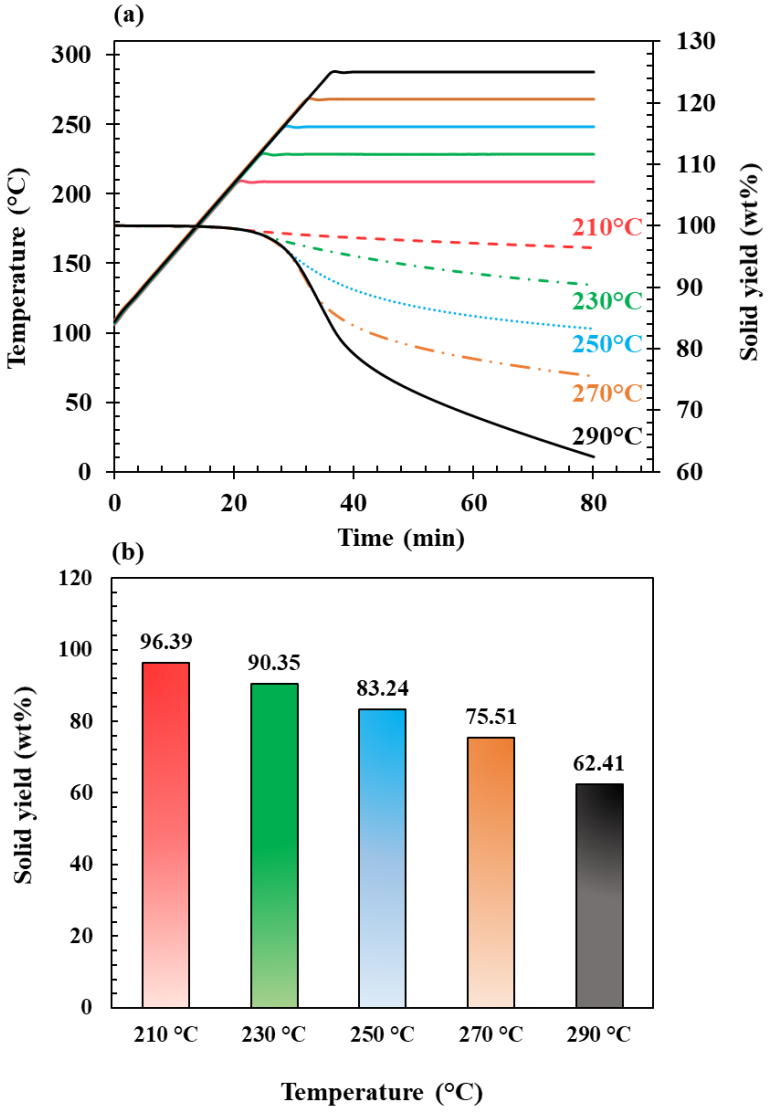

Figure 27. Solid yield dynamic profiles (a) and final solid product yield (b) for micro samples torrefaction treatment.

The torrefaction experiment was carried out for five different temperatures: 210, 230, 250, 270 and 290°C. For a better readability of the figure the normalized solid yield evolution

profiles are presented after the drying process (105°C). The yield curves were constructed by plotting the calculated $\eta_S(t)$ (Eq. 21) against treatment time.

Treatment temperature strongly influences wood thermodegradation. Figure 27 (b) shows the solid yield at the end of the treatment for different temperatures and highlights the temperature effects. The solid yield decreases when the temperature increases, and the final values are 96.39, 90.35, 83.84, 75.51 and 62.41wt%, for the treatments at 210, 230, 250, 270 and 290°C respectively agreeing with literature for micro-size particles TG (LU et al., 2012).

Considering that temperature and time are the two main key parameters in torrefaction treatment a 3D surface (data from Figure 27 (a)) an its 2D contour is presented in Figure 28.

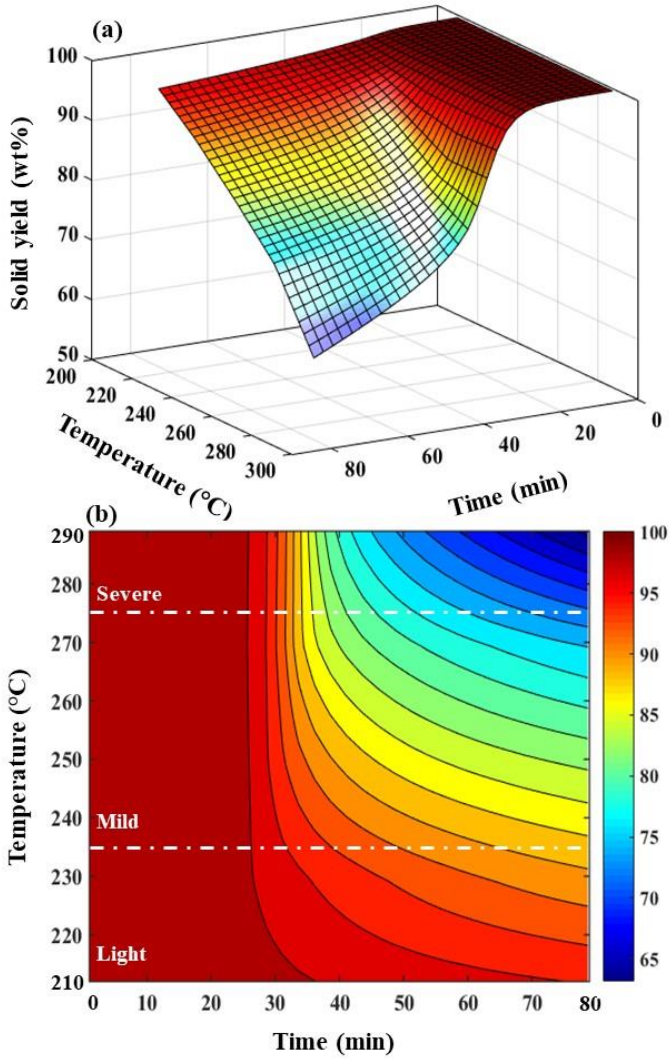

Figure 28. (a) Solid yield surface in function of the temperature and time and (b) surface contour.

A better characterization of the solid yield dynamics can be taken from Figure 28 and provide a more detailed interpretation of thermal degradation. Chen et al., (2015) reported in

(CHEN; PENG; BI, 2015) a comparison classification for the intensity of torrefaction experiments where the torrefaction can be characterized by the temperature treatment as light (200-235°C), mild (235-275°C) and severe (275-300°C).

Analyzing the contour illustrated in Figure 28 (b) it can be observed that the three classification groups are well defined. Treatments until 235°C has a light degradation (maximum of 12wt% at 235°C), the mild torrefaction is a transition area where the final product degradation variates from 12 to 25wt% and the higher temperatures presents higher degradations (30 to 40wt%).

In order to identify the intensity of thermal degradation, the solid yield derivative (DTG) profile is plot in Figure 29. Some studies have pointed out that the thermal degradation of wood started at temperatures of 180-200°C (CANDELIER et al., 2016; ESTEVES; PEREIRA, 2009) agreeing with obtained results where the degradation starts around 18 min (180°C). The three degrees of severity reported by (CHEN; PENG; BI, 2015) are identified, being the 210 and 230°C part of the light torrefaction with a maximum decomposition 0.170 and 0.333wt%. min^{-1} respectively, the 250°C the mild with 0.857$wt\%.min^{-1}$ and the 270 and 290°C de severe with 1.697 and 1.799wt%. min^{-1}.

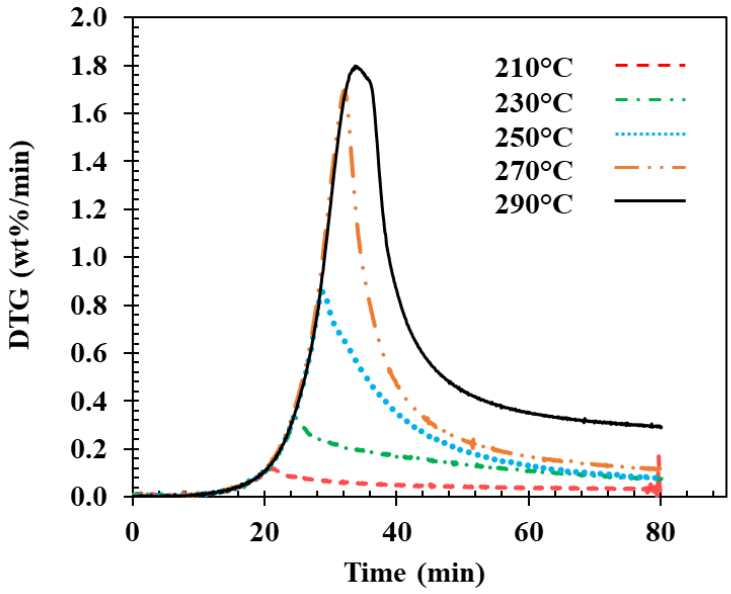

Figure 29. Solid yield derivative in time (DTG) for the five torrefaction treatments.

The 3D surface (data from Figure 27 (a)) an its 2D contour is presented in Figure 30 for the DTG data in Figure 29. In Figure 30 (b) is easier to identify the torrefaction classification ranges proposed by (CHEN; PENG; BI, 2015). An important point to notice is that the intensity peak of the degradation takes place between 20 and 40 min for all treatments.

Under the effect of temperature wood hemicelluloses are depolymerized into oligomeric and monomeric units and further dehydrated to aldehydes under acidic conditions, leading to fewer hydroxyl groups and thus to a less hygroscopic material. The degradation starts by deacetylation where the acetyl groups (-$COCH_3$) of hemicelluloses are broken and acetic acid is generated. After deacetylation, the produced acetic acid is regarded as a catalyst of depolymerization which further increases the decomposition of polysaccharides (COLLARD; BLIN, 2014; ESTEVES; PEREIRA, 2009). The acid catalyzed degradation leads to the formation of formaldehyde, furfural, and aldehydes. At the same time, the dehydration of hemicelluloses develops, decreasing the number of hydroxyl groups (CHAOUCH et al., 2010; CANDELIER et al., 2013).

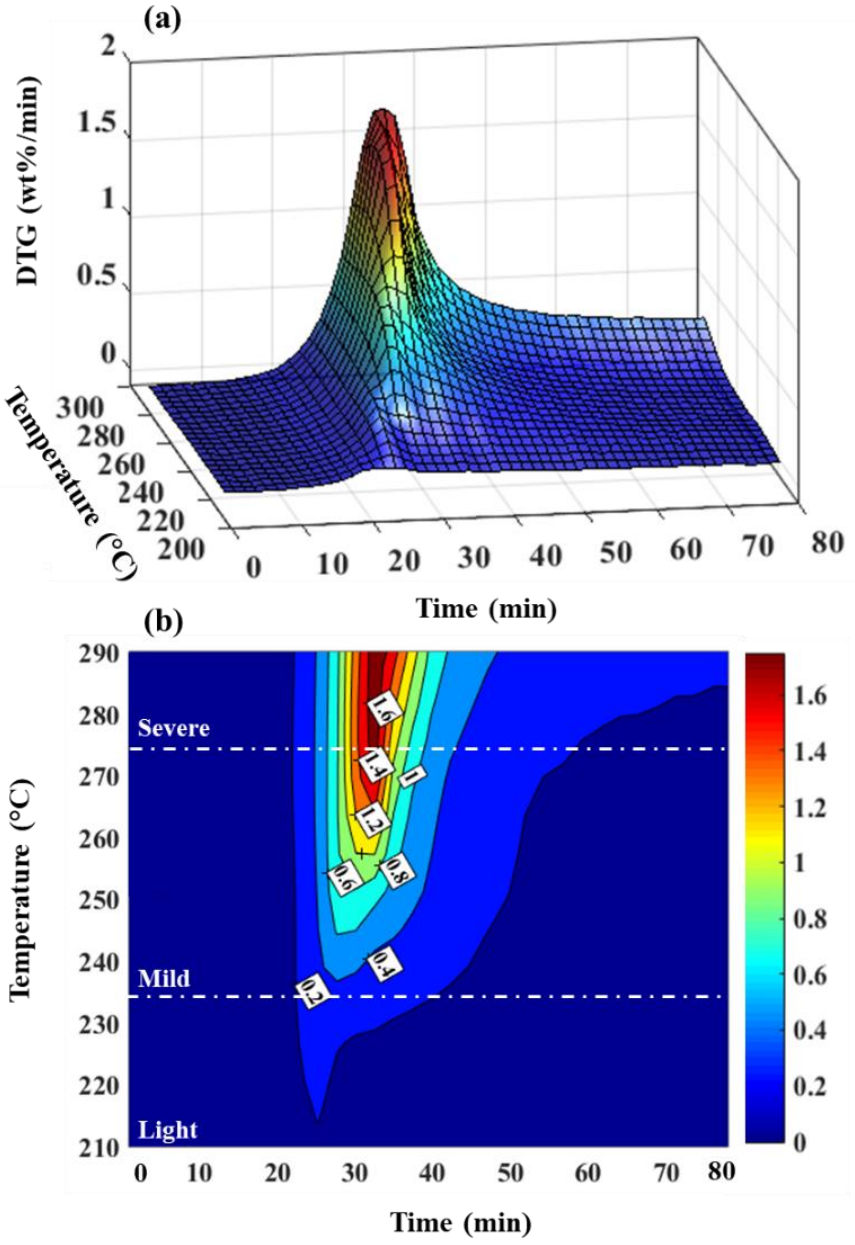

Figure 30. (a) DTG surface in function of the temperature and time and (b) DTG surface contour.

Cellulose and lignin are characterized by stronger molecular structure, their depolymerisation during the heat treatment is rather limited. Amorphous cellulose is degraded leading to a slight increase of the cellulose crystallinity ratio. The lignin is the least reactive polymer. However, its structure is modified through reactions of polymerization.

Until the 230°C temperature is observed only a slight peak due to the hemicelluloses degradation in the beginning of degradation (between 20 and 30 min of treatment). During the mild torrefaction range the degradation peaks start to be more evident after the 245°C temperature becoming more aggressive after 255°C. The degradation becomes severe after the 270°C having values almost 100% higher than the average value of the mild range (250°C).

4.2.2 FTIR results

TG-FTIR can monitor the devolatilization of the eucalyptus wood sample, recording the mass and identifying the major volatile species and their corresponding release temperature allowing the characterization of the released volatiles functional groups, from which specific species are identified. The commonly detected torrefaction products include non-condensable gases, such as CO, CO_2 and CH_4, and condensable volatiles, such as H_2O, methanol, acids and phenols (WANG et al., 2017; LIU et al., 2008; SHEN; GU, 2009; SHEN; GU; BRIDGWATER, 2010; WANG et al., 2015, 2017; YANG et al., 2007).

The obtained FTIR spectrum of gas products from torrefaction experiment (Figure 27) at the maximum evolution rate (DTG peaks Figure 29) spectrogram were separated and are presented in Figure 31. The average intensity of volatiles during the mass loss was determined and depicted in the Gram-Schmidt (G-S) curves based on vector analysis.

Based on TG-FTIR analysis of the wood constituents (hemicellulose, cellulose and lignin) the behaviors of the evolved gas products during the torrefaction treatments have been determined. It is possible to notice here the severity of the treatments analyzing the intensity of the released volatiles at the maximum evolution rate for each temperature treatments.

For the light torrefaction (210 and 230°C) only the CO_2 (2240 to 2390 cm^{-1}) is well identified. For the mild torrefaction the intensity of the functional groups starts to appear. At 250°C (mild torrefaction), water (3450 to 4000 cm^{-1}; 1300 to 1590 cm^{-1}), methanol (3600 to 3700 cm^{-1}; 2700 to 3100 cm^{-1}; 900 to 1100 cm^{-1}), formic acid (3450 to 3650 cm^{-1}; 1710 to 1850 cm^{-1}; 1030 to 1150 cm^{-1}), CO_2 (2240 to 2390 cm^{-1}), and small amounts of CO (2040 to 2240 cm-1) were slight observed agreeing with the studies for the individual analyses of wood components (LV; ALMEIDA; PERRÉ, 2015) . The characteristic bands of the G-S peaks were

similar to those at 250°C during torrefaction at 270°C and 290°C exhibiting stronger peak intensities for the released functional groups.

The discussed classification of torrefaction in light, mild, and severe are evidenced in the IR spectra. During mild torrefaction, hemicellulose decomposition and volatile liberation are intensified. Hemicellulose is substantially depleted and cellulose is also consumed to a certain extent (LV; ALMEIDA; PERRÉ, 2015). When torrefaction undergo to severe treatments, hemicellulose is almost completely depleted, and cellulose is oxidized to a great extent. Analyzing the biomass thermal degradation, lignin is the most difficult constituent to be consumed, its consumption within the temperature range of torrefaction is thus very low. By substantial removal of hemicellulose and cellulose from biomass by severe torrefaction, the weight and energy yield of biomass are usually lowered significantly although the energy density of the fuel is intensified to a great extent (CHEN; PENG; BI, 2015).

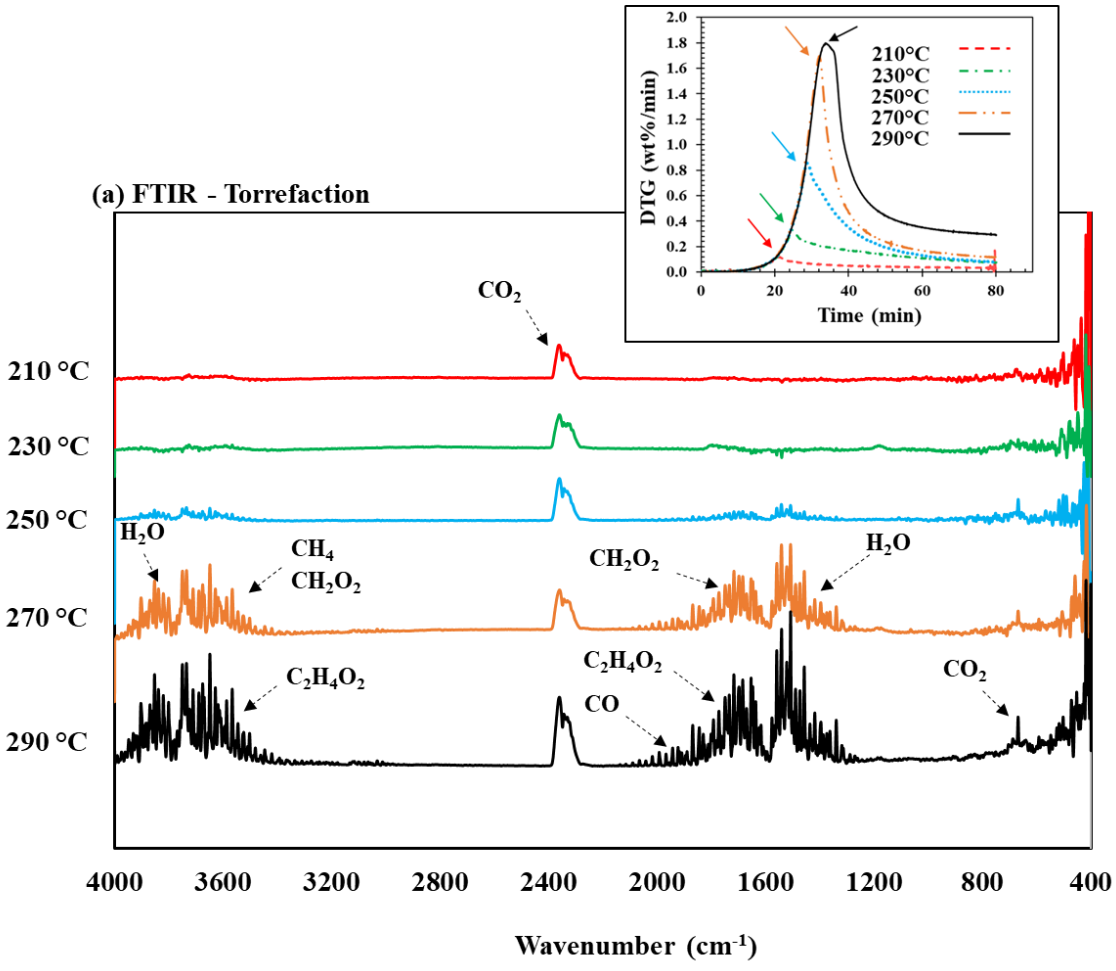

Figure 31. IR spectra obtained at the maximum evolution rate for torrefaction experiments (detailed).

4.2.3 Torrefied solid product pyrolysis results

After the samples undergoes torrefaction treatments, the torrefied product where pyrolyzed to obtain more information about the thermal degradation during process. The results of the thermogravimetric analyses (TGA) and derivative thermogravimetric (DTG) analyses are illustrated in Figure 32. Those analysis allowed to proceed further into the impact of the torrefied eucalyptus wood.

A slightly weight drop is observed during the first step of the treatment (removal of moisture content) being the drop of the raw sample bigger characterizing the hydrophobic behavior of the torrefied product.

A noticeable difference during the wood thermal degradation for the raw wood and the different torrefaction conditions is evidenced. Figure 32 shows that the degradation starts earlier for the raw sample followed by the torrefaction treatments ensuing the intensity of the pretreatment. The final solid yield is lower for the treatments performed in higher temperatures due to the fact that the wood components were already consumed during the pretreatment.

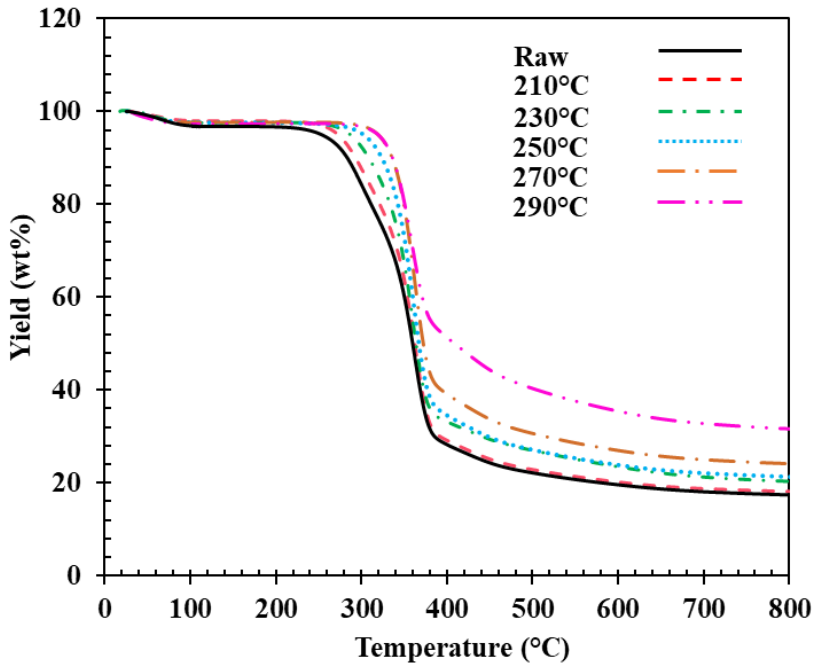

Figure 32. Solid yield profiles of pyrolysis experiment for torrefied product pyrolysis.

The solid yield 3D surface (data from Figure 32) an its 2D contour is presented in Figure 33. The surface as well as the contour allows to have a better interpretation of the degradation process during the pyrolysis showing that the classification for the severity of torrefaction process can be identified for the 3 pre-treatment zones. The torrefied products treated with the light classification (200-235°C) had a faster degradation showing that the torrefaction had a

slight effect on wood degradation. The mild treatment reported a similar behavior between 235 and 250°C temperature. The severe classification for the pre-treatment is noticed with the lower degradation from 27 min until the end of the degradation.

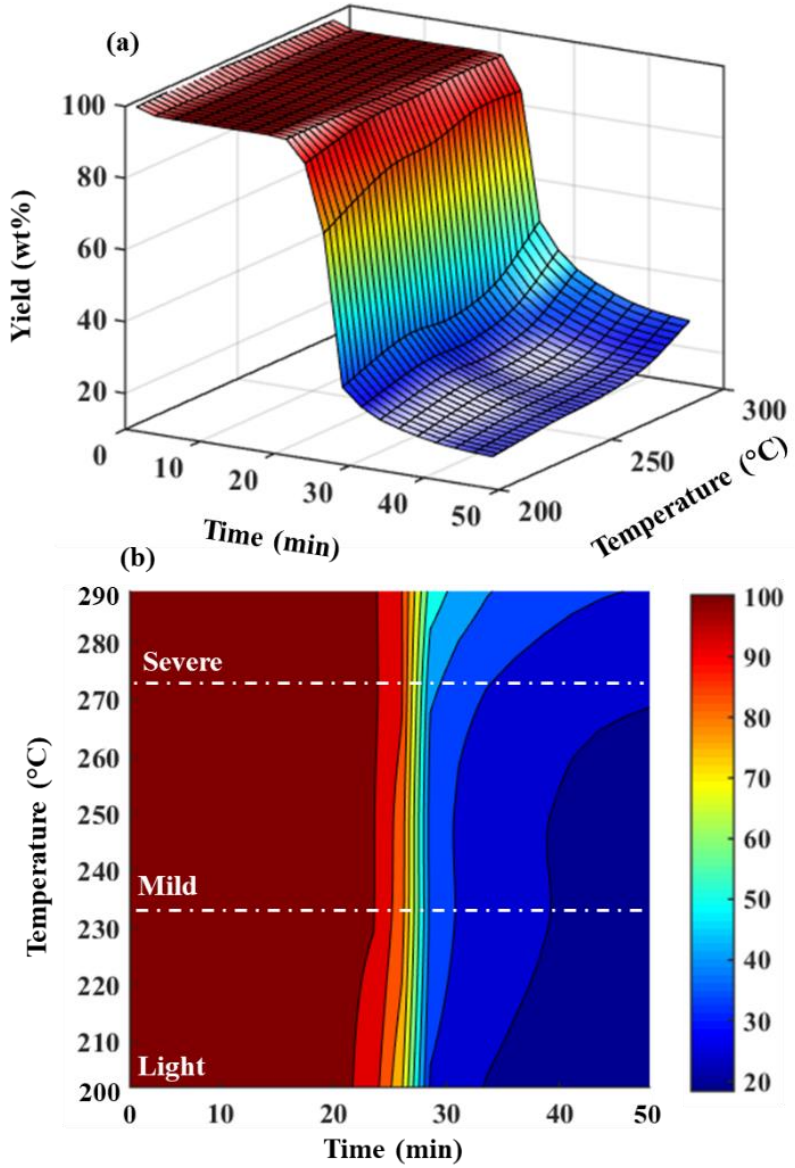

Figure 33. (a) Solid yield surface in function of the temperature and time. (b) surface contour of torrefied product pyrolysis.

Figure 34 presents the derivatives (DTG) of the pyrolysis yield profiles from Figure 32. Analyzing the curves when in the light torrefaction classification (200-235°C), it is possible to see that for the raw profile as well as for 210°C a mild degradation of the hemicellulose followed by a slight cellulose and lignin degradation. For the 230 and 250°C a mild to severe degradation of the hemicellulose is observed differing those curves in the beginning of degradation. A slight degradation of cellulose and lignin are observed being the 250°C higher

than the 230°C. The beginner of the degradation profile of the 270 and 290°C are very similar differing after the temperature of 340°C. One important observation is that the severe degradation of cellulose during the pretreatment can be observed on the DTG pic and a higher degradation for lignin can explain the difference on the final yield when compared to the other treatments profiles.

A detailed surface and contour of the DTG analysis in Figure 34 were illustrated in Figure 35. The profiles were reduced (treatment time between 20 and 30 min temperature correspondent to the temperatures between 200 to 600°C) to a better readability of the treatment intensity dynamics. The DTG profiles surface (data from Figure 34) are presented in Figure 35 (a) and the contours are presented in Figure 35 (b).

The degradation of hemicelluloses for the torrefied product can be identified by the characteristic shoulders before the cellulose degradation peaks in Figure 34 and it is represented by the 0.2 intensity value in the contour Figure 35 (b) between 23 and 26 minutes. It is possible to observe that, after biomass undergoes torrefaction, the shoulders got smaller until the 270°C temperature where this component reach almost total degradation being the shoulder of the 270 and 290°C treatments very similar and the contour line after the severe linear stage.

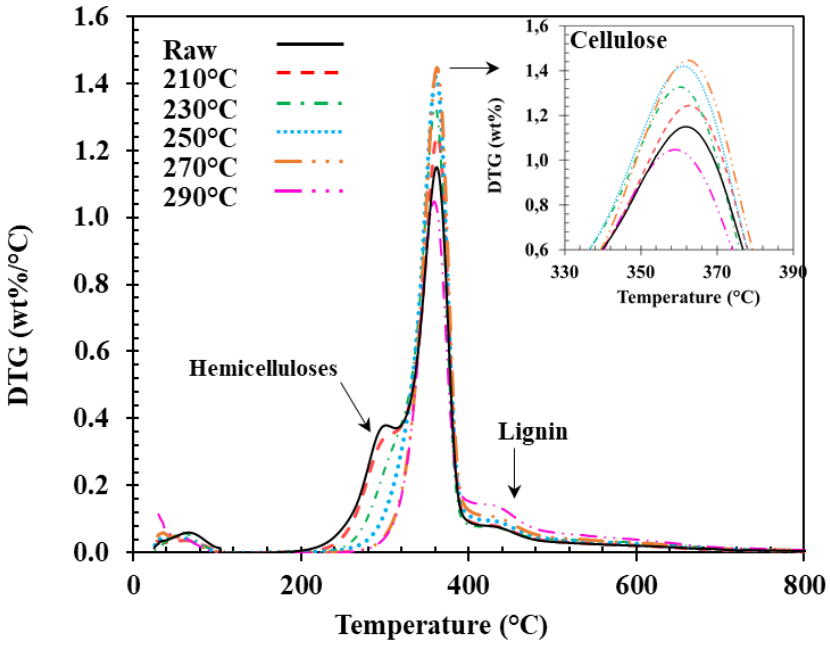

Figure 34. DTG profiles of pyrolysis experiment for the five (210,230,250,270 and 290°C) torrefied product.

The DTG peaks in Figure 34 are reached at approximately 365 °C and are attributed to the thermal decomposition of cellulose (CHEN; KUO, 2010b)(LIN et al., 2018). For the torrefied

biomass materials treated until 270°C, the obtained DTG peaks are higher than those of the untreated (raw biomass) and for the severe torrefaction classification, these peak decreases, showing a stronger degradation of celluloses during the pretreatment, also evidenced by the IR spectra for the higher temperatures in Figure 31. Figure 35 (b) contours show this behavior illustrating in the torrefaction mild temperature range higher values for the peaks due to slight degradation of cellulose. The DTG peaks width also decreases after treatment Figure 34 due to the amorphous cellulose degradation after treatment (a lower cohesive energy density is resulted because the amorphous cellulose reactivity is higher than that of crystalline one) (LIN et al., 2018; ESTEVES; PEREIRA, 2009).

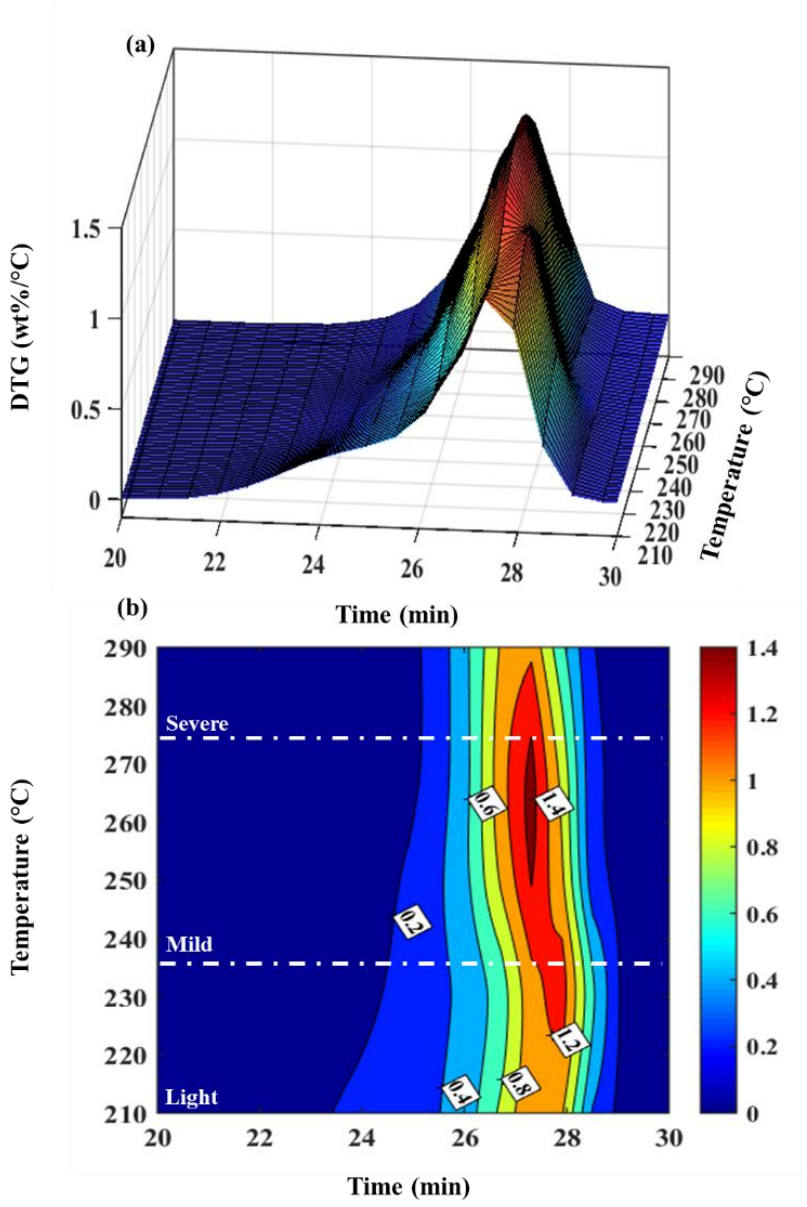

Figure 35. (a) Pyrolysis DTG surface in function of the temperature and time and (b) pyrolysis DTG surface contour.

The DTG curves corresponding to lignin degradation increases slightly with increasing treatment temperature (temperature between 400-500°C), as a consequence of relatively more lignin retained after treatment as can be seen in Figure 34 agreeing with (CHEN; LU; TSAI, 2012a; CHEN; KUO, 2010b; LIN et al., 2018). When the temperature is higher than 600°C, the curves are nearly characterized by a flat region and approach zero, implying that lignin is almost completely depleted (LIN et al., 2018).

4.2.4 Thermogravimetric (TGA): Macro-samples results

Torrefaction control experiments for treatment without acoustic were performed for 250°C and 270°C temperatures allowing to validate the reactor performance, solid yield evolution as well as the torrefied wood properties for a *Eucalyptus grandis* macro-size particle. The results provide the bases of comparison for torrefaction experiments under acoustic influence in section 4.3.2. Considering the wood sample solid yield, Figure 36 illustrates the results comparison for torrefaction treatments under similar conditions for *Eucalyptus grandis* (ALMEIDA; BRITO; PERRÉ, 2010; LU et al., 2012; ROUSSET et al., 2012). As expected (ALMEIDA; BRITO; PERRÉ, 2010; BERGMAN; KIEL, 2005) the combined effect of time and temperature, greatly affects mass loss being a very effective indicator of the torrefaction process severity.

The solid yield decreases with increasing temperature showing a linear relationship founded for all compared solid yield data ($R^2 = 0.923$). A mass loss percentage of 11.94wt% for 250°C and 17.8wt% for 270°C agrees with previous studies for *Eucalyptus grandis* (ALMEIDA; BRITO; PERRÉ, 2010; RODRIGUES; ROUSSET, 2009). Values reported by (LU et al., 2012) has a more significant mass loss due to the higher heating rate applied in treatment. Larger heating rate leads to higher mass loss speed under the same temperature and small differences in final solid yield (ZHAO et al., 2017).

Literature results for fixed carbon and volatile matter of torrefied eucalyptus wood are summarized in Figure 36 (b) for comparison. As expected, an increase in fixed carbon (hence a decrease in volatiles) with increased torrefaction temperature was observed for all the compared data. Raw biomass data agrees with literature (ARIAS et al., 2008; LU et al., 2012; ROUSSET et al., 2012) despites of the data from (ALMEIDA; BRITO; PERRÉ, 2010) that obeys the linear tendency but has higher values for V.M and lower F.C. Each temperature treatment is well represented in a linear relationship ($R^2 = 0.9987$). Values from (ALMEIDA; BRITO; PERRÉ, 2010) for 220, 250 and 280°C has the same linear behavior, however has similar results values of higher temperature treatments. Maybe due to the size of the utilized sample or raw biomass properties. The obtained result for 250°C is well placed after 240°C

treatment performed by (ROUSSET et al., 2012) and closer to results obtained by (LU et al., 2012; RODRIGUES; ROUSSET, 2009). Result for 270°C agrees with (LU et al., 2012) and is well placed when comparing to 280°C data.

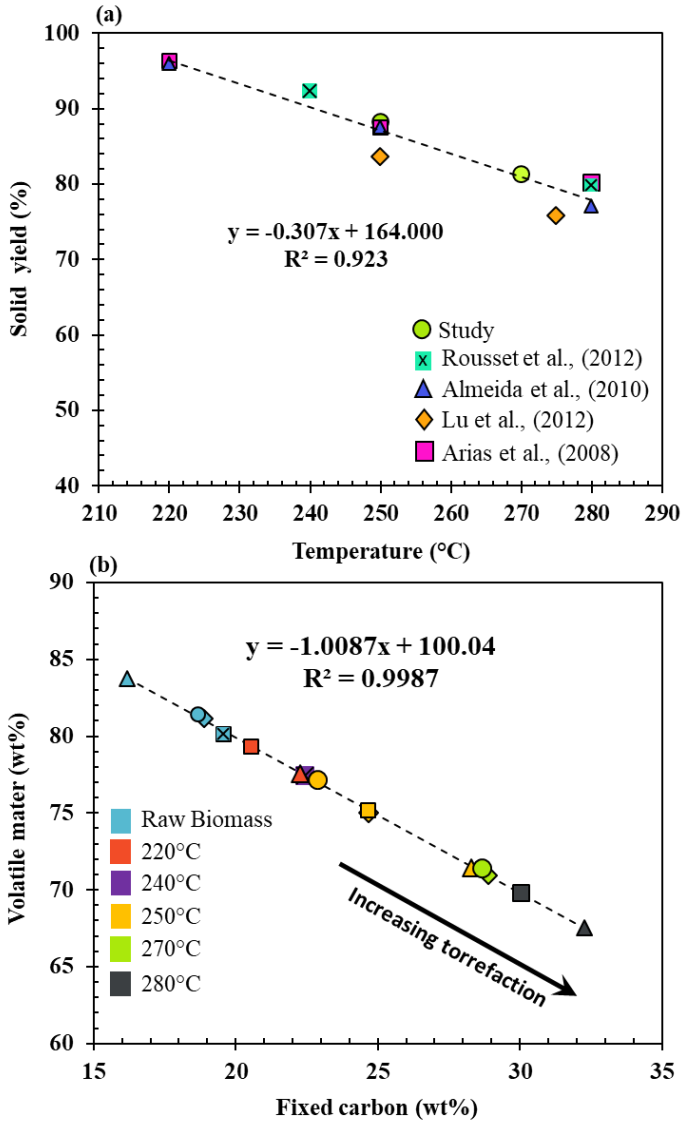

Figure 36. (a) Solid yield (%) versus temperature (°C) and (b) fixed carbon versus volatile matter comparison for *Eucalyptus grandis* torrefaction under similar conditions for 220, 250, 270 and 280°C treatments.

The raw sample volatile content decreased from 77.17 to 71.12wt% while the fixed carbon increased significantly from 22.77wt% to 28.79wt% with the elevation of the temperature from 250 to 270°C as reported by (RODRIGUES; ROUSSET, 2009; ROUSSET et al., 2012).

The energy yield is defined by the energy content ratio between torrefied biomass and the corresponding raw biomass, which is equivalent to the multiplication of the solid yield and the enhancement factor of HHV (Eq. 22) (CHEN; PENG; BI, 2015; CHEN; LU; TSAI, 2012a; PARK et al., 2012). Almeida et al., (ALMEIDA; BRITO; PERRÉ, 2010) indicated that the calorific value of a material decreased almost linearly with increasing torrefaction mass loss.

The plot of obtained energy yield versus solid yield in Figure 37 in comparison with (ALMEIDA; BRITO; PERRÉ, 2010; RODRIGUES; ROUSSET, 2009) showed that a decrease in solid yield linearly (R^2 = 0.918) decreases the energy yield of biomass as suggested by (CHEN; PENG; BI, 2015).

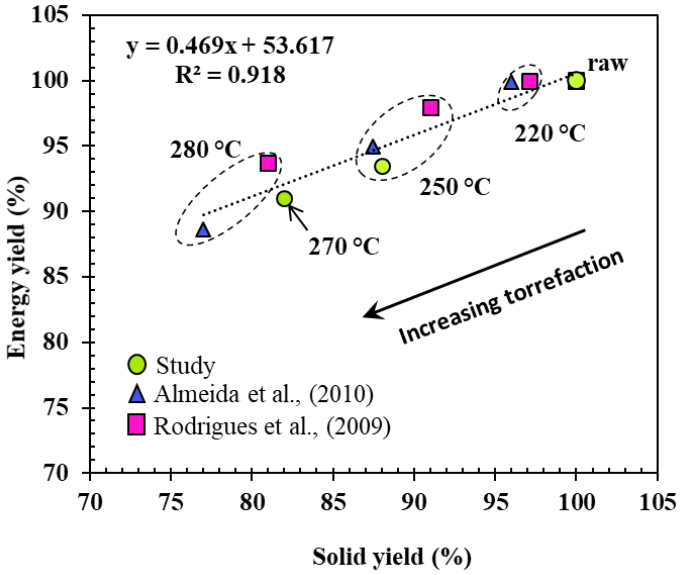

Figure 37. Solid yield (%) versus energy yield (%) for torrefaction treatment of *Eucalyptus grandis* under similar conditions for 220, 250, 270 and 280°C treatments.

4.3 Biomass thermoacoustic torrefaction results

The results for standard torrefaction (without acoustic) are presented in section 4.3.1, to validate the macro-scale torrefied biomass properties and provide the reference values for acoustic treatments comparison. The experimental analysis and statistical results for torrefaction under acoustic are presented in section 4.3.2 for all explored frequencies. Section 4.3.3 discusses and shows the results for the optimum identified frequencies.

4.3.1 Temperature and solid yield dynamics

The results for the temperature evolution (core and surface thermocouples) during the 250 and 270°C torrefaction treatments are illustrated in Figure 38 for the control (no acoustic) and acoustic treatments (1411, 1810, 2478 and 2696Hz). The illustrated temperature profiles are an average of 3 treatments that undergoes at the same conditions. As the heat system is controlled by an on/off PID some oscillations were observed on the temperature curves.

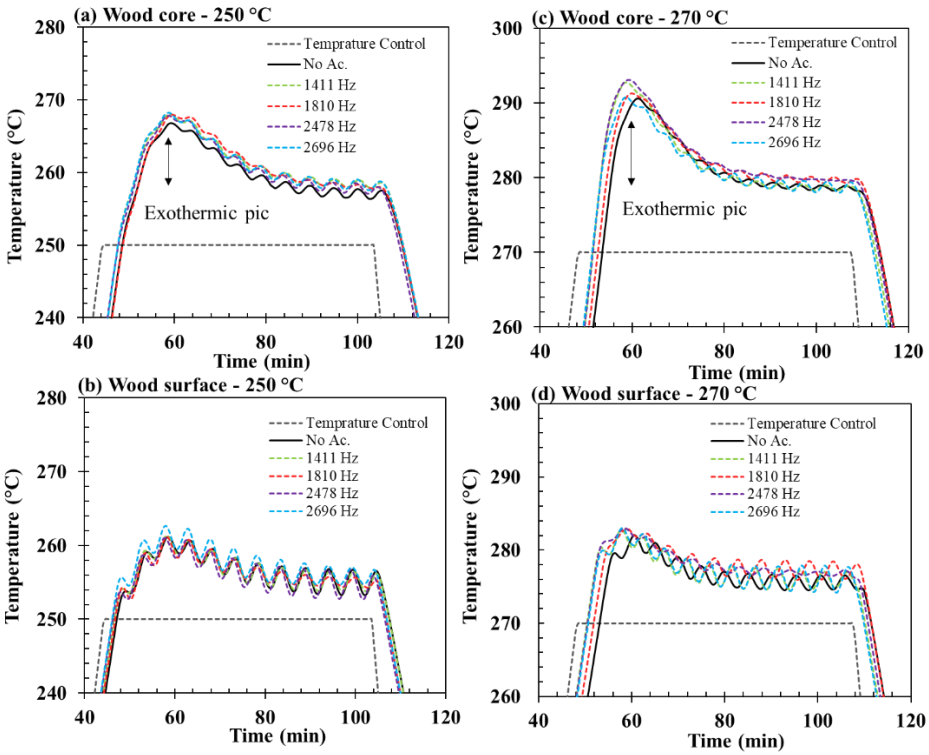

Figure 38. Average temperature profiles of the thermocouple located in the center of the samples for 250°C (a) and 270°C (c) treatments; Average temperature obtained by the thermocouple located at the surface of the samples for 250°C (b) and 270°C (d) treatments.

Analyzing the 250°C experiments (Figure 38 (a) and (b)), the acoustic treatments had a maximum temperature higher than the control treatment. An increase of the temperature was observed for the treatments under acoustic effect. It was also observed that the treatments under acoustics influence reached the level of 250°C with approximately 2 minutes and 30 seconds before the control, except for the frequency 1810Hz. The wood surface temperatures profiles for the acoustic treatments remained close to the control (no acoustic), except for the frequency 2696Hz. The maximum exothermic peak temperature was registered for the 2696Hz frequency with a temperature of 268.8°C, being 2.3° C higher than the control.

Figure 38 (c) and (d) shows, respectively, the average temperatures for the core and surface for the 270°C experiment. At 270°C, the treatments under acoustic influence were more evident in comparison to the control. The temperature profiles at the sample core indicate that all treatments reached the 270°C plateau before the control, especially the frequencies 1411, 2478 and 2696Hz (3 and a half minutes faster).

All treatments reached the exothermic peak (maximum temperature) between 58 and 62 minutes, and the treatments that undergoes acoustic influence reached their temperature peaks before the control. The 1411 and 2478Hz treatments reached a similar peak of 293.5°C and the control of 290.5°C. After the exothermic peak (TURNER et al., 2010), the temperatures of all

the treatments stabilize between 270 and 280°C during the plateau of 270°C, and there are no significant differences between the treatments.

Turner et al., (2010) and Rodrigues and Rousset (2009) reported that the average temperatures measured on the surface of the wood during torrefaction process are higher than in the core during the heating phase, with an inversion when the treatment reaches the plateau. This behavior change is due to the exothermic reactions that occur inside the wood, increasing the temperature and consequently the production of volatile materials (ROUSSET et al., 2004).

Figure 39 shows the solid yield dynamics for the temperature of 250 and 270°C. Analyzing the 250°C treatment Figure 39 (a) the degradation starts at about 25 minutes for the 1411 and 1810Hz frequencies and for the 2478 and 2696Hz frequencies at 30 minutes. The control biomass degradation begins only at 35 minutes. Note that the degradation of the control experiment is lower than the treatments under acoustic.

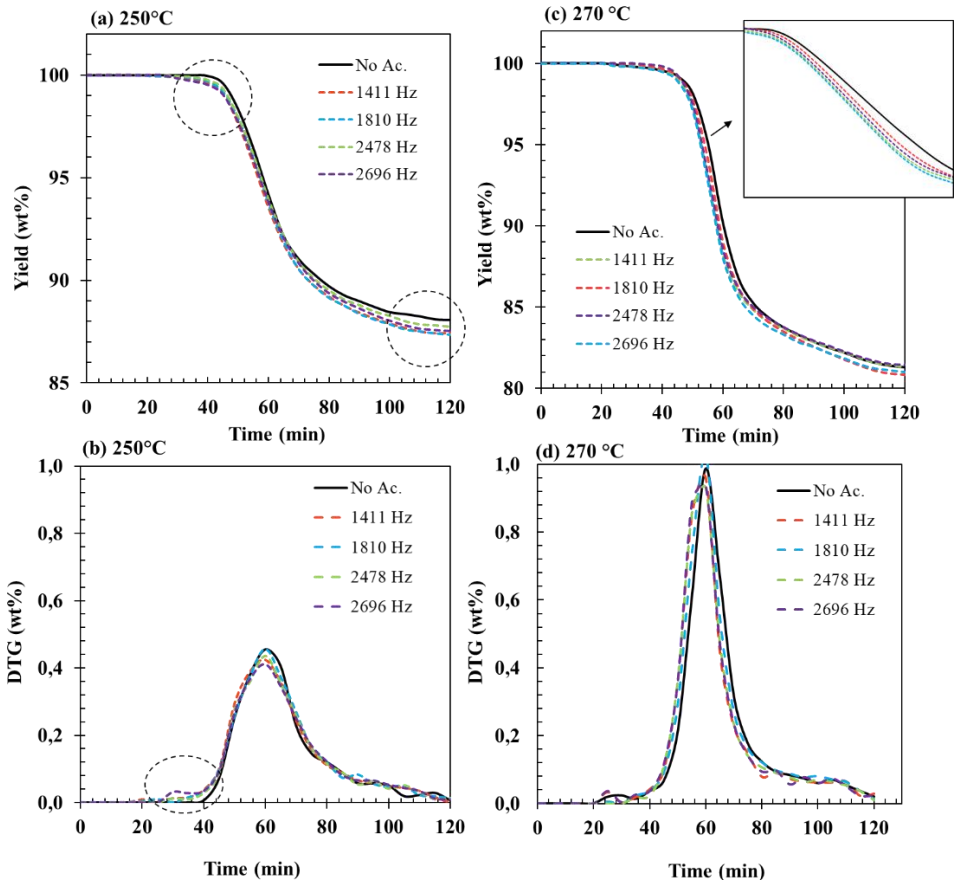

Figure 39. Average solid yield profiles for 250°C (a) and 270°C (c) treatments; Average DTG profiles for 250°C(b) and 270°C (d) treatments.

For the 270°C temperature Figure 39 (c) different behavior were observed for degradation in relation to the temperature of 250°C. After reaching the plateau of 270°C, the acoustic

treatments differ from the control and present a faster and more intense degradation until almost equaling at the end of the process Figure 39 (c).

In Figure 39 (d), the 270°C DTG differences were observed during the process for the treatments without acoustics and under acoustic effect, such as early biomass degradation and exothermic phase for acoustic treatments.

4.3.2 Chemical analysis

The proximate analyses result for all the torrefied samples under acoustic frequencies and statistics summary for the experimental factorial design performed, are shown in Table 8. An analysis of variance (ANOVA) were carried out considering possible interactions between the two explanatory variables: acoustic frequencies (F) and temperature (T). When the temperature condition is assessed, a statistical significance is observed comparing 250 and 270°C treatments, agreeing with (PARIKH; CHANNIWALA; GHOSAL, 2005; ROUSSET et al., 2012). Considering the acoustic treatments for each temperature condition, the results showed that there were no significant differences between acoustic frequencies. The resulting values for ash content were inexpressive, even after the thermal treatment for both temperatures agreeing with (LU et al., 2012) which obtained values close to 0wt% for the temperatures of 250 and 275°C.

Table 8. Properties of the torrefied solid with and without acoustic (Control). Classification by Tukey's test of averaged results considering 3 replicates per treatment. For each group, the means with the same letter in a column were not significantly different at 5% ($\alpha = 0.05$).

Treatments		Proximate analyses (wt%)*		
T(°C)	Frequency	V.M	F.C	Ash
Raw.		81.4	46.03	0.09
250	**Control**	**77.17^{a}**	**22.77^{a}**	**0.054^{a}**
	1411Hz	76.69^{a}	23.24^{a}	0.067^{a}
	1810Hz	76.59^{a}	23.35^{a}	0.059^{a}
	2478Hz	77.40^{a}	22.52^{a}	0.082^{a}
	2696Hz	76.37^{a}	23.56^{a}	0.069^{a}
270	**Control**	**71.12^{b}**	**28.79^{b}**	**0.086^{b}**
	1411Hz	71.21^{b}	28.70^{b}	0.094^{b}
	1810Hz	71.89^{b}	28.02^{b}	0.095^{b}
	2478Hz	71.14^{b}	28.77^{b}	0.093^{b}
	2696Hz	70.07^{b}	29.81^{b}	0.116^{b}

V.M.: volatile matter; F.C.: fixed carbon. * Dry basis.

Table 9 presents the energetic analysis results for the solid product. Considering only the temperature assessment, obtained results for 250 and 270°C showed a good agreement with the 90wt% energy yield obtained by Bergman et al. (BERGMAN; KIEL, 2005) and with

energy yield results of 93.7 and 88.5 obtained by Lu et al., (LU et al., 2012) at 250 and 275°C for eucalyptus.

Parikh et al., (PARIKH; CHANNIWALA; GHOSAL, 2005) reported that HHV is the most important property for biomass as fuel and is highly related to proximate analysis. A higher gain of HHV is usually associated with the percentage gain of FC. In this context, according to Table 8 and Table 9, treatments that had the highest percentage gains in FC also had higher gains in HHV, except for the treatment under 2478Hz frequency at a temperature of 250°C, in which, although the gain of F.C was low in relation to the other treatments, the HHV was higher than the control and 2696Hz treatment. Resulting values for treatments under acoustic influence were superior to the control (without acoustic), except for the frequency 1810Hz at 270°C. Table 9 shows that the best results for HHV occurred at the temperature of 270°C. At the temperature of 250°C the treatments with acoustics did not differentiate between them but were statistically better than the control.

At the temperature of 270°C the treatments 2696 and 1411Hz achieved the best results differing statistically from the control (no acoustic). The 1810Hz frequency was the one that presented the worst result for HHV. In absolute values, the energy yields average for the acoustics treatments were higher than the control, both at the temperature of 250 and 270°C, except for the frequency 1810Hz at the temperature of 270°C.

Table 9. Energy properties. Classification by Tukey's test of averaged results considering 2 replicates per treatment. For each group, the means with the same letter were not significantly different at 5% ($\alpha = 0.05$). Lowercase letters differ in the line and uppercase letters differ in column. (Lowercase letters statistical difference in line and uppercase letters in column).

Treatments	HHV		η_S		η_E	
T(°C)	250	270	250	270	250	270
Frequency						
Control	21.3347^{bB}	22.2893^{aC}	88.06^{a}	81.29^{b}	93.13^{a}	90.09^{b}
1411Hz	21.6207^{bA}	22.4037^{aAB}	87.43^{a}	81.44^{b}	94.02^{a}	90.64^{b}
1810Hz	21.5844^{bA}	22.1638^{aD}	87.38^{a}	80.81^{b}	93.79^{a}	89.61^{b}
2478Hz	21.5703^{bA}	22.3280^{aBC}	87.75^{a}	81.43^{b}	94.11^{a}	90.65^{b}
2696Hz	21.5306^{bA}	22.4326^{aA}	87.54^{a}	81.03^{b}	93.86^{a}	90.45^{b}
Raw	20.09		100		100	

HHV: Higher Heating Value; η_S: Solid yield (wt%); η_E: Energy yield (wt%)

According to the analysis of variance in Table 10 there was a statistical difference only for the temperature when evaluating the immediate analysis parameters (V.M, F.C and Ash content) and solid yield (η_S)). For the energy yield (η_E), there were a statistical difference for both temperature and frequency. and their interaction. Thus. the 1411 and 2696Hz treatments

also showed to be statistically significant for HHV for 270°C when compared to treatments without acoustic and the other two frequencies (1810 and 2478Hz) and were retained for a more detailed analysis in section 4.3.3.

Table 10. Analysis of variance of the temperature (T) and the acoustic frequency (F) parameters, along with their first and second order interactions for the six response variables. CV = Coefficient of variation; * = statistically significant; ns = not statistically significant at 1%. The values correspond to the F test.

Response variable	VM (%)	FC (%)	Ash (%)	HHV	η_S	η_E
T	373.785 *	350.124 *	46.238 *	4133.566 *	3205.022*	835.068 *
F	1.714 ns	1.663 ns	3.092 ns	34.968*	1.322 ns	6.981 *
T x F	1.035 ns	1.005 ns	1.748 ns	27.762*	1.018 ns	2.385 ns
CV (%)	1.42	4.06	19.5	0.13	0.46	0.46

V.M.: volatile matter; F.C.: fixed carbon HHV: Higher Heating Value; η_S: Solid yield (wt%); η_E: Energy yield (wt%)

4.3.3 Optimum frequencies

The chemical analysis showed that both frequencies 1411 and 2696Hz presented the best results considering the energy properties of torrefied biomass. A deep investigation exploring treatment dynamics and chemical correlations diagrams was performed for torrefied final product for these two frequencies.

4.3.3.1 Thermo-acoustic dynamics

The lower and highest identified frequencies in Table 9 (1411Hz and 2696Hz) were selected for a further analysis of the heat treatment. Figure 40 (a) and (b) shows the evolution of the average temperature at the wood sample surface and core for 250 and 270°C respectively.

As expected (TURNER et al., 2010), the temperature at the surface was higher than in the core during the linear heating phase, with and without acoustic frequencies. An inversion of the temperature occurred at treatment temperature due to exothermic reactions inside of the wood sample as identified in (CHAOUCH, 2011; ROUSSET, 2004).

Figure 40 also illustrates a detailed view from temperatures after 230°C for (a) and after 250°C for (b). There is a modification on temperature profiles for treatments under acoustic. Frequencies mainly affected the core temperatures due to the exothermic reactions.

Indeed, a maximum temperature gradient of 2.3°C (270°C - 1411Hz) was observed over the temperature evolution, with and without acoustic. In agreement with literature, the higher the treatment, more evident is the exothermic pic due to exothermic reactions inside of the wood (CHAOUCH, 2011). The heat release effect of this exothermic reactions can be seen as well at the surface temperature when the treatment is performed for the higher temperature of 270°C

(heat release from the inside of the wood affect the surface temperature). The time taken to reach the treatment temperature level was reduced by 2 min for 250°C and 2.3 min for 270°C treatments.

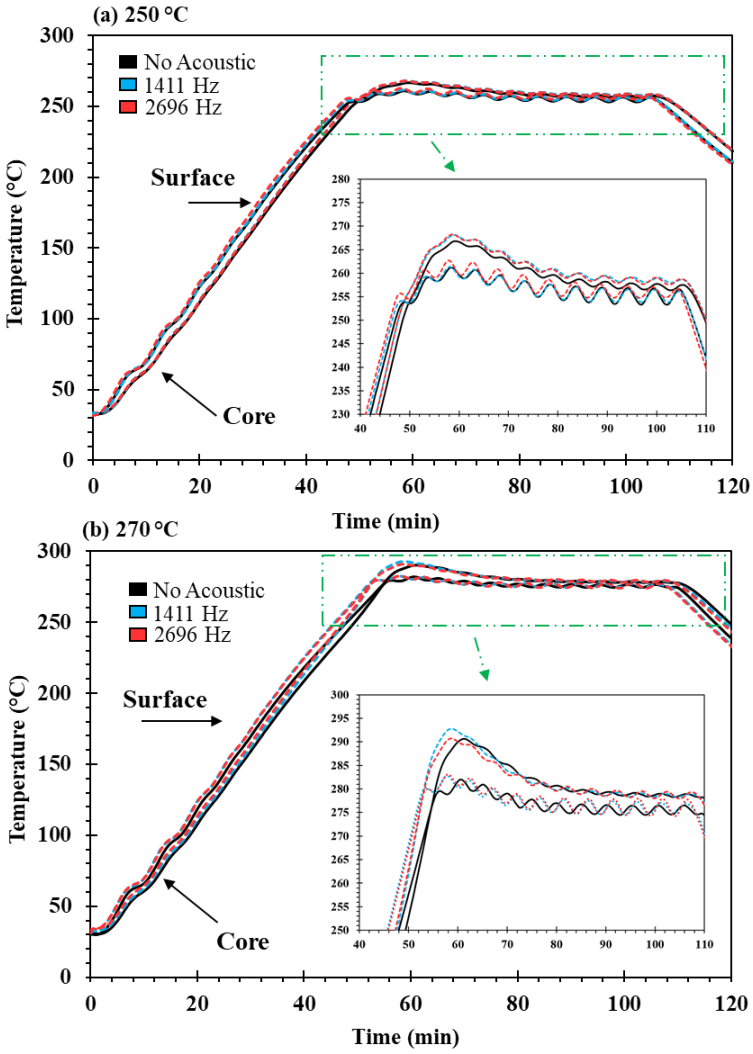

Figure 40. Average of the surface and core temperature profiles for treatments without acoustic (No Acoustic) and treatments with 1411Hz and 2696Hz frequencies performed at 250°C (a) and 270°C (b). Dashed-double-dot arrows indicate the zoomed-in profiles.

The effect of the acoustic field combined with the different treatment temperatures was also assessed from the solid yield and conversion rate of the wood samples. Figure 41 shows the evolution of the solid yield as a function of time along with the differential thermal gravimetry calculated from the derivative of the solid yield curves during time for 250°C (a) and 270°C (b) treatments.

For the torrefaction experiments without acoustics (continuous black line), wood starts to decompose after 180°C as described by (CHEN; PENG; BI, 2015). The mass loss increases with increasing temperature and mass loss percentage of 11.5wt% for 250°C and 18.71wt%

for 270°C obtained for torrefaction without acoustics agree with studies for *Eucalyptus grandis* at the same conditions (ALMEIDA; BRITO; PERRÉ, 2010; RODRIGUES; ROUSSET, 2009; ROUSSET et al., 2012). Considering the solid yield profiles for 250 and 270°C treatments, an earlier degradation is observed for treatments under 1411 and 2696Hz frequencies.

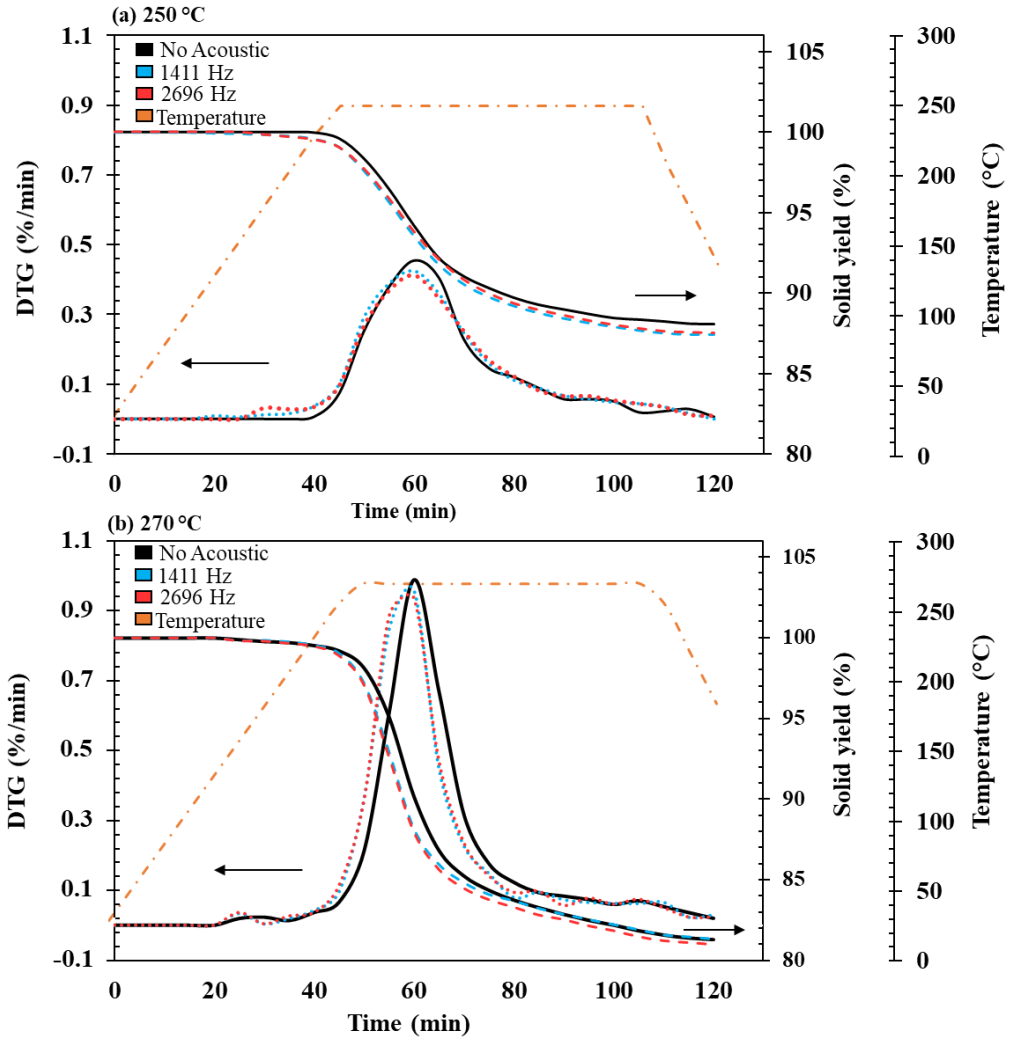

Figure 41. Solid yield (%) and solid yield deviation (g/min) for treatments without acoustic (No Acoustic) and treatments with 1411Hz and 2696Hz frequencies performed at 250°C (a) and 270°C (b).

Solid yield profiles for treatments under acoustic influence has a comparable comportment for both temperatures and shows an interesting shift in time comparable to treatments performed with different heating rates. Similar shifts were reported by (CHAOUCH, 2011) for poplar wood under 230°C temperature treatment with a heating rate of 1°C.min^{-1} and 2°C.min^{-1}. In fact. the temperature gradient founded in the temperature profiles (Figure 40) can explain these results for the solid yield.

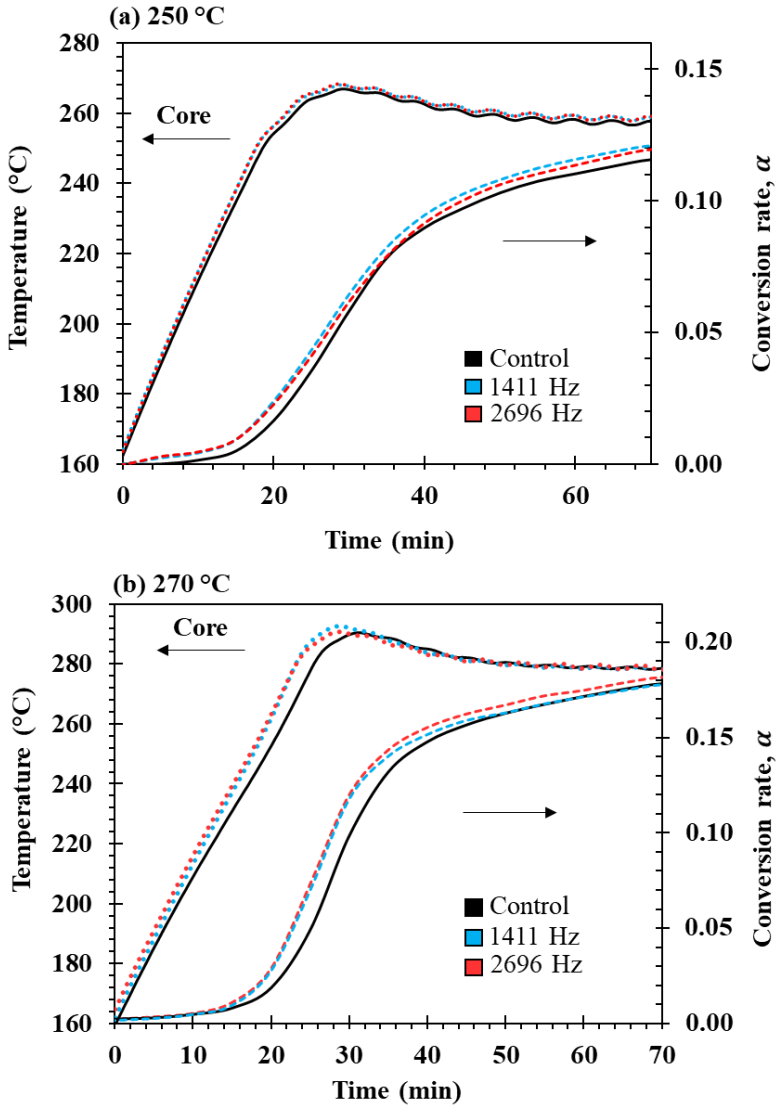

Figure 42. Conversion rate for treatments without acoustic (control) and treatments with 1411Hz and 2696Hz frequencies performed at 250°C (a) and 270°C (b).

In both cases under acoustic influence, the tendency revealed an increase in differential thermal gravimetry showing two small peaks in the beginning of degradation for 250°C and a shift in time showing an earlier degradation for both temperatures. For 250°C the peak is less intense compared to 270°C peak, showing a stronger degradation for higher temperatures.

The calculated conversion rate α and wood core temperature are illustrated in Figure 42 **Figure 41** (a) for 250°C and (b) for 270°C. As the torrefaction process is assumed to start at about 180°C (CHEN; PENG; BI. 2015), the yield at 160°C was normalized as the initial yield, and the time was counted as $t = 0$ for a better reability of the results.

Resulting values for the conversion rates agree with literature for no acoustic treatments at the same conditions (ROUSSET et al., 2012). Treatments performed under acoustic shows a noticeable difference compared to the control experiment (no acoustic). Higher conversion

rates were obtained for 270°C experiments due to the higher temperatures registered inside of the wood leading to a higher releasing of volatiles (Figure 31).

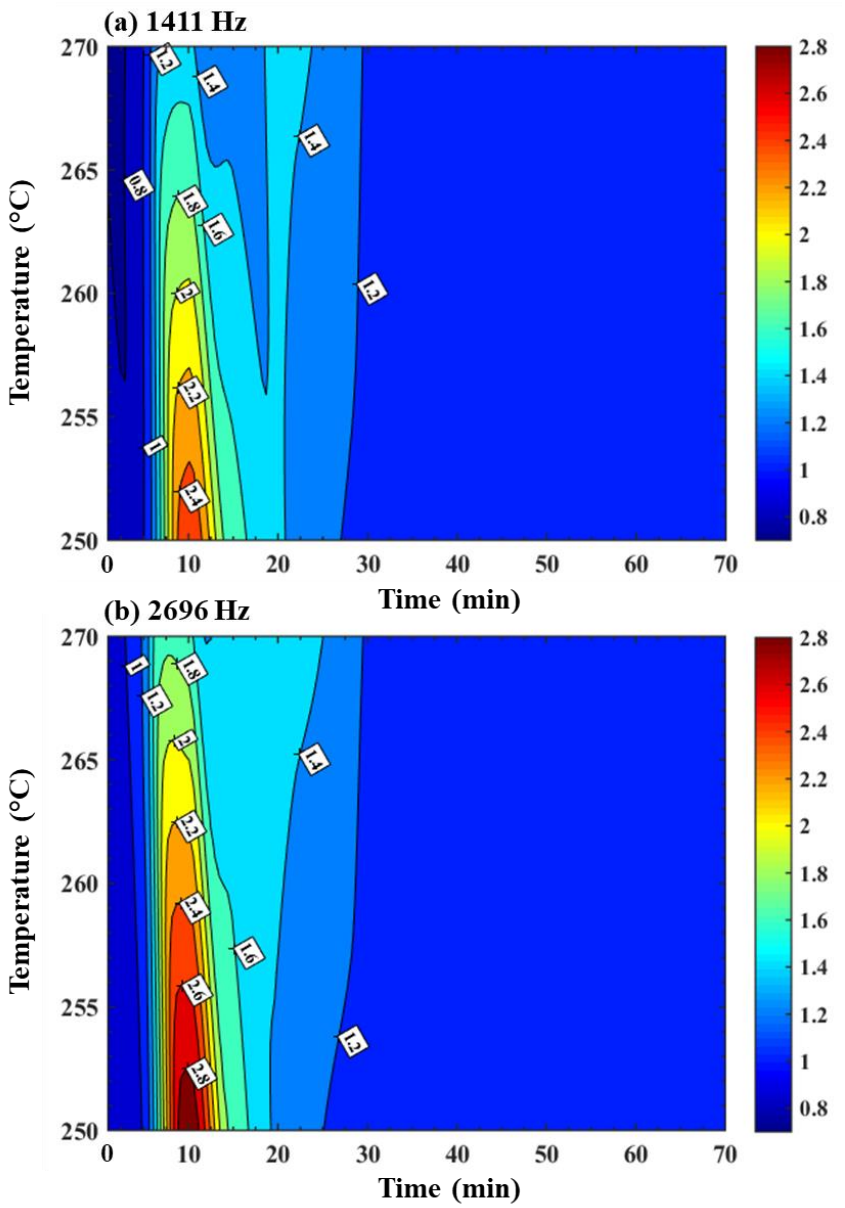

Figure 43. Calculated conversion rates enhancements for treatments (a) 1411Hz and (b) 2696Hz performed at 250°C and 270°C.

For a better comparison beetwen treatments with and without acoustic the conversiton rates enhancements were calculated and are illustrated in the Figure 43**Figure 42** for (a) 1411Hz and (b) 2696Hz treatments. Results shows a similar behavior for both acoustic treatments an enhancement factor of 2.4 and 2.8 for 250°C and 270°C respectively. In other words, the conversation rate can be intensified up to 140% for 250°C and 180% for 270°C in the beginning of torrefaction when compared to experiments without acoustic.

As can be noticed in temperature profiles results as well as for the solid yield and conversion rates analysis, the main stage of treatment affected by the acoustic influence was the linear heating and the begging of the settled temperature treatment for both temperatures. Treatment performed under 2696Hz were more effective showing a higher modification for temperature profiles and for the solid conversion rates.

An important aspect to be pointed out is that the acoustics affected the middle of the torrefaction treatment, showing very similar solid yield for the final products and final temperatures. The results are interesting if the objective of the applied thermal modification is to reduce treatment time. For example, to achieve 10wt% of mass loss treatment time was reduce up to 4 min for 250°C and 2.8 minutes for 270°C. Similar patterns and treatment reducing time are reported when torrefaction treatment is performed with different heating rates for standard torrefaction (CHAOUCH, 2011).

4.3.3.2 Solid product pyrolysis

The thermogravimetric (TGA) and derivative thermogravimetric (DTG) analyses results are illustrated in Figure 44 for the pyrolysis of thermo-acoustic torrefied product treatment at 250 and 270°C.

Those analysis allowed to obtain more information about the effect of the interaction between acoustic waves and temperature on the torrefied eucalyptus wood. The same analysis was performed for the standard torrefaction procedure and was discussed in the section 4.2.3 and illustrated in Figure 34.

Comparing the solid yield behavior, it is possible to conclude from Figure 34 that the treatments performed with higher temperature intensities had a lower degradation (wood components had a higher consumption during the torrefaction) when the pyrolysis of the torrefied product was performed. Figure 44 (a) and (b) illustrate that the experiments performed under acoustic influence had a slight lower degradation presenting the behavior of a more intensive treatment when compared to the control.

Figure 44 (b) and (d) displays the solid yield DTG for the 250 and 270°C treatment without (control) and with (1411 and 2696Hz) acoustic. Comparing with the Figure 34 it is possible to observe that the difference during wood components degradation were obtained for the cellulose (peak). The acoustic treatments showed a higher degree of degradation being difficult to point out which treatment was better due to the slight difference. The chemical analysis discussed in the next section provided more information to understand the physical phenomena.

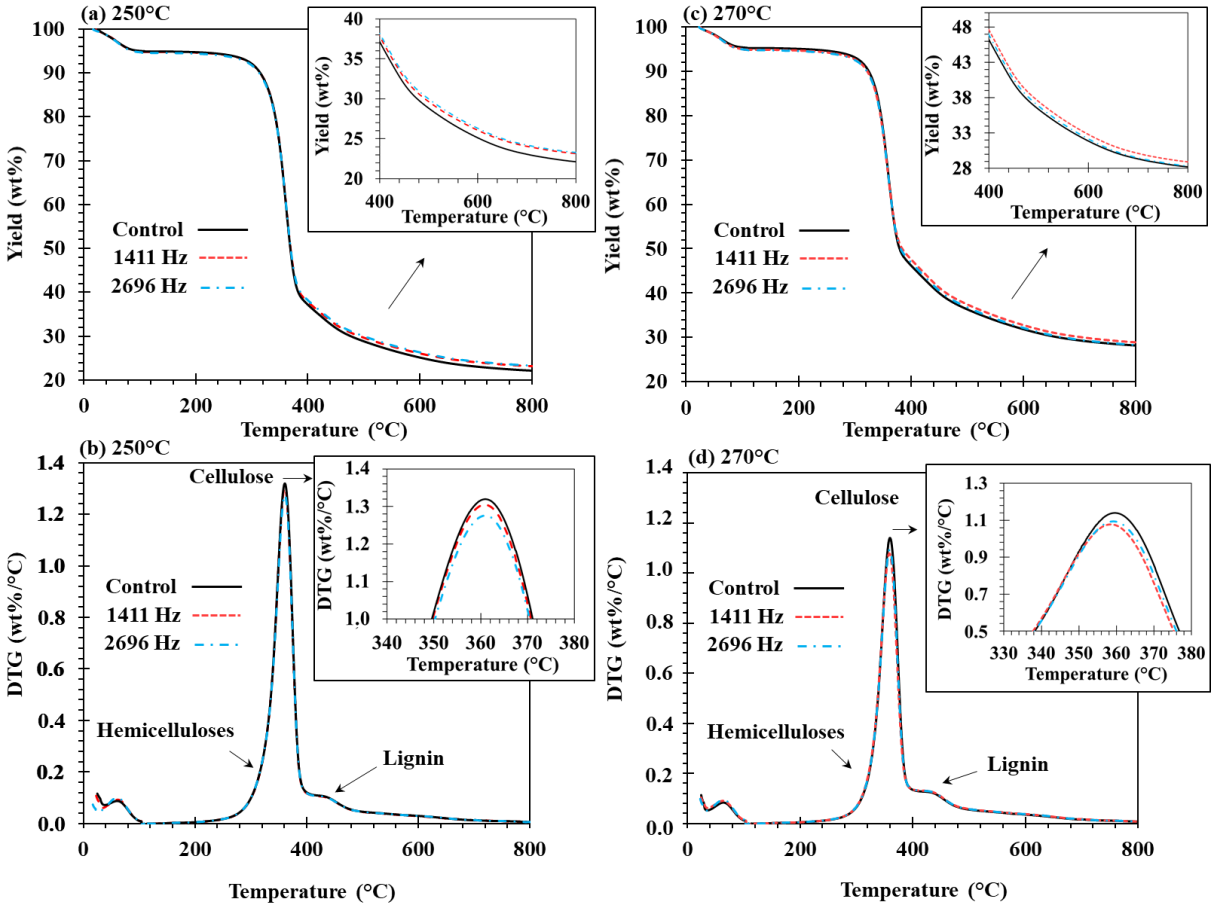

Figure 44. (a) Solid yield in function of the temperature (b) detailed DTG (200-600°C) of thermo-acoustic torrefied product (250°C) pyrolysis.

4.3.3.3 Chemical analysis interpretation

Figure 45 illustrates for the identified optimum frequencies the listed values (Table 8) of VM and FC contents (Figure 45 (a)) and the atomic oxygen-to-carbon (O/C) and hydrogen-to-carbon (H/C) (Figure 45 (b)) correlations for optimum frequencies. Raw biomass volatile matter content is higher when compared to treated wood, while its FC content is lower agreeing with (ALMEIDA; BRITO; PERRÉ, 2010; CHEN; LU; TSAI, 2012a; PARIKH; CHANNIWALA; GHOSAL, 2005). During biomass torrefaction a dehydration process takes place releasing moisture and light volatiles from raw materials.

As can be seen in Figure 45 (a), treatments performed with acoustic coupled to temperature presented a higher degradation aspect. The linear tendency shows a increasing torrefaction agreeing with solid yield curves (Figure 41). Resulting values are in agreement when analyzing the torrefaction dynamics and chemical analysis.

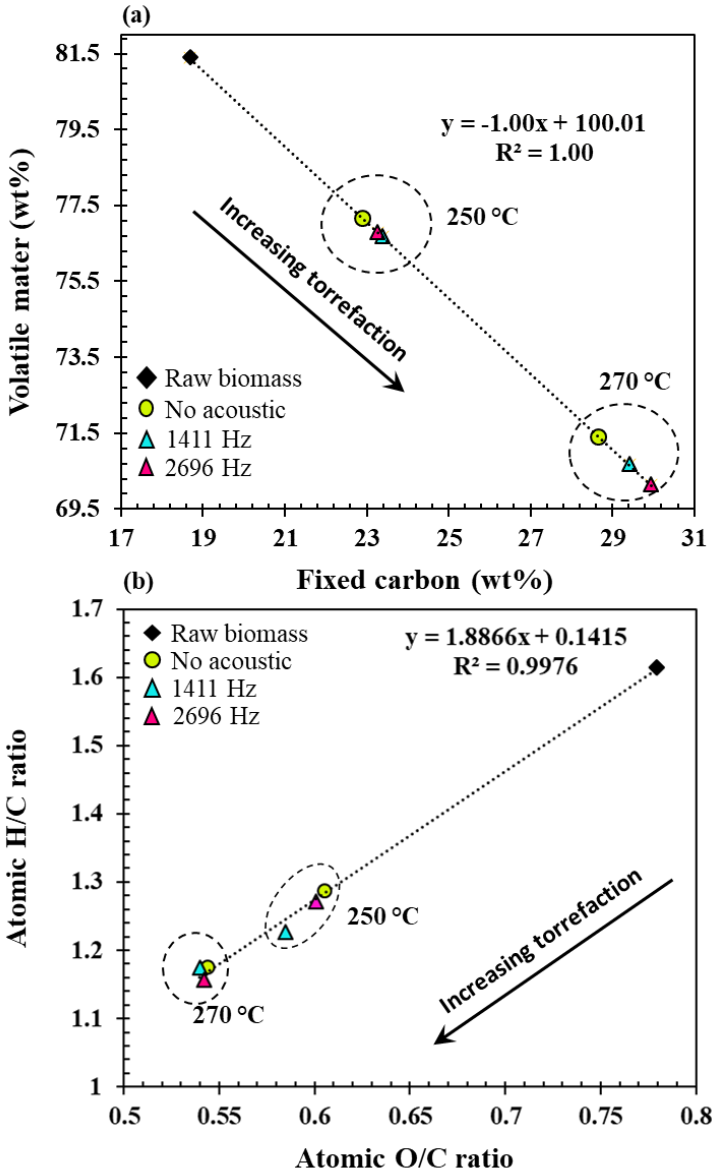

Figure 45. Results for fixed carbon (F.C) versus volatile matter (V.M) (a) and van Krevelen diagram (b) for optimum frequencies treatment.

For 250°C the 1411Hz treatment reported better resutls when compared to 2696Hz treatment and the oposite for the 270°C. This can be explained due to the different comportments that de acoustic field have for different temperature atmospheres or due to the different organic compounds that are released for the different temperature conditions. The hypothesis is that the acoustic energy helps the heavier compounds (cellulose decomposition takes place) released during 270°C.

The van Krevelen diagram is illustrated in Figure 45 (b). After undergoing torrefaction, moisture and light volatiles, which contain more hydrogen and oxygen are removed from biomass, whereas relatively more carbon is retained (CHEN; PENG; BI, 2015). The obtained values for the atomic oxygen-to-carbon (O/C) and hydrogen-to-carbon (H/C) ratios for raw

biomass and torrefied biomass showed a linear regression (R^2 = 0.9976) corroborated with the literature (CHEN; LU; TSAI, 2012a; MCKENDRY, 2002; PARIKH; CHANNIWALA; GHOSAL, 2005). Figure 45 (b) shows that the 1411Hz treatment has a higher impact when compared to the highest frequency (2696Hz) at 250°C. For the 270°C treatment, not significant difference was reported.

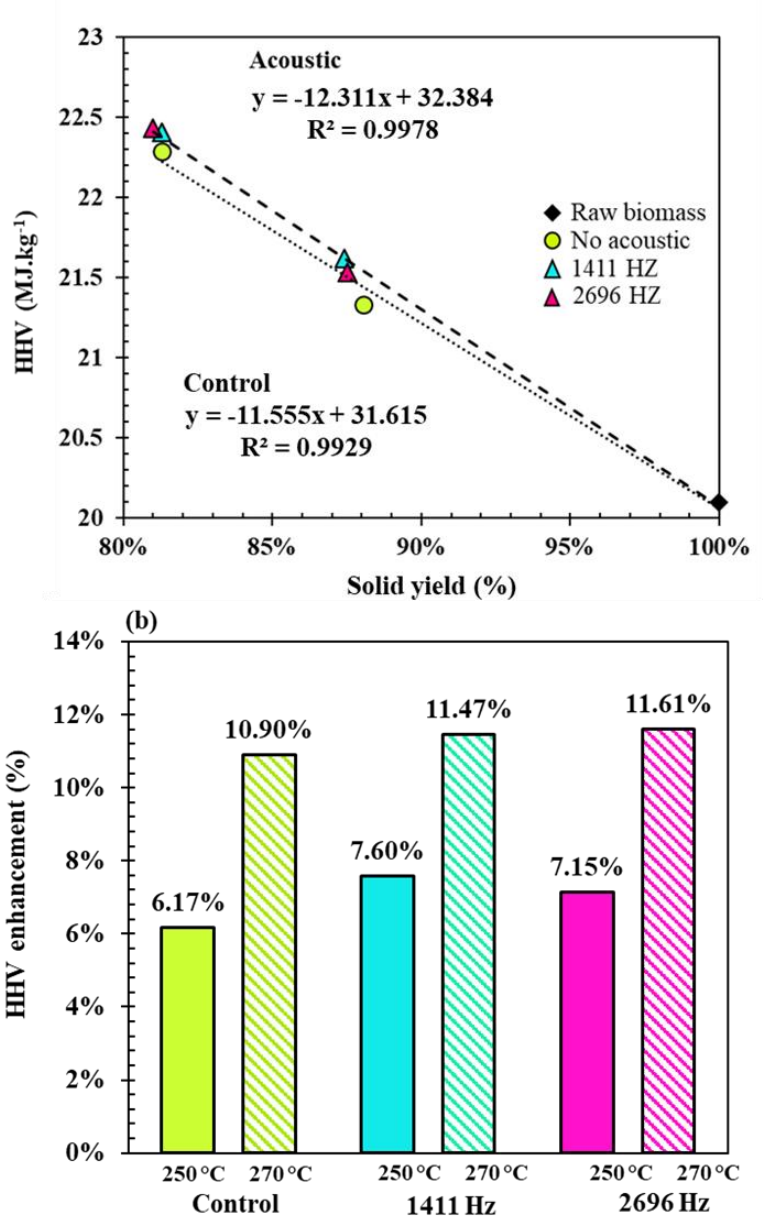

Figure 46. Higher heating value in function of the solid yield (a) and HHV enhancement (solid bar – 250°C treatment, hatched bar - 270°C treatment) (b) for the identified optimum treatments and control treatments.

Figure 46 displays the higher heating value (HHV) as a function of the solid yield (a) and de HHV enhancement (b) for treatments performed under 1411Hz and 2696Hz. Making a comparison between temperature treatments (control) and coupled treatments (temperature and acoustic), it is possible to notice the same behavior for Figure 46 (a) and (b) where for the

250°C temperature treatment coupled to 1411Hz frequency a higher value for the HHV as well as for the HHV enhancement (solid bar) are reported. For the 270°C temperature treatment, the 2696Hz frequency had better result for both parameters.

From an industrial point of view, the ideal energy aspect is to obtain a high energy yield at a low solid volume (higher mass losses) dispending less energy during pre-treatment process. Lu et al, (LU et al., 2012) determined an energy-mass co-benefit index (EMCI) that means the difference between the energy yield and the solid yield ($EMCI = \eta_E - \eta_S$). This INDEX was defined to seek the optimum condition operation between torrefaction treatments where a higher EMCI represent a better treatment to be applied to the raw material.

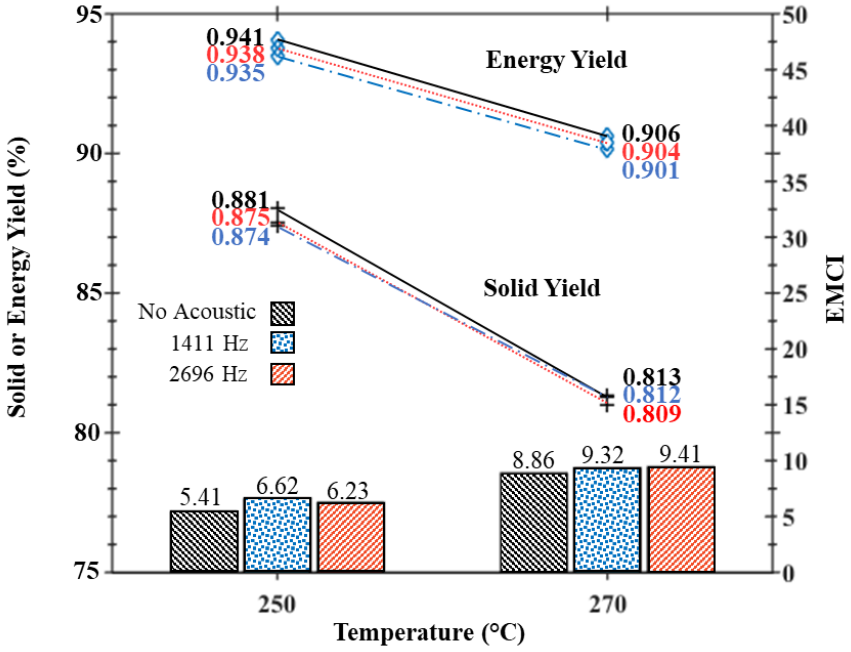

Figure 47. Solid and energy yields and energy-mass co-benefit indexes (EMCI) of eucalyptus in for standard ad acoustic (optimum frequencies) treatment.

Figure 47 illustrates the solid and energy yields and the calculated energy-mass co-benefit indexes (EMCI) of *Eucalyptus grandis* for torrefaction treatments under temperature influence and coupled temperature and frequencies (1411 and 2696Hz).

During torrefaction, the weight loss will lessen the energy yield, whereas the enhancement of HHV facilitates energy yield (CHEN; PENG; BI, 2015). Seeing that the impact of the former on energy yield is over the latter, the energy yield decreases with increasing temperature and duration. For 250°C treatment, the bar chart in Figure 47 shows a maximum value of 6.62 EMCI (1411Hz treatment) and for 270°C treatment a maximum value of 9.41 EMCI (2696Hz) implying that optimum operations occur at these conditions. This result agrees with the entire torrefied product assessment.

4.4 Biomass numerical model

4.4.1 Biomass kinetic model validation

For the kinetic model validation experimental data from (CHAOUCH, 2011) were used. Experimentally recorded temperature and solid yields profiles during the heating process are shown in Figure 48. Experimental data comes from a Macro-TGA experiments. Wood heat treatment was carried out at five different temperatures: 200, 210, 220, 230 and 240°C.

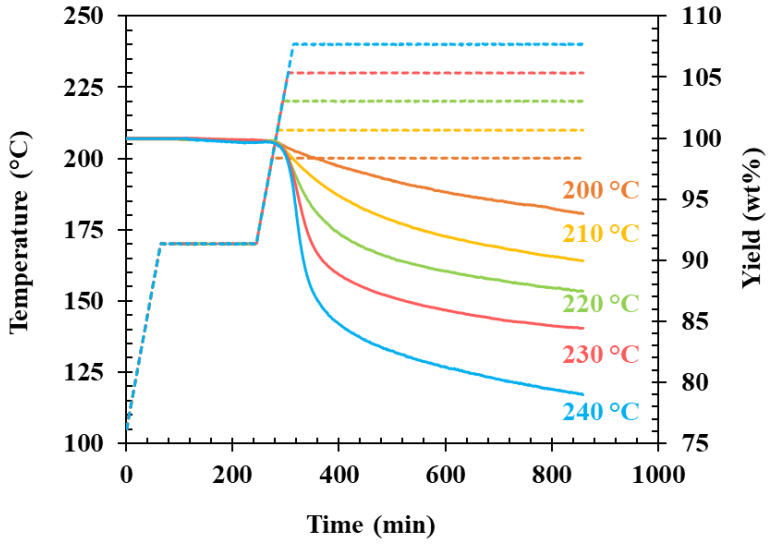

Figure 48. Temperature profiles and solid yield during heat treatment of poplar (CHAOUCH et al. 2010).

4.4.1.1 Definition of model parameters

First of all, kinetic parameters were determined for each treatment temperature individually. Pre-exponential factors and activation energies were initialized using data from the literature (COLIN et al., 2015) and upgraded by the minimization of $diff^{(T)}$ (Eq. 29) using a multidimensional unconstrained nonlinear minimization solver Nelder-Mead (Matlab® software) with admitted convergence criterion of 10^{-4}. The numerical method is illustrated in Figure 49.

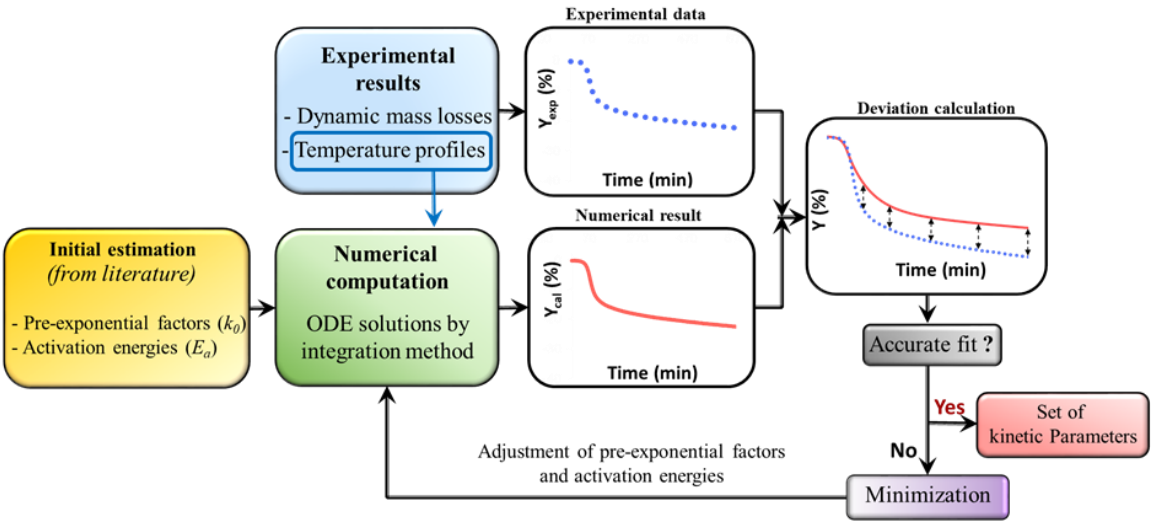

Figure 49. Numerical schematic flow for kinetic model.

The results obtained with this individual approach are presented in Figure 50. For a better readability of the figure, mass yields evolutions are presented after the thermal stabilization plate of 170°C. Indeed, as mentioned above, no significant mass loss can be observed for temperatures lower than 170°C.

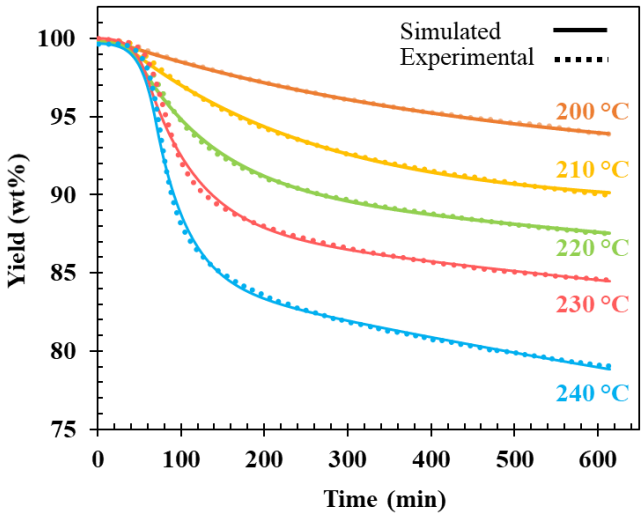

Figure 50. Numerical kinetics simulation (solid line) fitted with experimental data (dotted line) for individual analysis.

For a deeper observation of kinetic parameters variation, pre-exponential factors and activation energies of all considered temperatures have been compared in Figure 51 and Figure 52. Whatever the considered reaction, a gap is observed between the parameters obtained for the low temperatures (200 and 210°C) and those obtained at high temperature (220, 230 and 240°C). This first numerical step suggests the existence of two thermal sensitivity groups. in which the reactions differ.

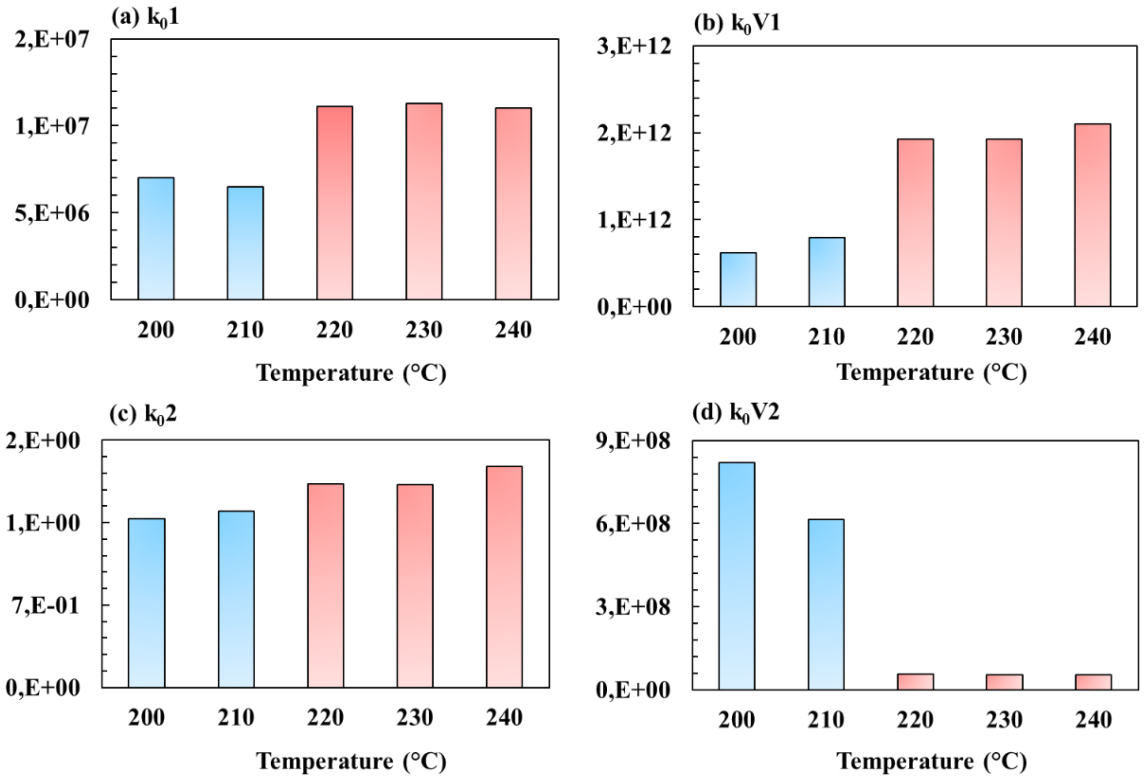

Figure 51. Comparison for obtained pre-exponential factors for individual kinetics analysis.

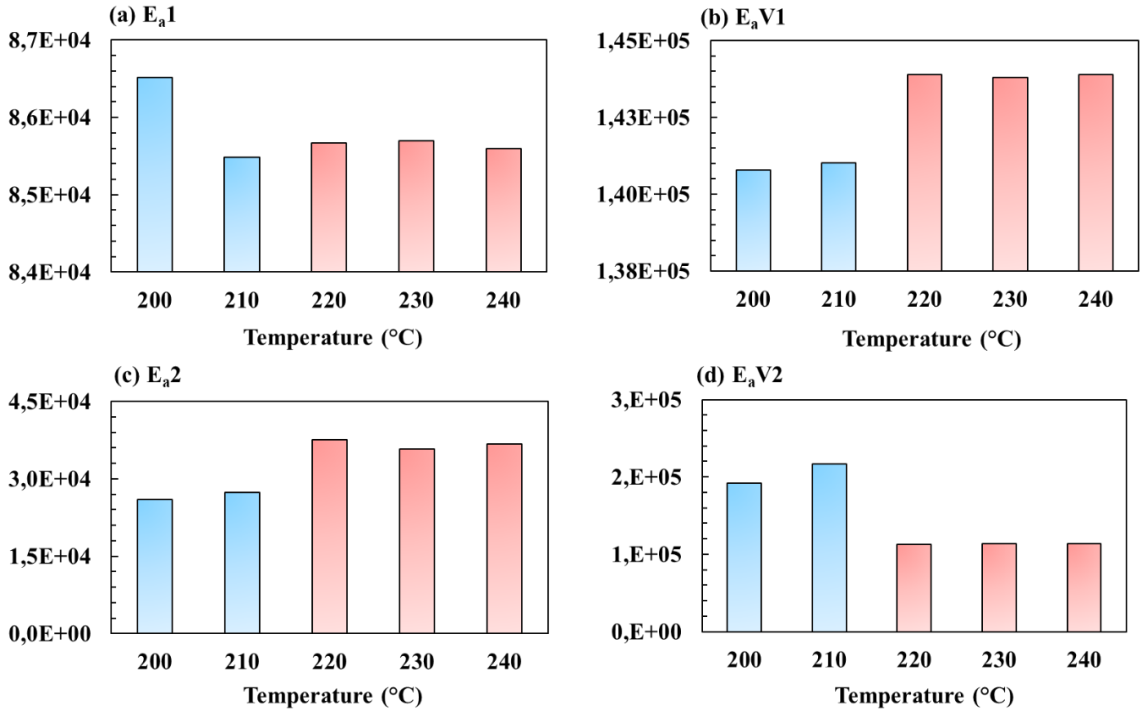

Figure 52. Comparison for obtained activation energies for individual kinetics analysis.

4.4.1.2 Optimization of model parameters

Even if the previous results were satisfying, two major drawbacks have to be noticed. From a scientific point, such a simulation assesses that different reaction paths exist depending on the treatment temperature. Moreover, for industrial applications, this involves that information about kinetic parameters are required for each temperature and each wood species. The target of the following step is thus to determine a common set of kinetic parameters leading to an accurate mass yield prediction whatever the treatment temperature ranging between 200 and 240°C. In order to achieve this objective, for a given set of kinetic parameters, mass yield profiles are calculated for all the temperatures. The deviations $diff^{(T)}$ are then determined and a global deviation between experimental and numerical results for all the temperatures is computed according to Eq. (41).

$$deviation = diff^{(200)} + diff^{(210)} + diff^{(220)} + diff^{(230)} + diff^{(240)} \quad (41)$$

As previously, the Nelder-Mead solver was used to find the optimal set of kinetic parameters. To improve the solution finding, a change of variable (Eq. (42)) has been applied (REVERTE, 2007).

$$\begin{cases} k_{m,i} = \ln(k_{0,i}) \\ E_{m,i} = \frac{E_{a,i}}{R} \end{cases} \quad (42)$$

Where $k_{m,i}$ and $E_{m,i}$ are respectively modified (subscript m) kinetic constant and activation energy of the i^{th} (subscript i) peudo-component. This modification aims to reduce the difference of order of magnitude between the values of pre-exponential factors and activation energies. Rate constants k_i with modified Arrhenius law becomes Eq. (43):

$$k_i(T) = exp(k_{r,i}).\, exp\left(\frac{-E_{r,i}}{T}\right) \quad (43)$$

in a direct approach, the procedure to find a common set of kinetic parameters was initialized with data available in the literature. Simulated and experimental solid yields (Figure 53) show

an acceptable agreement only for the lowest temperatures. A careful analysis of the solver convergence allowed to observe that multiple solutions are possible according to the parameters initialization. For this reason, a strategy based on the thermal sensitivity was built up. The method leading to the best results is schematically represented in Figure 54.

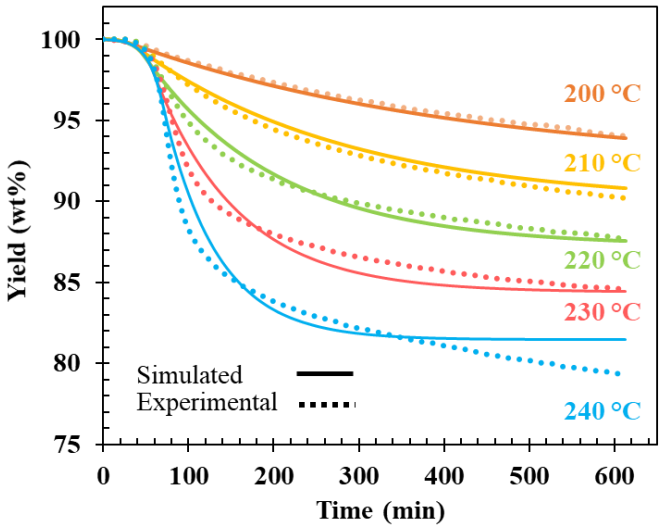

Figure 53. Simulated and experimental solid yields applying direct approach method.

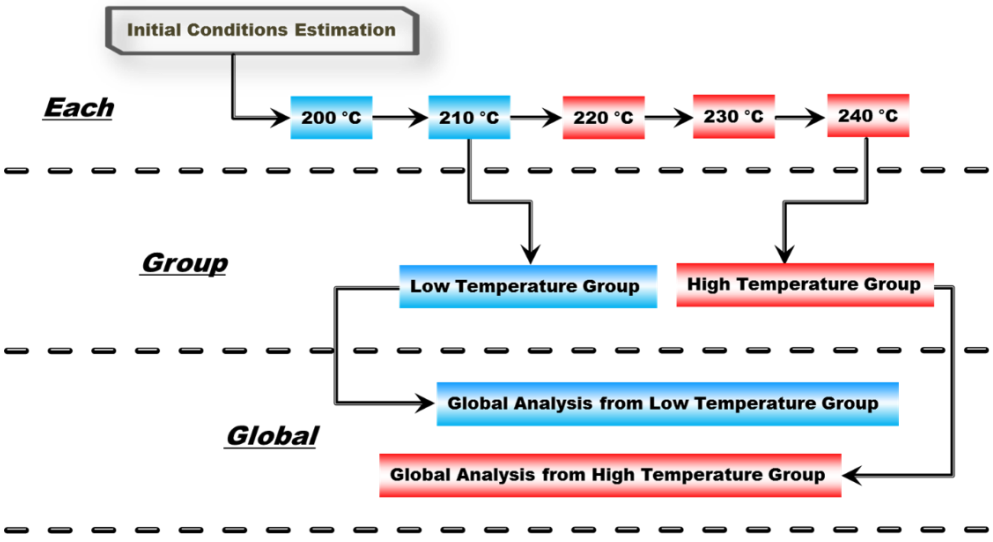

Figure 54. Methodology for the numerical thermal sensitivity analysis.

Kinetic parameters are firstly determined according to the individual approach temperature by temperature. The kinetic parameters obtained for the treatment at 240°C are then used as initialization to find an optimal set of parameters for the group of high temperatures (220, 230 and 240°C) identified in the previous step.

Finally, these kinetic parameters are used as initialization to determine a unique set for all the studied temperatures. Simulation results of this approach are shown in Figure 55. Good results accordance is achieved between experimental and numerical results. The largest divergence between experimental and calculated values appears for a heat treatment at 210°C.

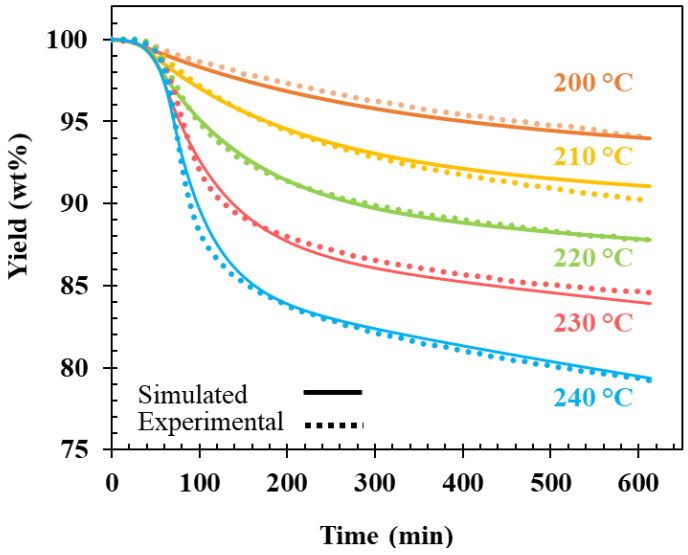

Figure 55. Simulated and experimental solid yields applying thermal sensitivity analysis.

Actually, it seems important to notice that the dispersion of experimental results at 210°C is more pronounced and leads to deduce that calculated values are included into the experimental uncertainty. The larger uncertainty at this temperature is assumed to be a consequence of the change in the reaction path previously identified.

It should be emphasized that a good fitting has been achieved both at the beginning and at the end of the treatment process. This observation confirms that the chosen model is able to consider from a macroscopic point of view, all thermodegradation reactions occurring in the treatment temperatures range 200 to 240°C. Owing to the better simulation quality and reasonable computation time, the set of kinetic parameters obtained using the thermal sensitivity approach is retained.

4.4.1.3 Characteristics of kinetics parameters

To provide a better understanding of obtained kinetic values and establish an equivalent comparison, pre-exponential factors and activation energies issued from the literature are presented in Table 11**.** Studied species and treatment conditions are detailed in the table.

Comparison between poplar and pure xylan (major constituent of hardwoods hemicelluloses) points out that in both materials activation energy associated to k_1 is bigger than in k_2 and activation energy in k_{V1} is bigger than in the k_{V2}. Some authors observed, for other species, another behavior giving activation energy of k_1 smaller than that of k_2 (BACH et al., 2016; BATES; GHONIEM, 2012; SHANG et al., 2013). It is important to keep in mind that kinetic parameters values result from a numerical minimization function.

Table 11. Literature of kinetic parameters.

Material	Experimental condition	Kinetics parameter	Reference
Poplar	Temperature: 200-240°C Heating rate: 1°C min^{-1} Isothermal period: 10 h	$k_1 = 1.04\times10^{7}\exp(\frac{-85850}{RT})$ $k_{v_1} = 1.91\times10^{12}\exp(\frac{-144130}{RT})$ $k_2 = 2.05\times10^{1}\exp(\frac{-36060}{RT})$ $k_{v_2} = 7.00\times10^{7}\exp(\frac{-114890}{RT})$	Present study
Xylan	Temperature: 200-340°C Heating rate: 40 to70°C s^{-1} Isothermal period: 800-2000 s	$k_1 = 1.74\times10^{4}\exp(\frac{-66235}{RT})$ $k_{v_1} = 3.31\times10^{6}\exp(\frac{-91540}{RT})$ $k_2 = 3.43\times10^{2}\exp(\frac{-56396}{RT})$ $k_{v_2} = 5.87\times10^{1}\exp(\frac{-52628}{RT})$	DI BLASI et al., 1997
Willow	Temperature: 230-300°C. Heating rate: 10°C min^{-1} Isothermal period: 10-50 min	$k_1 = 2.48\times10^{4}\exp(\frac{-75976}{RT})$ $k_{v_1} = 3.23\times10^{7}\exp(\frac{-114214}{RT})$ $k_2 = 1.1\times10^{10}\exp(\frac{-151711}{RT})$ $k_{v_2} = 1.59\times10^{10}\exp(\frac{-151711}{RT})$	BATES et al., 2012

Wheat straw	Temperature: 250-300°C. Heating rate: 10 and 50°C min^{-1} Isothermal period: 90 min	$k_1 = 3.48\times10^{4}\exp(\frac{-70999}{RT})$ $k_{v_1} = 3.91\times10^{10}\exp(\frac{-139460}{RT})$ $k_2 = 4.34\times10^{3}\exp(\frac{-76566}{RT})$ $k_{v_2} = 3.48\times10^{7}\exp(\frac{-118620}{RT})$	SHANG et al., 2013
Spruce	Temperature: 220-300°C. Isothermal period: 120 min	$k_1 = 1.04\times10^{1}\exp(\frac{-20792}{RT})$ $k_{v_1} = 1.26\times10^{7}\exp(\frac{-90262}{RT})$ $k_2 = 2.76\times10^{4}\exp(\frac{-70605}{RT})$ $k_{v_2} = 3.48\times10^{6}\exp(\frac{-93473}{RT})$	BACH et al., 2016
Birch	Temperature: 220-300°C. Isothermal period: 120 min	$k_1 = 2.25\times10^{7}\exp(\frac{-87705}{RT})$ $k_{v_1} = 1.02\times10^{10}\exp(\frac{-119850}{RT})$ $k_2 = 2.39\times10^{1}\exp(\frac{-93506}{RT})$ $k_{v_2} = 1.03\times10^{8}\exp(\frac{-109617}{RT})$	BACH et al.. 2016
Beech	Temperature: 220-260°C. Isothermal period: 80 min	$k_1 = 2.48\times10^{10}\exp(\frac{-76000}{RT})$ $k_{v_1} = 3.94\times10^{7}\exp(\frac{-11400}{RT})$ $k_2 = 1.10\times10^{10}\exp(\frac{-151700}{RT})$ $k_{v_2} = 4.12\times10^{6}\exp(\frac{-11400}{RT})$	REPELLIN et al., 2010
Pine	Temperature: 250-300°C. Heating rate: 10-50°C min^{-1} Isothermal period: 90 min	$k_1 = 7.714\times10^{1}\exp(\frac{-46854}{RT})$ $k_{v_1} = 2.68\times10^{8}\exp(\frac{-122110}{RT})$ $k_2 = 1\times10^{-5}\exp(\frac{-0.0061}{RT})$ $k_{v_2} = 5.75\times10^{4}\exp(\frac{-94396}{RT})$	SHANG et al., 2014

The separate consideration of pre-exponential factor and activation energy is not suitable because there is a possibility of compensation between them. For a better interpretation of the competition between the occurring reactions, the kinetic rates are graphically disposed in an Arrhenius plot for temperatures between 200-240°C (Figure 56).

It is thus possible to observe that, for Poplar heat treatment, similarly to the pure Xylan, the ranking of reaction rates from largest to smallest is $k_1 > k_{v1} > k_2 > k_{v2}$. The kinetic rates indicate that the first reaction step $A \rightarrow B$ and $A \rightarrow V_1$ is faster than the second $B \rightarrow C$ and $B \rightarrow V_2$ as pointed out by (BACH et al., 2016; SHANG et al., 2013). From the Arrhenius plot, it can be concluded that when the temperature increases, the second step becomes more important, especially the reaction that leads to the formation of V_2.

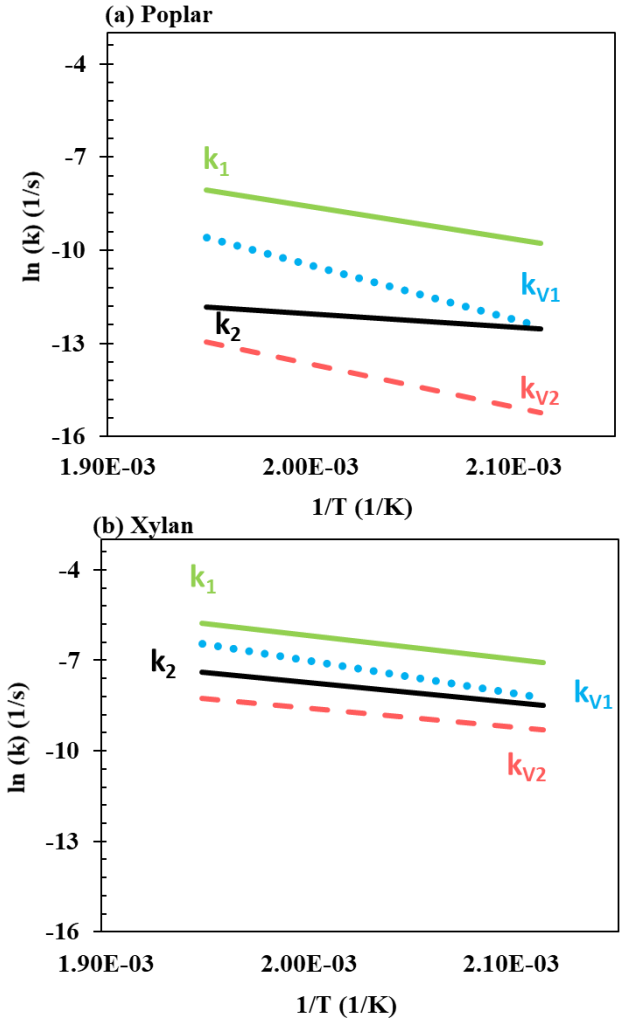

Figure 56. Reaction rates competition for (a) Poplar and (b) Xylan (DI BLASI et al., 1997).

4.4.2 Eucalyptus Kinetics

The thermo-acoustics torrefaction experiments were performed using the *Eucalyptus grandis* wood species. Solid and volatile yield dynamics as well as chemical analysis showed that the interaction between temperature (T) and frequency (F) during the thermo-acoustic torrefaction had a slight higher and faster degradation.

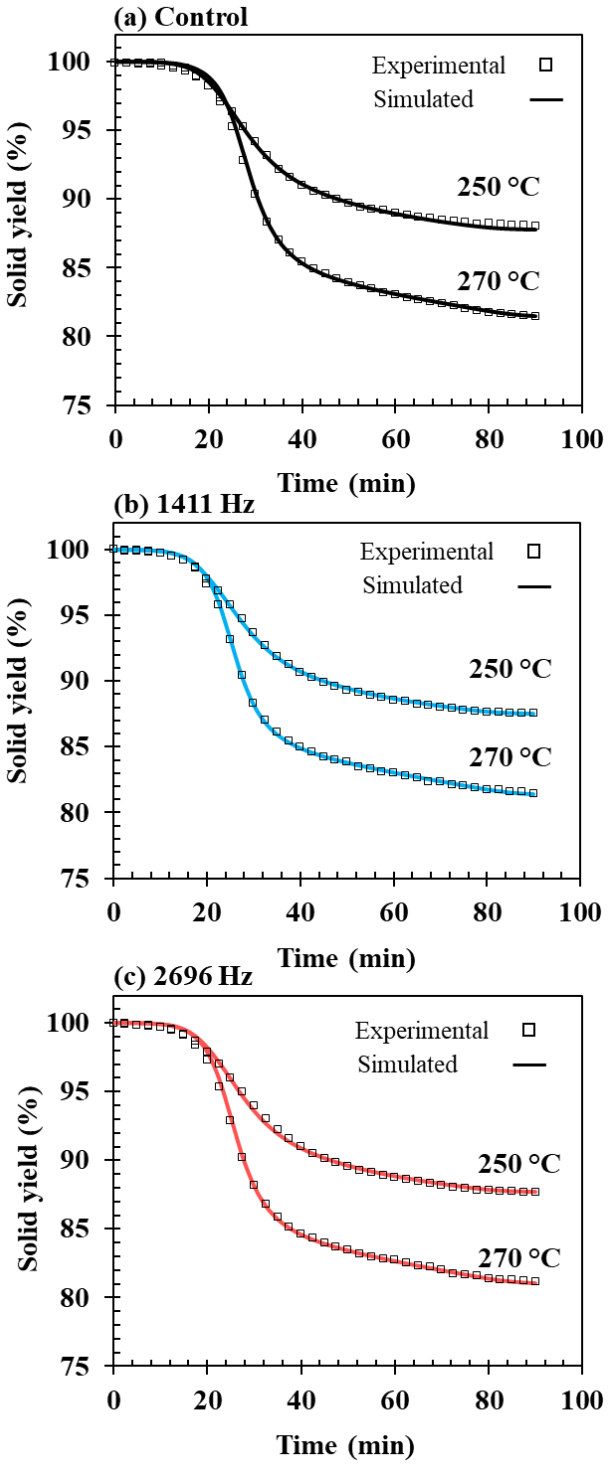

Figure 57. Simulated and experimental curves for control (a) and acoustic treatments (b) 1411 and (c) 2696Hz.

A calculus of kinetic parameters and a numerical kinetic simulation were performed to obtain more information about the eucalyptus wood thermodegradation under the temperature, as well as, coupled temperature and frequency interaction effect. For that, the validated thermal sensitivity model in section 4.4.1 was used to calculate the kinetic parameters and simulate the solid yield. The experimental data (Figure 41) from standard torrefaction (control) and for the identified optimum frequencies (1411 and 2696Hz) of the coupled thermo-acoustic torrefaction were used as input data. The resulting fitted curves are presented in Figure 57. As mentioned in section 4.4.1. no significant mass loss can be observed for temperatures lower than 170°C. For a better conversion during the simulation the input data was established before the 170°C temperature.

For the kinetics study, three set of kinetic parameters groups (k_1, k_{v1}, k_2, k_{v2}) for control, 1441 and 2696Hz experiments were obtained for both temperatures (250 and 270°C). Figure 57 (a) present the fitted curves for experiments without acoustic (control) and Figure 57 (b) and (c) presented the fitted curves for 1411 and 2696Hz thermo-acoustic torrefaction respectively.

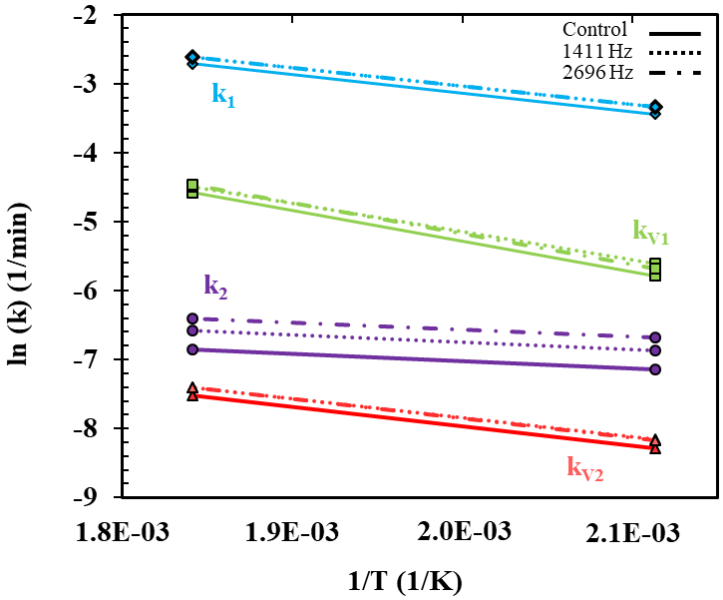

Figure 58. Reaction rates comparison for control (no acoustic), 1411 and 2696Hz treatments.

The simulated curves from the obtained kinetic parameters present an accurate fitted for the three cases. The calculated kinetic rates with the obtained pre-exponential factors and activate energy are illustrated in Figure 58.

As can be seen in Figure 58 the same kinetics behavior (line slope) is obtained for all treatments, being that acoustic ones faster than the control. The obtained kinetics for the

acoustic experiments presented very similar behavior showing fasters reaction rates in comparison to control (without acoustic) for the first step $k_1, k_{v1.}$ as well as for the second step k_2, k_{v2}.

Analyzing the torrefied product pyrolysis results that undergoes with acoustic influence (Figure 44) it is possible to observe that during the degradation, the identified difference in the curves pointed out to a higher wood celluloses degradation (releasing of heavier volatile groups). Bates et Ghoniem (BATES; GHONIEM. 2012) reported that the faster first stage of torrefaction is primarily attributable to the decomposition of hemicellulose (with an increasing contribution from cellulose decomposition at higher temperatures). The mass loss during the second stage is primarily due to cellulose decomposition, with minor lignin decomposition and charring of the remaining hemicellulose.

An interesting resulting obtained in this investigation is that the parameter k_2, that represents the second stage of thermodegradation (remaining hemicelluloses and mainly the cellulose), had a higher displacement in comparison to the other kinetic parameters, agreeing with the pyrolysis of torrefied product results (Figure 44). The 2696Hz treatments presented the faster kinetics for this parameter.

4.4.2.1 Characteristics of products

Kinetics rates obtained from the thermal sensitivity approach were used to calculate the instantaneous solid and volatile yields for each pseudo-component. Firstly, investigating only the control (no acoustic) experiments, the solid dynamics during both temperature treatment (Figure 59 (a) and (c)) had a huge temperature dependence as expected. For 250°C treatment a small amount of A was retained after a smooth degradation curve and for the 270°C (severe treatment) the initial biomass A was totally consumed and entirely converted into B and V_1 during a more aggressive and faster degradation (mainly between 20-40 minutes). Looking only for the formation of B, the maximum value (around 80wt%) is similar for both treatments temperatures. However, due to the entire consumption of B during 270°C, the intermediate product had a higher consumption when compared to 250°C, leading to a higher formation of C.

The observed decreasing of the solid yield throughout experiments is numerically introduced through the volatile productions V_1 and V_2 during the first and the second step of the consecutive reactions respectively. It can be seen on Figure 58 that k_{V1} is much more important than k_{V2}. As a result, the amount of V_1 produced during the treatment is higher than the amount of V_2 for both treatments (Figure 59 (b) and (d)).

The beginning of the V_1 and V_2 formation for both treatments is the same comparing 250 and 270°C treatments. However, the intensity of formation and final amount of each volatile groups is higher for the 270°C due to the stronger thermal decomposition. This behavior was also reported during the assessment of torrefaction in micro-scale by FTIR where the 270°C treatment presented a higher amount and intensity of functional groups (Figure 31). The solid yield decrease is thus mainly due to the production of V_1. Consequently, the faster consumption of the raw biomass A at the beginning of the process leads to faster releasing of the volatile V_1.

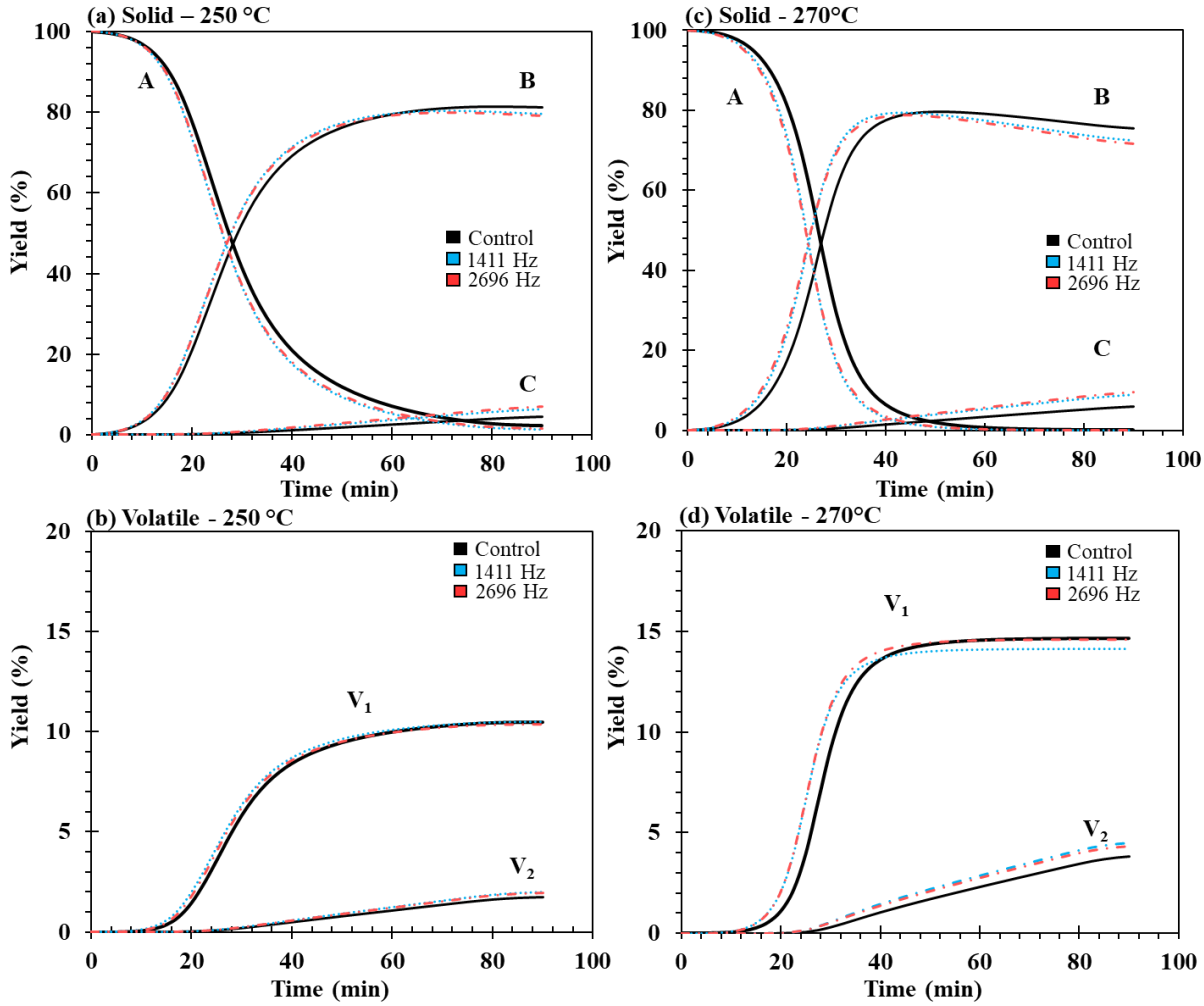

Figure 59. Solid and volatiles pseudo-components evolution for treatments under 250 and 270°C without (control) and with (1411 and 2696Hz) acoustic.

Analyzing the torrefaction by the classification on light mild and severe, it is possible to compare the 250 and 270°C experiment (mild and severe torrefaction respectively). It can be observed that during the first stage of torrefaction ($A \rightarrow B$ and $A \rightarrow V_1$) the decomposition of hemicellulose takes place for both treatments with an increasing contribution from cellulose decomposition at 270°C. For the 270°C the V_1 production is stabilized due to complete

degradation of hemicelluloses. These results can be validated by the experimental analyses with FTIR (Figure 31) and the pyrolysis DTG profiles (Figure 34).

Investigating the second stage of degradation ($B \rightarrow C$ and $B \rightarrow V_2$), there is a slight consumption of B leading to a small formation of V_2 during 250°C experiment. For the 270°C a higher amount of B is consumed (primarily due to cellulose decomposition, with minor lignin decomposition and charring of the remaining hemicellulose) resulting in a higher percentage of volatiles V_2 (also identified in FTIR experiments).

The acoustic coupling resulted in a faster degradation of solid pseudo-components (a shift in time starting the degradation of A earlier and accelerating the formation of B leading to a stronger degradation of this intermediate product). The volatiles V_1 and V_2 had an earlier releasing. Comparing the control with acoustic treatments the final amount of V_1 (hemicelulose consumption) are very similar for both temperatures and a higher amount of V_2 (a higher degradation of cellulose and lignin took place) is reported for the two temperatures.

4.4.3 Composition Model

BACH et al., (2016) showed a direct method to predict the biochar elemental composition presenting good agreements. A new formulation based on the study (BACH et al., 2016) was developed in section 4.4.2 and the results are presented here. The direct model provides a simple and accurate numerical prediction of the carbon (C), hydrogen (H) and oxygen (O) evolution during time for each temperature analysis based on the kinetic evolution discussed in section 4.4.1 and the initial (raw biomass) and final (torrefied product) values of C, H and O. First a validation of the model is presented in section 4.4.3.1 and thereafter the model is used to simulate the composition of the thermo-acoustic experiments.

4.4.3.1 Biomass composition model validation

For the composition model validation, the Eq. (30) to (41) were solved using a multidimensional unconstrained nonlinear minimization solver Nelder-Mead (Matlab® software) with admitted convergence criterion of 10^{-4}. The obtained results for the temperature dependence of the solid an volatile composition were compared to (BATES; GHONIEM, 2012) to validate the model. Figure 60 illustrated this comparison.

The raw biomass (A) has a constant composition (BACH et al., 2016; BATES; GHONIEM, 2012). The obtained temperature dependence for the composition of the intermediate solid B had a very accurate fitting to the result of (BATES; GHONIEM, 2012) as well as for the final

product C. However, the developed model obtained a higher percentage of carbon and a lower percentage of oxygen for higher temperatures Figure 60 (a) and (b).

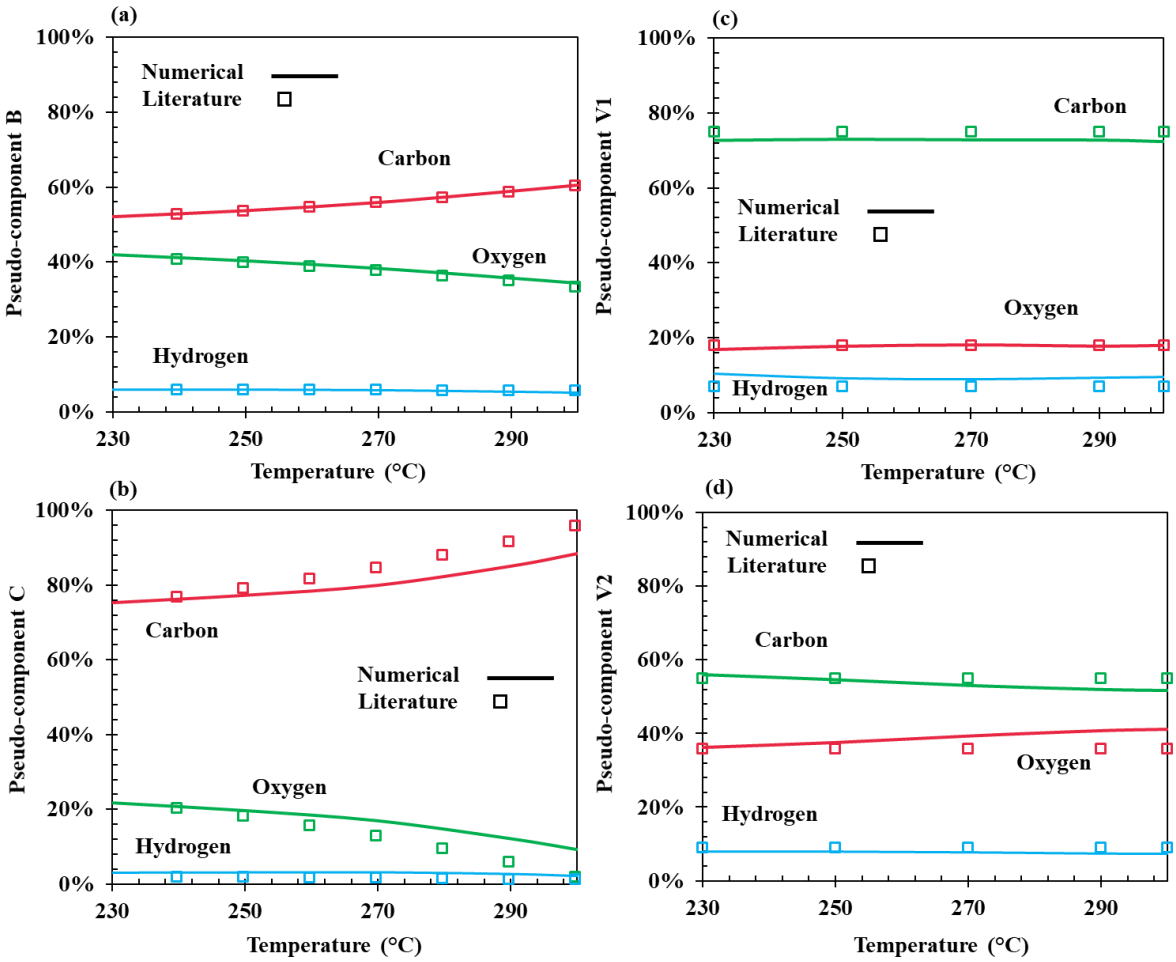

Figure 60. Validation of the temperature dependence for the composition of the intermediate solid B (a) and char (C).

In Bates et Ghoniem (2012) work, the composition percentage of V_1 and V_2 were estimated with experimental data and established as constants for all temperatures. As can be seen in the FTIR results (Figure 31), the volatile release (functional groups intensities) is not constant, having a highest intensity for the higher temperatures, remaining more carbon in the final solid and releasing more oxygen and hydrogen. For the numerical solution, the V_1 and V_2 composition were not assumed as constants and are illustrated in Figure 60 (c) and (d).

A more realistic behavior for the composition is obtained with the model where the volatiles composition has a temperature dependence. Results showed that for higher temperature the quantity of oxygen and hydrogen are bigger, and the percentage of carbon are smaller (more carbon retained in the finals solid product), especially for the V_2 group that has a stronger

importance in higher temperature decomposition (remaining hemicelluloses and mainly cellulose decomposition).

4.4.3.2 Eucalyptus Composition

A numerical simulation of the composition evolution in time were performed to obtain more information about the eucalyptus wood thermodegradation under the temperature as well as coupled temperature and frequency effect.

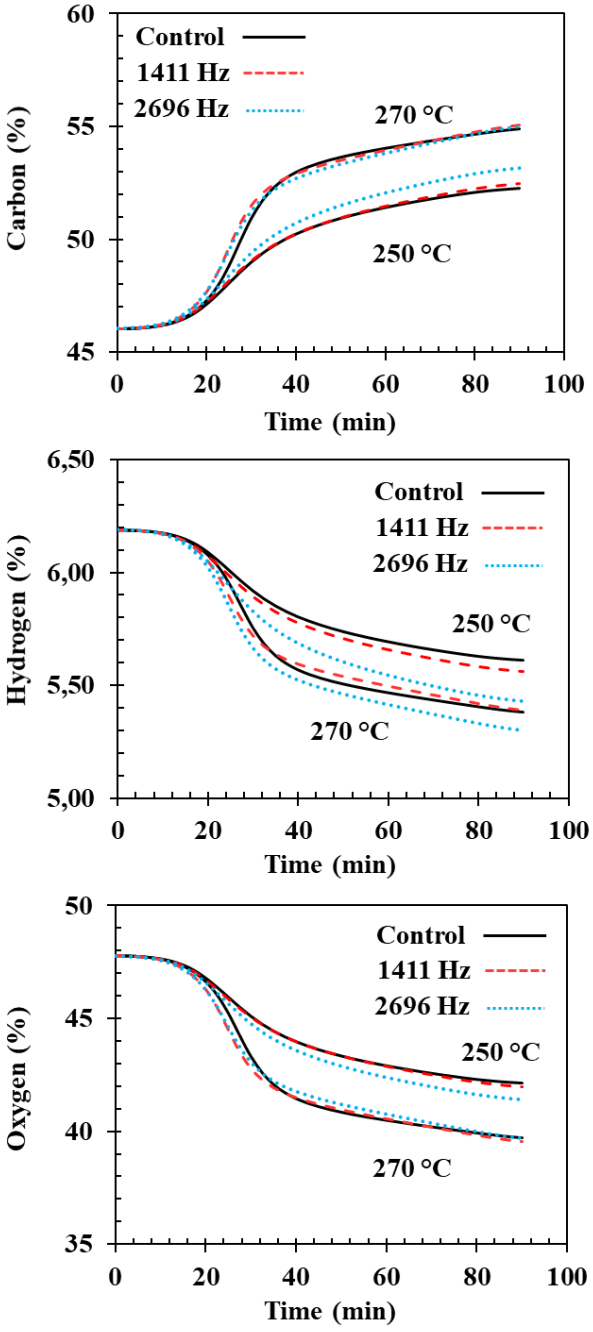

Figure 61. Carbon (a) Hydrogen (b) and Oxygen (c) evolution in time for 250 and 270°C treatments without (control) and with acoustic (1411 and 2696Hz).

The validated composition model in section 4.4.3.1 was applied with the experimental data obtained for the thermoacoustic torrefaction (section 4.3.3.1) and the obtained kinetic evolution in section 4.4.2. The evolution in time for the control experiment (no acoustic) as well as for the thermo-acoustic experiments under influence of optimum frequencies (1411 and 2696Hz) are illustrated in Figure 61 for both temperatures (250 and 270°C).

In all profiles a slightly shift in time is evidenced not having a significant difference comparing the acoustic treatments, as were reported in the chemical analysis. This numerical composition model will be extended to a complex thermochemical and heat transfer model in future work, allowing to calculate the HHV evolution in time as well as the heat release during treatment.

5. CONCLUSIONS AND PERPSECTIVES

5.1 Conclusions

The present work is devoted to deep the knowledge in biomass thermo-degradation torrefaction process within a modified reactor environment by acoustic waves. This study allowed the development of an innovative technology to improve the wood heat treatment coupling acoustic field and temperature. Thanks to this double work of experimentation and modeling, a further understanding of the thermo-acoustic physical phenomena during the torrefaction of a solid wood sample was presented.

This research explored two approaches: an experimental and numerical analysis. Firstly, an experimental assessment of a *Eucalyptus grandis* micro-particle via the characterization of the fundamental mechanisms generated in the wood by the heat treatment, allowed a deeper understand of the thermo-physical phenomena and established experimental results to be compared.

Secondly, a sound system was implemented within an existing torrefaction reactor and characterized thereafter applying three different acoustic analysis methodologies in time and frequency domains. This characterization allowed the measurement of the flow rate and acoustic intensity at the exact spot where the sample is located within the reactor. Thereafter, macro-scale samples of *Eucalyptus grandis* were torrefied and the interaction effect between acoustic filed and temperature was investigated via chemical and physical analysis of torrefied product.

The numerical approach contemplates the development of a kinetic model (thermal sensitivity methodology) as well as a composition model allowing the prediction the biomass degradation and the composition dynamics.

Regarding the micro-scale torrefaction experimental study, some interesting results were obtained. The torrefaction experiment was carried out for five different temperatures: 210, 230, 250, 270 and 290°C with a heating rate of 5°C.min^{-1} in an inert atmosphere. The solid yield decreases when the temperature increases, and the final values are 96.39, 90.35, 83.84, 75.51 and 62.41wt%, for the treatments respectively. A better interpretation of the solid yield and DTG dynamics via the exploitation of 3D surfaces and 2D contour for the torrefaction and pyrolysis of torrefied product provided a more detailed discussion of thermal degradation, identifying the classification for the torrefaction intensity as light (200-235°C), mild (235-275°C) or severe (275-300°C). FTIR results during torrefaction allowed to characterize the presence and its intensity of volatile functional groups for each torrefaction temperature. These results were used to discuss the thermo-acoustic physical phenomena and determine the two temperatures to be applied during the acoustic torrefaction.

Regarding the thermo-acoustic experiments, the concept of the acoustic system was presented and detailed. Starting from a basic experimental reactor, some physical improvement of the device was performed in order to characterize and control the acoustic frequencies during the heat treatment of wood. A modal characterization with calibrate source was investigated and showed a limitation due to the exponential comportment of the modal density in high frequencies. Thereafter, the acoustic behaviour within the reactor was characterized and mapped by applying frequency and time domain methodologies. The acoustic frequencies were explored in the range of 0 to 3000Hz applying both Lissajous/Hilbert techniques in the time domain and the cross-spectrum technique in the frequency domain. The results showed an agreement between the two techniques with identification of higher particle velocities around the wood sample for the following frequencies: 1411, 1810, 2478 and 2696Hz.

The thermo-acoustic torrefaction was performed for the identified frequencies providing the degradation dynamics as well as temperate profiles. The torrefied solid product were assessed by chemical experiments. The standard torrefaction for the macro-particle scale showed a good agreement with literature. Considering the acoustic torrefaction experiments results, some meaningful conclusions can be taken from the chemical and dynamic analysis:

- The final solid yields were very similar whatever the acoustic frequency, however its dynamic profiles show that acoustic may accelerate the degradation process.
- The acoustic field effect influenced slightly the elemental composition of the wood, by decreasing the H/C and O/C atomic ratios.

- Proximate analyses showed that torrefaction coupled to acoustic waves presented lower VM and higher FC when compared to standard torrefaction. The statistical analysis did not show any significant differences for acoustic torrefied biomass except for the higher heating value.
- The 1411 and 2696Hz frequencies were investigated as they presented better results when compared to other treatments conditions. For 250°C treatment, the 1411Hz frequency presented both a higher final solid yield and HHV enhancement compared to 2696Hz. At 270°C, results showed a higher value for 2696Hz.
- Comparing the solid yield behavior during the pyrolysis of the torrefied products under 1441 and 2696Hz it is possible to conclude that the treatments had a lower degradation compared to the standard torrefaction. The difference during wood components degradation were obtained for the cellulose component where for both treatments showed a higher degree of degradation being difficult to point out which treatment was better due to the slight difference.

Applying the frequencies of 1411 and 2696Hz for 250 and 270°C, a maximum temperature gradient of 2.3°C for 270°C was reported for treatment under influence of 1411Hz. The solid yield profile for 250 and 270°C treatment had an earlier degradation for treatments under 1411Hz and 2696Hz frequencies and showed an interesting shift in time comparable to treatments performed when different heating hates are applied. Considering the conversion rates, noticeable results for the enhancement factors of 2.4 and 2.8 for 250°C and 270°C respectively were reported. These results indicate that the combined effect of heat and acoustics affected the interaction between gaseous environment and wood sample modifying degradation processes development under the same experimental conditions.

Regarding the numerical models, a new thermal sensitive methodology was developed for the kinetic simulation. For the kinetics validation, the thermodegradation of poplar wood was performed by using a pilot scale reactor by conduction at five different temperatures (200, 210, 220, 230, and 240°C). A mathematical model was developed and implemented to predict dynamic mass yield of macro-scale samples during the heat treatment. The model developed is based on the two-step kinetic scheme with three-stage approach (thermal sensitivity analysis). The results indicate that the ranking of reaction rates is $k_1 > k_{v1} > k_2 > k_{v2}$. It means the first step of reaction ($A \rightarrow B$ and $A \rightarrow V_1$) is faster than the second step ($B \rightarrow C$ and $B \rightarrow V_2$). The heat treatment kinetics obtained in this study give the possibility to predict the treatment duration in order to reach a particular level of wood modification under industrial conditions.

It should be emphasized that a good fitting has been achieved both at the beginning and at the end of the treatment process confirming that the chosen model is able to consider from a macroscopic point of view, all thermodegradation reactions occurring in the treatment temperatures range owing to the better simulation quality and reasonable computation time. Overall, the obtained results are encouraging for a future development of a numerical tool able to give recommendations and conduct efficiently the heat treatment of wood in industry.

The validated model was applied to simulate the acoustic thermodegradation for *Eucalyptus grandis* macro-particles. The acoustic coupling resulted in a faster degradation of solid pseudo-components (a shift in time is observed starting the degradation of A earlier and accelerating the formation of B leading to a stronger degradation of this intermediate product). The volatiles V_1 and V_2 had an earlier releasing. Comparing the control with acoustic treatments the final amount of V_1 (hemicellulose consumption) are very similar for both temperatures and a higher amount of V_2 (a higher degradation of cellulose and lignin took place) is reported for the two temperatures.

Investigating the second stage of degradation ($B \rightarrow C$ and $B \rightarrow V_2$) there was a slight degradation for B leading to a small formation of V_2 during 250°C experiment. For the 270°C a higher amount of B is degraded (primarily due to cellulose decomposition, with minor lignin decomposition and charring of the remaining hemicellulose) resulting in a higher number of volatiles V_2 (also identified in FTIR experiments).

The composition model was validated and the obtained temperature dependence for the composition of the intermediate solid B had a very accurate fitting as well as for the final product C, however the developed model obtained a higher percentage of carbon and a lower percentage of oxygen for higher temperatures. The numerical solution presented for the V_1 and V_2 composition a more realistic behavior for the composition where the volatiles composition is not constant and for higher temperature the quantity of oxygen and hydrogen are bigger and the percentage of carbon are smaller, especially for the V_2 group that has a stronger importance in higher temperature decomposition (remaining hemicelluloses and mainly cellulose decomposition).

The model was used to simulate the composition of *Eucalyptus grandis* that undergoes the thermo-acoustic torrefaction for the optimum frequencies. In all profiles a slightly shift in time is evidenced, showing as earlier degradation not having a significant difference between the acoustic treatments as were reported in the chemical analysis. This numerical composition model will be extended to a complex thermochemical and heat transfer model, allowing to calculate the HHV evolution in time as well as the heat release during treatment.

5.2 Perspectives

Regarding the thermo-acoustic torrefaction system development and the experimental study developed some perspectives were taken:

- The exploratory acoustic characterization was performed in a range of 300- 3000Hz. It is recommended to go further into a more complex characterization for a larger range of frequencies, including ultrasound frequencies.
- It would be interesting to design a thermo-acoustic reactor in a smaller scale and with a cylindrical configuration, where it would have a greater control in relation to the collect of gases, as well as a greater control and quality for the acoustic propagation.
- The presence of a second sound actuator could contribute to the modification of the atmosphere, modifying the interaction of gaseous environments and wood sample in other ways.
- The coupling of a volatile analysis system to the output of the thermo-acoustic reactor (FTIR or gas chromatography (GC)) would provide information of the volatiles release dynamics over time and would contribute to the identification of which functional groups were released in greater quantity during the thermo-acoustic torrefaction.
- The variation of some parameters such as heating rates and final treatment temperatures, as well as the use of other wood species in the study, especially those with a higher content of cellulose, could contribute with more information about the interaction of acoustics at the thermodegradation.

In relation to the developed numerical models:

- During the development of the kinetic model it was observed a significant dependence of the initialization parameters of the simulation. A parametric study of these initial conditions and the convergence time for the solution is recommended.
- A method to capture the released volatiles during the thermo-acoustic experiment have been developed and will be used to validate the evolution of the elemental composition in time.
- The two developed models have been extended in to a more complex model. Applying a finite element approach to simulate the heat of reactions from the obtained elemental composition for solid and volatile. The calculated heat of reaction will be inserted as heat sources and will provide a more accurate characterization the wood degradation inside a heat transfer domain.

6. REFERENCES

ABRAF. Anuário Estatístico-Associação Brasileira de Produtores de Florestas Plantadas. **Anuário Estatístico ABRAF**, p. 146, 2013.

AKGÜL, M.; GÜMÜŞKAYA, E.; KORKUT, S. Crystalline structure of heat-treated Scots pine [Pinus sylvestris L.] and Uludağ fir [Abies nordmanniana (Stev.) subsp. bornmuelleriana (Mattf.)] wood. **Wood Science and Technology**, v. 41, n. 3, p. 281–9, 2006.

AL-KHAZALI, H. A. H.; ASKARI, M. R. Geometrical and Graphical Representations Analysis of Lissajous Figures in Rotor Dynamic System. v. 2, p. 971–978, 2012.

ALMEIDA, G.; BRITO, J. O.; PERRÉ, P. Alterations in energy properties of eucalyptus wood and bark subjected to torrefaction: The potential of mass loss as a synthetic indicator. **Bioresource Technology**, v. 101, n. 24, p. 9778–9784, 2010.

ANCA-COUCE, A. et al. Kinetic scheme to predict product composition of biomass torrefaction. **Chemical Engineering Transactions**, v. 37, p. 43–48, 2014.

ANCA-COUCE A, MEHRABIAN R, SCHARLER R, O. I. Kinetic scheme to predict product composition of biomass torrefaction. **Chemical Engineering Transactions**, v. 37, p. 43–8, 2014.

ARIAS, B. et al. Influence of torrefaction on the grindability and reactivity of woody biomass. **Fuel Processing Technology**, v. 89, n. 2, p. 169–175, 2008.

BACH, Q. V. et al. Predictions of biochar yield and elemental composition during torrefaction of forest residues. **Bioresource Technology**, v. 215, p. 239–246, 2016.

BACH, Q. V.; SKREIBERG, O. Upgrading biomass fuels via wet torrefaction: A review and comparison with dry torrefaction. **Renewable and Sustainable Energy Reviews**, v. 54, p. 665–677, 2016.

BACH, Q. V.; TRAN, K. Q.; SKREIBERG, Ø. Comparative study on the thermal degradation of dry- and wet-torrefied woods. **Applied Energy**, v. 185, p. 1051–1058, 2017.

BAHNG, M. K. et al. Current technologies for analysis of biomass thermochemical processing: A review. **Analytica Chimica Acta**, v. 651, n. 2, p. 117–138, 2009.

BALAT, M.; BALAT, H.; OZ, C. Progress in bioethanol processing. **Progress in Energy and Combustion Science**, v. 34, n. 5, p. 551–573, 2008.

BASU, P. **Biomass Gasification and Pyrolysis: Practical Design**. [s.l: s.n.]. v. 28

BASU, P. et al. An experimental and theoretical investigation on torrefaction of a large wet wood particle. **Bioresource technology**, v. 159, p. 215–22, maio 2014.

BATES, R. B. **MODELING THE COUPLED EFFECTS OF HEAT TRANSFER, THERMOCHEMISTRY, AND KINETICS DURING BIOMASS TORREFACTION**. [s.l: s.n.].

BATES, R. B.; GHONIEM, A. F. Biomass torrefaction: Modeling of volatile and solid product evolution kinetics. **Bioresource Technology**, v. 124, p. 460–469, 2012.

BATIDZIRAI, B. et al. Biomass torrefaction technology: Techno-economic status and future prospects. **Energy**, v. 62, p. 196–214, 2013.

BENDAT, J. S.; PIERSOL, A. G. **Random Data, Analysis and Measurement Procedures**. 2nd. ed. New York: John Wiley and Sons, 1986.

BENNETT, G. J. et al. Heat Transfer Enhancement in Ducts Due to Acoustic Excitation. **7th World Conference on Experimental Heat Transfer, Fluid Mechanics and Thermodynamics**, 2009.

BERGMAN, P. C. et al. Torrefaction for biomass co-firing in existing coal-fired power stations. **Energy research Center of Netherlands**, 2005.

BERGMAN, P. C. A.; KIEL, J. H. A. Torrefaction for biomass upgrading. **Proc. 14th European Biomass Conference, Paris, France**, n. October, p. 17–21, 2005.

BHUTTO, A. W. et al. Insight into progress in pre-treatment of lignocellulosic biomass. **Energy**, v. 122, p. 724–745, 2017.

BIAGINI, E.; BARONTINI, F.; TOGNOTTI, L. Devolatilization of biomass fuels and biomass components studied by TG/FTIR technique. **Industrial and Engineering Chemical Research**, v. 45, p. 4486–4493, 2006.

BLONDEAU, J.; JEANMART, H. Biomass pyrolysis at high temperatures: Prediction of gaseous species yields from an anisotropic particle. **Biomass and Bioenergy**, v. 41, p. 107–121, jun. 2012.

BRIDGEMAN, T. G. et al. An investigation of the grindability of two torrefied energy crops. **Fuel**, v. 89, p. 3911–8, 2010.

BROUST, F.; GIRARD, P.; VAN DE STEENE, L. Biocarburants de seconde génération. **Techniques de l'ingénieur**, v. RE 110, p. 1–13., 2008.

CAILLAT, S. et al. Cocombustion de charbon et de biomasse. Cas des chaudières industrielles. **Techniques de l'ingénieur.**, p. 1–16., 2010.

CANDELIER, K. et al. Thermodesorption coupled to GC–MS to characterize volatiles formation kinetic during wood thermodegradation. **Journal of Analytical and Applied Pyrolysis**, v. 101, p. 96–102, maio 2013.

CANDELIER, K. et al. Control of wood thermal treatment and its effects on decay resistance: a review. **Annals of Forest Science**, v. 73, n. 3, p. 571–583, 2016.

CARRIER, M. et al. Production of char from vacuum pyrolysis of South-African sugar cane bagasse and its characterization as activated carbon and biochar. **Journal of Analytical and Applied Pyrolysis**, v. 96, p. 24–32, 2012.

CAVAGNOL, S. et al. Inverse analysis of wood pyrolysis with long residence times in the temperature range 210–290°C: Selection of multi-step kinetic models based on mass loss residues. **Thermochimica Acta**, v. 574, p. 1–9, 2013.

CHAOUCH, M. et al. Use of wood elemental composition to predict heat treatment intensity and decay resistance of different softwood and hardwood species. **Polymer Degradation and Stability**, v. 95, n. 12, p. 2255–2259, dez. 2010.

CHAOUCH, M. **Effet de l'intensité du traitement sur la composition élémentaire et la durabilité du bois traité thermiquement : développement d'un marqueur de prédiction de la résistance aux champignons basidiomycètes Soutenue**. [s.l.] Université Henri Poincaré Spécialité, 2011.

CHEN, W.-H.; PENG, J.; BI, X. T. A state-of-the-art review of biomass torrefaction, densification and applications. **Renewable and Sustainable Energy Reviews**, v. 44, p. 847–866, 2015.

CHEN, W. H. et al. An evaluation on improvement of pulverized biomass property for solid fuel through torrefaction. **Applied Energy**, v. 88, n. 11, p. 3636–3644, 2011a.

CHEN, W. H. et al. Thermal pretreatment of wood (Lauan) block by torrefaction and its influence on the properties of the biomass. **Energy**, v. 36, n. 5, p. 3012–3021, 2011b.

CHEN, W. H.; KUO, P. C. A study on torrefaction of various biomass materials and its impact on lignocellulosic structure simulated by a thermogravimetry. **Energy**, v. 35, n. 6, p. 2580–2586, 2010a.

CHEN, W. H.; KUO, P. C. A study on torrefaction of various biomass materials and its impact on lignocellulosic structure simulated by a thermogravimetry. **Energy**, v. 35, n. 6, p. 2580–2586, 2010b.

CHEN, W. H.; KUO, P. C. Torrefaction and co-torrefaction characterization of hemicellulose, cellulose and lignin as well as torrefaction of some basic constituents in biomass. **Energy**, v. 36, n. 2, p. 803–811, 2011a.

CHEN, W. H.; KUO, P. C. Isothermal torrefaction kinetics of hemicellulose, cellulose, lignin and xylan using thermogravimetric analysis. **Energy**, v. 36, n. 11, p. 6451–6460, 2011b.

CHEN, W. H.; LU, K. M.; TSAI, C. M. An experimental analysis on property and structure variations of agricultural wastes undergoing torrefaction. **Applied Energy**, v. 100, p. 318–325, 2012a.

CHEN, W. H.; LU, K. M.; TSAI, C. M. An experimental analysis on property and structure variations of agricultural wastes undergoing torrefaction. **Applied Energy**, v. 100, p. 318–325, 2012b.

CHEW, J. J.; DOSHI, V. Recent advances in biomass pretreatment - Torrefaction

fundamentals and technology. **Renewable and Sustainable Energy Reviews**, v. 15, n. 8, p. 4212–4222, 2011.

CHUNG, J. . Cross-spectral method of measuring acoustic intensity without error caused by instrument phase mismatch. **The Journal of the Acoustical Society of America**, v. 64, p. 1613–1616, 1978.

CINTRA, B.F.C. FERNANDES, E. C. Thermoacoustic instabilities of lean disc flames. **Fuel**, v. 184, p. 973–986, 2016.

CIOLKOSZ, D.; WALLACE, R. No Title. **Biofuels, Bioproducts & Biorefining**, v. 5, n. 3, p. 317–319, 2011.

COLIN, B. **Modélisation de la torréfaction de plaquettes de bois en four tournant et validation expérimentale à l'échelle d'un pilote continu de laboratoire**. [s.l.] École Nationale Supérieure des Mines d'Albi-Carmaux conjointement avec l'INP Toulouse, 2014.

COLIN, B. et al. Wood chips flow in a rotary kiln: Experiments and modeling. **Chemical Engineering Research and Design**, v. 98, p. 179–187, 2015.

COLLARD, F. X.; BLIN, J. A review on pyrolysis of biomass constituents: Mechanisms and composition of the products obtained from the conversion of cellulose, hemicelluloses and lignin. **Renewable and Sustainable Energy Reviews**, v. 38, p. 594–608, 2014.

CORAZZARI, I. et al. Advanced physico-chemical characterization of chitosan by means of TGA coupled on-line with FTIR and GCMS: Thermal degradation and water adsorption capacity. **Polymer Degradation and Stability**, v. 112, p. 1–9, 2015.

COUHERT, C.; COMMANDRE, J.; SALVADOR, S. Is it possible to predict gas yields of any biomass after rapid pyrolysis at high temperature from its composition in cellulose , hemicellulose and lignin ? **Fuel**, v. 88, n. 3, p. 408–417, 2009.

CUNDY, H.; ROLLETT, A. **Lissajous's figures in mathematical models**. Stradbroke, England: [s.n.].

DEGLISE, X.; DONNOT, A. Bois énergie. **Techniques de l'ingénieur.**, p. 1–21, 2004.

DEMIRBAS, A. Biorefineries: Current activities and future developments. **Energy Conversion and Management**, v. 50, n. 11, p. 2782–2801, 2009.

DENG, J. et al. Pretreatment of agricultural residues for co-gasification via torrefaction. **Journal of Analytical and Applied Pyrolysis**, v. 86, n. 2, p. 331–337, 2009.

DI BLASI, C.; LANZETTA, M. Intrinsic kinetics of isothermal xylan degradation in inert atmosphere. **Journal of Analytical and Applied Pyrolysis**, v. 40–41, p. 287–303, 1997.

EPE. Brazilian Energy Balance 2016, Year 2015. **Empresa de Pesquisa Energética - EPE (Brasil)**, p. 292, 2016.

ESTEVES, B. M.; PEREIRA, H. M. Wood modification by heat treatment: a review.

BioResources, v. 4, n. 1965, p. 370–404, 2009.

FAHY, F. **Sound Intensity**. 2nd. ed. [s.l.] CRC Press Book, 1995.

FELDMAN, M. Non-linear system vibration analysis using Hilbert transform--II. Forced vibration analysis method “Forcevib”. **Mechanical Systems and Signal Processing**, v. 8, n. 3, p. 309–318, 1994a.

FELDMAN, M. Non-linear system vibration analysis using Hilbert transform-I. Free vibration analysis method “Freevib”. **Mechanical Systems and Signal Processing**, v. 8, n. 2, p. 119–127, 1994b.

FELFRI, F. F. et al. Wood briquette torrefaction. **Energy Sustain. Dev.**, v. 9, p. 19–22, 2005.

FRANCISCO, DE A. S. E S.; CARLOS, A. V. DE A. The Assistat Software Version 7.7 and its use in the analysis of experimental data. **African Journal of Agricultural Research**, v. 11, n. 39, p. 3733–3740, 29 set. 2016.

GARCÌA-PÉREZ, M. et al. Vacuum pyrolysis of softwood and hardwood biomass. Comparison between product yields and bio-oil properties. **Journal of Analytical and Applied Pyrolysis**, v. 78, n. 1, p. 104–116, 2007.

GAUR, S.; REED, T. B. **Thermal data for natural and synthetic fuels**. New York: Marcel Dekker, 1998.

GAUTHIER, G. et al. Pyrolysis of thick biomass particles : experimental and kinetic modelling. **Chemical Engineering Transactions**, v. 32, p. 601–6, 2013a.

GAUTHIER, G. et al. Pyrolysis of thick biomass particles: Experimental and kinetic modelling. **Chemical Engineering Transactions**, v. 32, n. May 2016, p. 601–606, 2013b.

GERGES, S. N. **Ruídos e Vibrações Veiculares**. 1st. ed. [s.l: s.n.].

GRAY, A. **Modern differential geometry of curves and surfaces with mathematica**. 2nd. ed. Boca Raton, FL: CRC Press, 1997.

GUÉDRA, M. et al. Parameter estimation for the characterization of thermoacoustic stacks and regenerators. **Applied Thermal Engineering**, v. 80, p. 229–237, 2015.

HILL, S. J.; GRIGSBY, W. J.; HALL, P. W. Chemical and cellulose crystallite changes in Pinus radiata during torrefaction. **Biomass and Bioenergy**, v. 56, p. 92–98, 2013.

HUANG, Y. F. et al. Co-torrefaction of sewage sludge and leucaena by using microwave heating. **Energy**, v. 116, p. 1–7, 2016.

HUANG, Y. F. et al. Leucaena biochar produced by microwave torrefaction: Fuel properties and energy efficiency. **Applied Energy**, v. 204, p. 1018–1025, 2017.

JENKINS, G. M.; WATTS, D. G. **Spectral Analysis and Its Applications**. Holden-Day, San Francisco: [s.n.].

JOSHI, Y. et al. Torrefaction: Unit operation modelling and process simulation. **Applied**

Thermal Engineering, v. 74, p. 83–88, 2014.

KIEL, J. H. A. **Torrefaction for upgrading biomass into commodity fueleEuropean developments**Presentation at the European pellet conference. **Anais**...Wels, Austria: 2011

KINSLER, L. E. et al. **Fundamentals of Acoustics,**. 3rd. ed. [s.l.] JohnWiley & sons, 1982.

KOMAROV, S.; HIRASAWA, M. Enhancement of gas phase heat transfer by acoustic field application q. v. 41, p. 289–293, 2003.

LAWRENCE, J. D. **A catalog of special plane curves**. New York: Dover, 1972.

LI, H. et al. Torrefaction of sawdust in a fluidized bed reactor. **Bioresource Technology**, v. 103, n. 1, p. 453–458, 2012.

LIN, B. J. et al. Thermal degradation and compositional changes of wood treated in a semi-industrial scale reactor in vacuum. **Journal of Analytical and Applied Pyrolysis**, v. 130, n. December 2017, p. 249–255, 2018.

LIU, Q. et al. Mechanism study of wood lignin pyrolysis by using TG-FTIR analysis. **Journal of Analytical and Applied Pyrolysis**, v. 82, n. 1, p. 170–177, 2008.

LU, K. M. et al. Torrefaction and low temperature carbonization of oil palm fiber and eucalyptus in nitrogen and air atmospheres. **Bioresource Technology**, v. 123, p. 98–105, 2012.

LV, P.; ALMEIDA, G.; PERRÉ, P. TGA-FTIR analysis of torrefaction of lignocellulosic components (cellulose, xylan, lignin) in isothermal conditions over a wide range of time durations. **BioResources**, v. 10, n. 3, p. 4239–4251, 2015.

MATVEEV, K. I.; CULICK, F. E. C. A study of the transition to instability in a Rijke tube with axial temperature gradient. **Journal of Sound and Vibration**, v. 264, p. 689–706, 2003.

MCKENDRY, P. Energy production from biomass (part 1): overview of biomass. **Bioresource Technol**, v. 83, n. 1, p. 37–46, 2002.

MEDIAVILLA I, ESTEBAN LS, F. M. Optimisation of pelletisation conditions for poplar energy crop. **Fuel Processing Technology**, v. 104, p. 7–15, 2012.

MEDIC, D. et al. Effects of torrefaction process parameters on biomass feedstock upgrading. **Fuel**, v. 91, n. 1, p. 147–154, 2012.

MELKIOR, T. et al. NMR analysis of the transformation of wood constituents by torrefaction. **Fuel**, v. 92, n. 1, p. 271–280, 2012.

MELO, N. G. R. **Análise modal experimental de cavidade acústica com fonte calibrada.** [s.l.] Universidade de Brasília, 2013.

MOHAN, D.; PITTMAN, C. U.; STEELE, P. H. Pyrolysis of wood/biomass for bio-oil: a critical review. **Energy Fuel**, v. 20, p. 848–89, 2006.

NAG, A. **Biosystems engineering**. New York: MCGraw-Hill, 2010.

NOCQUET, T. **Torréfaction du bois et de ses constituants : expériences et modélisation des rendements en matières volatiles Torrefaction of wood and its constituents : experiments and modelling of volatile species**. [s.l.] Université de Toulouse, 2012.

NOCQUET, T. et al. Volatile species release during torrefaction of biomass and its macromolecular constituents: Part 2 - Modeling study. **Energy**, v. 72, p. 188–194, 2014a.

NOCQUET, T. et al. Volatile species release during torrefaction of wood and its macromolecular constituents : Part 1 e Experimental study. **Energy**, v. 72, p. 180–187, 2014b.

OPPENHEIM, A.V. SCHAFER, R. W. **Discrete Time Signal Processing**. New Jersey: Prentice Hall, 1989.

PARIKH, J.; CHANNIWALA, S. A.; GHOSAL, G. K. A correlation for calculating HHV from proximate analysis of solid fuels. **Fuel**, v. 84, n. 5, p. 487–494, 2005.

PARK, C. et al. Effect of process operating conditions in the biomass torrefaction: A simulation study using one-dimensional reactor and process model. **Energy**, v. 79, p. 127–139, jan. 2015.

PARK, S. W. et al. Torrefaction and low-temperature carbonization of woody biomass: Evaluation of fuel characteristics of the products. **Energy**, v. 45, n. 1, p. 676–685, 2012.

PEDUZZI, E. et al. Torrefaction modelling for lignocellulosic biomass conversion processes. **Energy**, v. 70, p. 58–67, 2014.

PENG, J. H. et al. Development of torrefaction kinetics for British Columbia softwoods. **Int J Chem React Eng**, v. 10, n. 1, p. 1542–6580, 2012.

PENG, J. H. et al. Torrefaction and densification of different species of softwood residues. **Fuel**, v. 111, p. 411–421, 2013.

PÉREZ-FORTES, M.; LAÍNEZ-AGUIRRE, J.M. BOJARSKI, A. D.; PUIGJANER, L. Optimization of pre- treatment selection for the use of woody waste in co-combustion plants. **Chemical Engineering Research and Design**, v. 1, p. 24, 2014.

PERRÉ, P.; DEGIOVANNI, A. Simulation par volume finis des transferts couplés en milieu poreux anisotropes: séchage du bois à basse et à haute température. **International Journal of Heat and Mass Transfer**, v. 33, n. 11, p. 2463–2478, 1990.

PRINS, M. J.; PTASINSKI, K. J.; JANSSEN, F. J. J. G. Torrefaction of wood. Part 1. Weight loss kinetics. **Journal of Analytical and Applied Pyrolysis**, v. 77, n. 1, p. 28–34, 2006a.

PRINS, M. J.; PTASINSKI, K. J.; JANSSEN, F. J. J. G. Torrefaction of wood. Part 2. Analysis of products. **Journal of Analytical and Applied Pyrolysis**, v. 77, n. 1, p. 35–40, 2006b.

RANZI, E.; CUOCI, A.; FARAVELLI, T. Chemical Kinetics of Biomass Pyrolysis. **Energy & Fuels**, v. 22, n. 6, p. 4292–300, 2008.

RATTE, J. et al. Mathematical modelling of slow pyrolysis of a particle of treated wood waste. **Journal of Hazardous Materials**, v. 170, n. 2–3, p. 1023–1040, 2009.

RATTE, J. et al. Mathematical modelling of a continuous biomass torrefaction reactor: TORSPYD^{TM} column. **Biomass and Bioenergy**, v. 35, n. 8, p. 3481–3495, ago. 2011.

RAVEN, P.H. & EICHHORN, E. R. F. **Biology ofplants**. 7th. ed. New York: W.H. Freeman and Company, 2005.

RENEWABLE ENERGY POLICY NETWORK FOR THE 21ST CENTURY (REN21). **Renewables 2016: global status report**. [s.l: s.n.].

REPELLIN, V. et al. Modelling anhydrous weight loss of wood chips during torrefaction in a pilot kiln. **Biomass and Bioenergy**, v. 34, n. 5, p. 602–609, 2010.

REPELLIN, V.; GUYONNET, R. Evaluation of heat treated wood swelling by differential scanning calorimetry in relation with chemical composition. **Holzforschung**, v. 59, n. 1, p. 28–34, 2005.

REVERTE, C. **Stratégie expérimentale pour la détermination de modèles stoechio-cinétiques des réactions de dégradation thermique**. [s.l.] Institut National Polytechnique de Toulouse, 2007.

RODRIGUES, T. O.; ROUSSET, P. L. A. Effects of torrefction on energy properties of Eucalyptus grandis wood. **Cerne**, v. 15, n. 4, p. 446–452, 2009.

ROGAUME, Y. Production de chaleur à partir du bois - Installations industrielles. **Techniques de l'ingénieur**, p. 1–13, 2005.

ROSSETO, G. D. **Contribution to the theory and practice of experimental acoustical modal analysis**. [s.l.] Universidade Estadual de Campinas, 2001.

ROUSSET, P. **CHOIX ET VALIDATION EXPERIMENTALE D ' UN MODELE DE PYROLYSE POUR LE BOIS TRAITE PAR HAUTE TEMPERATURE : DE LA MICRO-PARTICULE AU BOIS MASSIF Patrick Rousset**. [s.l.] ENGREF (AgroParis-Tech), 2004.

ROUSSET, P. et al. Effect of severe thermal treatment on spruce and beech wood lignins. **Annals of Forest Science**, v. 66, n. 1, p. 1–7, 2009.

ROUSSET, P. et al. Enhancing the combustible properties of bamboo by torrefaction. **Bioresource Technology**, v. 102, n. 17, p. 8225–8231, 2011.

ROUSSET, P. et al. Biomass torrefaction under different oxygen concentrations and its effect on the composition of the solid by-product. **Journal of Analytical and Applied Pyrolysis**, v. 96, p. 86–91, 2012.

SADDAWI, A. et al. Commodity fuels from biomass through pretreatment and torrefaction: effects of mineral content on torrefied fuel characteristics and quality. **Energy & Fuels**, v.

26, p. 6466–74, 2012.

SALEH, S. B. et al. Efficient fuel pretreatment : simultaneous torrefaction and grinding of biomass. **Energy & Fuels**, v. 27, p. 7531–40, 2013a.

SALEH, S. B. et al. Influence of biomass chemical properties on torrefaction characteristics. **Energy & Fuels**, v. 27, p. 7541–8, 2013b.

SANTOS, E. A.; MARTINS, C. A.; NASCIMENTO, C. L. A new approach to treating pressure oscillations in combustion instability phenomena. **Applied Acoustics**, v. 114, p. 27–35, 2016.

SARVARAMINI, A.; ASSIMA, G. P.; LARACHI, F. Dry torrefaction of biomass - Torrefied products and torrefaction kinetics using the distributed activation energy model. **Chemical Engineering Journal**, v. 229, p. 498–507, 2013.

SAS, P. **Acoustic intensity measurements**Seminar on Applied Acoustics (ISAAC11), Seminar on Advanced Techniques in Applied and Numerical Acoustics, Leuven-Belgium. **Anais**...2000

SHANG, L. et al. Intrinsic kinetics and devolatilization of wheat straw during torrefaction. **Journal of Analytical and Applied Pyrolysis**, v. 100, p. 145–152, 2013.

SHANG, L. et al. Kinetic model for torrefaction of wood chips in a pilot-scale continuous reactor. **Journal of Analytical and Applied Pyrolysis**, v. 108, p. 109–116, 2014.

SHEN, D. K.; GU, S. The mechanism for thermal decomposition of cellulose and its main products. **Bioresource Technology**, v. 100, n. 24, p. 6496–6504, 2009.

SHEN, D. K.; GU, S.; BRIDGWATER, A. V. Study on the pyrolytic behaviour of xylan-based hemicellulose using TG-FTIR and Py-GC-FTIR. **Journal of Analytical and Applied Pyrolysis**, v. 87, n. 2, p. 199–206, 2010.

SHIN, K.; HAMMOND, J. K. **Fundamentals of Signal Processing for Sound and Vibration Engineers**. 1. ed. [s.l.] Wiley, 2008.

SILVEIRA, E. A. et al. Coupling of an acoustic emissions system to a laboratory torrefaction reactor. **Jornaul of Analytical and Applied Pyrolysis**, n. December, p. 0–1, 2017.

SINGH, T. et al. Chemical characterisation and durability assessment of torrefied radiata pine (Pinus radiata) wood chips. **International Biodeterioration and Biodegradation**, v. 85, p. 347–353, 2013.

STELTE, W. et al. No Title. **Fuel pellets from biomass: The importance of the pelletizing pressure and its dependency on the processing conditions. Fue**, v. 90, n. 11, p. 3285–90, 2011.

SVOBODA, K. et al. Pretreatment and feeding of biomass for pressurized entrained flow gasification. **Fuel Processing Technology**, v. 90, n. 5, p. 629–35, 2009.

TRAN, K. Q. et al. Stump torrefaction for bioenergy application. **Applied Energy**, v. 112, n. January 2005, p. 539–546, 2013.

TRIBOULOT, P.; TROUY-TRIBOULOT, M. C. Matériau bois. Structure et caractéristiques. **Techniques de l'ingénieur**, v. C 925, p. 1–26, 2001.

TUMULURU, J. S.; BOARDMAN, R.; WRIGHT, C. Changes in moisture, carbon, nitrogen, sulphur, volatiles, and calorific value of miscanthus duringtorrefaction. **AIChE Annual Meeting**, 2010.

TURNER, I. et al. An experimental and theoretical investigation of the thermal treatment of wood (Fagus sylvatica L.) in the range 200-260 °C. **International Journal of Heat and Mass Transfer**, v. 53, n. 4, p. 715–725, 2010.

USLU, A.; FAAIJ, A. P. C.; BERGMAN, P. C. Pre-treatment technologies, and their effect on international bioenergy supply chain logistics. Techno-economic evaluation of torrefaction, fast pyrolysis and pelletisation. **Energy**, v. 33, n. 8, p. 1206–23, 2008.

VALTER FRANCESCATO. Wood fuels handbook. p. 1–40, 2015.

VAN DER STELT, M. J. C. et al. Biomass upgrading by torrefaction for the production of biofuels: A review. **Biomass and Bioenergy**, v. 35, n. 9, p. 3748–3762, 2011.

WANG, S. et al. Pyrolysis behaviors of four O-acetyl-preserved hemicelluloses isolated from hardwoods and softwoods. **Fuel**, v. 150, p. 243–251, 2015.

WANG, S. et al. Kinetic modeling of biomass components pyrolysis using a sequential and coupling method. v. 185, p. 763–771, 2016.

WANG, S. et al. Lignocellulosic biomass pyrolysis mechanism : A state-of-the-art review. v. 62, 2017.

WANNAPEERA, J.; FUNGTAMMASAN, B.; WORASUWANNARAK, N. Effects of temperature and holding time during torrefaction on the pyrolysis behaviors of woody biomass. **Journal of Analytical and Applied Pyrolysis**, v. 92, n. 1, p. 99–105, 2011.

WEILAND, J. J.; GUYONNET, R. Study of chemical modifications and fungi degradation of thermally modified wood using DRIFT spectroscopy. **Holz als Roh-und Werkstoff**, v. 61, p. 216–20, 2003.

WIKBERG, H.; LIISA MAUNU, S. Characterisation of thermally modified hard- and softwoods by C CPMAS NMR. **Carbohydrate Polymers**, v. 58, n. 4, p. 461–6, 2004.

WINDEISEN, E.; STROBEL, C.; WEGENER, G. Chemical changes during the production of thermo-treated beech wood. **Wood Science and Technology**, v. 41, n. 6, p. 523–36, 2007.

YANG, H. et al. Characteristics of hemicellulose, cellulose and lignin pyrolysis. **Fuel**, v. 86, n. 12–13, p. 1781–1788, 2007.

ZHAO, Z. et al. Numerical analysis of Eucalyptus grandis x E. urophylla heat-treatment: A

dynamically detecting method of mass loss during the process. **Results in Physics**, v. 7, p. 5–15, 2017.

ZWART, R.; BOERRIGTER, H. The impact of biomass pretreatment on the feasibility of overseas biomass conversion to Fischer-Tropsch products. **Energy & Fuels**, p. 2192–7, 2006.